Zebrafish Larvae as a Model to Study Doxorubicin-Induced Cardiotoxicity

Master thesis in Pharmacy

Ingeborg Nerbø Reiten

Centre for Pharmacy,

Department of Clinical Science,

UNIVERSITY OF BERGEN

June 2020

Acknowledgements

First, I would like to thank my supervisor, Lars Herfindal, for all help and guidance through my master project.

I would like to thank the rest of the lab group; Edvin Tang Gundersen, Ronja Bjørnstad, Jan-Lukas Førde and Reidun Æsøy for helping me at the lab and answering all of my questions throughout the course of the project. Also, a thanks to Sarah Marie Vie Furevik for teaching me zebrafish larvae injections and handling at the beginning of my master project. You have all been to immense help.

Thank you to the Zebrafish Facility at the department of Bioscience for allowing us to retrieve zebrafish embryos nearly every week.

Also, a thanks to Endy Spriet and Hege Avsnes Dale at the Molecular Imaging Centre at the Department of Biomedicine for helping me with confocal microscopy and imaging.

I would like to give a special thanks to Martina Stipic for shared laughs and frustrations, especially throughout this last year. A thanks also to the rest of my pharmacy classmates and friends for lunches, dinners and study breaks the past five years.

Finally, thank you to my family and to Vegard for encouraging me through my studies and for believing in me.

Thank you,
Ingeborg Nerbø Reiten

Table of Contents

Abbreviations

ACN	Acetonitrile
ANOVA	Analysis of variance
ASB	Ammonium sulfate buffer
bpm	Beats per minute
CTG	5-chloromethylfluorescein diacetate (CellTracker™ Green CMFDA)
CVD	Cardiovascular disease
CYPs	Cytochrome P450 enzymes
DA	Dorsal aorta
DiI	1,1'-Dioctadecyl-3,3,3',3'-Tetramethylindocarbocyanine Perchlorate
DLS	Dynamic light scattering
DMEM	Dulbecco's Modified Eagle Medium
DMSO	Dimethyl sulfoxide
DNA	Deoxyribonucleic acid
DNR	Daunorubicin
DOX	Doxorubicin
dpf	Days post fertilization
dpi	Days post injection
EPI	Epirubicin
HDL	High density lipoprotein
HEPC	Hydrogenated egg phosphatidylcholine
HMG-CoA	3-hydroxy-3-methylglutaryl-coenzyme A
hpf	Hours post fertilization
hpi	Hours post injection
HPLC	High performance liquid chromatography
HR	Heart rate

IDA	Idarubicin
IR	Infrared
LDL	Low density lipoprotein
LSD	Least significant difference
MEM	Minimum Essentials Medium Eagle
MQ	Milli-Q water
MTD	Maximum tolerated dose
NDDS	Nanosized drug delivery systems
PBS	Phosphate buffered saline
PCE	Pericardial effusion
PCV	Posterior cardinal vein
PEG	Polyethylene glycol
PEG-PE	1,2-Distearoyl-sn-Glycero-3-Phosphoethanolamine-N-[Methoxy(Polyethylene glycol)-2000] (Ammonium salt)
PTU	1-phenyl 2-thiourea
RNA	Ribonucleic acid
ROS	Reactive oxygen species
SDCM	Spinning disk confocal microscope
SEC	Size elution chromatography
SIM	Simvastatin
TEM	Transmission electron microscopy
TFA	Trifluoroacetic acid
UV	Ultraviolet
WST-1	4-[3-(4-Iodophenyl)-2-(4-nitro-phenyl)-2H-5-tetrazolio]-1,3-benzene sulfonate

1 Abstract

Doxorubicin is one of the most versatile cytostatic drugs available and shows efficacy on most cancer forms. However, it also possesses the risk of cardiotoxicity that is hard to predict, can occur decades after treatment, and that limits the cumulative lifetime doses of the drug. Various approaches have been tested to avoid this toxicity, with liposomal forms of doxorubicin already being on the market. Additionally, some studies have shown that statins can limit doxorubicin induced cardiotoxicity, and also improve the anti-cancer effects of the drug.

The zebrafish has over the last decades emerged as a convenient and relevant model for human cancer research. The species has rapid development, the skin is optically transparent, their genome is comparable to that of humans, and they enable for very easy *in vivo* imaging. In this study zebrafish larvae were used to study the potential cardioprotective effect of simvastatin in co-treatment with doxorubicin, as well as how liposomal formulations of these drugs influence heart function. Moreover, the zebrafish larvae were tested as a model organism for cancer.

Doxorubicin was loaded into liposomes with or without simvastatin incorporated into the lipid bilayer and tested in *in vitro* cytotoxicity assays on H9C2 cardiomyoblast cells and MCF-7 breast cancer cells and *in vivo* in zebrafish larvae. Additionally, fluorescently stained MCF-7 cells were injected in zebrafish larvae and observed over two days.

In the zebrafish larvae injected with fluorescent MCF-7 cells in the yolk sac, the fluorescent signal was observed to spread to the tail of the zebrafish larvae after one- and two-days post injection and to increase in number and size. More experiments need to be conducted to verify this being viable MCF-7 cells.

Liposomal forms of doxorubicin were found to have less impact on zebrafish heart rate, death and pericardial edema and resulted in increased viability in the cytotoxicity assays compared to free doxorubicin. Co-loading with simvastatin did not give an observed additional cardioprotective effect in zebrafish larvae. In the *in vitro* studies, however, free simvastatin co-therapy with high-doses of free doxorubicin contributed to increased viability of H9C2 cardiomyoblast cells relative to free doxorubicin alone, while no such effect was observed for the MCF-7 breast cancer cells. The zebrafish larvae allow for direct observations of physiological functions in an intact, living organism, while still being an inexpensive model. Therefore, zebrafish larvae prove superior to cell cytotoxicity models in the study of toxicity and efficacy of anti-cancer drugs.

2 Introduction

2.1 Cancer and Cancer Therapies

Cancer is a group of diseases caused by abnormal cells dividing uncontrollably in the body, commonly forming tumors and invading other tissue. Today, approximately one in six deaths worldwide is due to cancers (1). Cancer occur in one of three people, and are commonly treated by surgery, drug therapy or radiation. Drug therapies are traditionally chemotherapy, but may also involve hormone therapy, and an increasing amount of biological compounds and immunotherapy are being used (2). Biological compounds can be monoclonal antibodies directed towards antigens on the cancer cell surface. With these it has become possible to specifically attack cancer cells, thereby lowering the toxicity in normal tissue and increasing the efficiency (3). Recent advances in immunotherapy also involves modifications of patient T-cells to recognize tumor specific antigens (4). Difficulties in finding tumor specific antigens and the heterogenicity in cancers however, often minimize the advantages of these drugs (3). Because the new, biological compounds is limited in many cases, modifying anti-cancer drugs already on the market can be a solution in the cancer drug discovery process.

Most anti-cancer treatments give adverse and toxic effects during treatment, as well as protracted effects which can occur years after recovery from cancer (5). The maximum tolerated dose (MTD) of a drug is the highest possible dose a patient can receive, without experiencing unacceptable toxicity (6). MTD is determined in phase I trials, and in cancer, because of the high lethality, quite extensive adverse effects, such as fatigue, nausea and vomiting, anaemia and infections will be tolerated (7, 8). Chemotherapy is particularly challenging because the target in cancer therapy is our own diseased cells, which are difficult to distinguish from normal cells. This can also lead to severe toxic effects on healthy tissue, and in some cases even death (9). Thus, there is a need for new and efficient treatments causing less side-effects.

During the early phases of anti-cancer drug development, cell models are often used to find efficacy and possible unwanted effects of lead compounds. *In vitro* cell assays can give indications of cytotoxic activity, and high throughput screenings of thousands of substances can easily be conducted at a low cost (10). The models make it possible to directly visualize cell processes of tumor development. However, cell lines do not represent the heterogeneity of a tumor and lack the ability to model the complete tumor microenvironment (11). More advanced cell models, for instance three-dimensional cell cultures, have been developed to better mimic

the *in vivo* situations, but cannot replicate the organs and tissues working together in an animal (12). Animal models, while being much more similar to humans, often lack the properties of easy cancer visualization, are time consuming, and expensive (11). The high cost and long time for preclinical mammalian trials limits the number of compounds that can be tested *in vivo.* However, *in vivo* testing in mammals is a requirement for drugs to ensure safety of drugs for human and veterinary use (13). Intermediary animal models prior to testing on mammals, could make it possible to inexpensively do larger *in vivo* screenings and tests to further increase safety and efficacy of new drugs.

2.2 Anthracyclines

Anthracyclines were first extracted from the actinobacteria *Streptomyces peucetius* and belong to the group of cytotoxic antibiotics (14). The main mechanisms of action for the drugs are intercalation in the deoxyribonucleic acid (DNA)-helix preventing both synthesis of ribonucleic acid (RNA) and DNA, and inhibition of the protein Topoisomerase II which is essential in DNA replication and protein synthesis (2). The most used anthracyclines are doxorubicin (DOX), daunorubicin (DNR), epirubicin (EPI) and idarubicin (IDA) (15), where EPI and IDA, are derivatives of DOX and DNR, respectively (16). The drugs are quite similar but contain small molecular differences in their chemical structure (Figure 2.1). DOX is one of the most commonly used cytostatic drugs, with only a few cancer types being unresponsive. The drug is for instance used in treating acute lymphatic leukemias in children and adults, and breast cancer (17-19). DOX and EPI are similar in dose-response relationships. However, EPI has shown a lower cardiotoxic risk at high-dose therapy (20, 21). DNR and IDA are both used in the treatment of leukemias (22, 23). The efficiency of the two drugs varies based on cancer, patient and tumor, but they have similar profiles in adverse effect and toxicity (24, 25). In this study, the main focus will be on DOX.

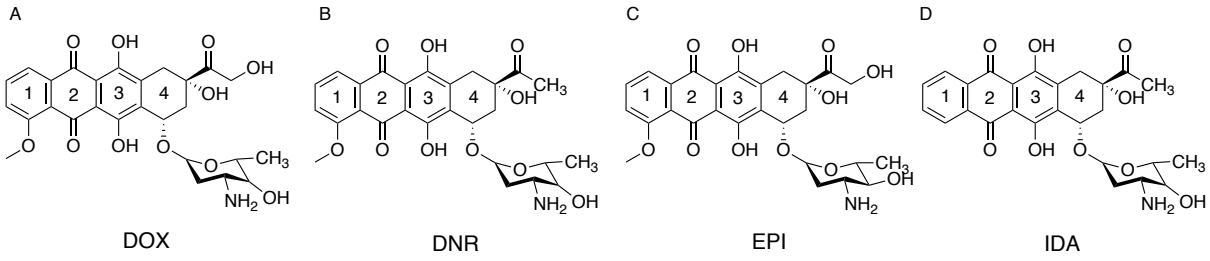

Figure 2.1: Chemical structures of the anthracyclines*. From the left, doxorubicin (DOX, A), daunorubicin (DNR, B), epirubicin (EPI, C) and idarubicin (IDA, D). In DOX there is an alcohol group connected to the ketone on ring 4, which is absent in DNR. IDA is a derivate of DNR and lacks the methoxy group on ring 1. The difference between DOX and EPI is an R/S conversion of the alcohol group on the sugar connected to ring 4.*

One of the biggest disadvantages with the anthracyclines, in particular DOX, is the cardiotoxic adverse effects (26). The cardiotoxic effects can be both acute and chronic. Acute cardiotoxic effects occur during or after the first days of treatment and are often reversible changes. These could for instance be arrythmias and nonspecific electrocardiogram changes like lowered QRS-T voltage, ST-segment depression and premature ventricular heartbeats (27, 28). Acute cardiotoxic effects occur in approximately 11% of patients receiving DOX (28). Chronic anthracycline cardiomyopathy, however, is hard to predict during treatment and causes all anthracyclines to have recommended restrictions in their cumulative lifetime dosage (15). The effects are dose related, and a retrospective study including three trials found an estimated increase of congestive heart failure from 5% to 48% of patients receiving a cumulative DOX dose of 400 mg/m^2 and 700 mg/m^2, respectively (29). Apart from cumulative dose, several risk factors for cardiotoxic effects are reported such as old age, young age (children), previous cardiovascular disease (CVD), and ethnicity (30). Chronic DOX cardiomyopathy can lead to congestive heart failure and death (26).

The mechanism for anthracycline cardiotoxicity is not fully understood, but there are several possible explanations. One of the main theories is by the generation of reactive oxygen species (ROS) (31). While anthracyclines inhibit topoisomerase IIα in cancer cells, they also inhibit topoisomerase IIβ in cardiomyocytes. This can cause double stranded DNA breaks and a possible accumulation of ROS, leading to cardiomyocyte injury and death (32). Anthracyclines is also shown to give both physical and functional damage to mitochondria like swelling of the mitochondria and is also found to interfere in the electron transport chain in the energy metabolism processes in cells *in vitro.* However, *in vivo* it is observed that the effect on energy metabolism continue after removal of the drug, indicating that other components than interference with the electron transport chain must be affected (33). The drugs also have high affinity for cardiolipin, a phospholipid localized only in the inner mitochondrial membrane.

The complex created between anthracyclines and cardiolipin ultimately leads to a overproduction of ROS, and following damage of the cardiomyocytes (34).

To summarize, cancer therapies are often treatments with many adverse effect and high toxicity, and there is a constant need for new, more effective, less toxic drugs. DOX is a cytostatic with effect on most cancer types, but still inhabits a risk of chronic cardiomyopathy in many patients. As this already is an effective cytostatic agent, an attractive approach is to reduce its cardiotoxicity and improve patient safety. In the following sections, both the use of statins and nanosized drug delivery systems (NDDS) will be discussed as possible protective mechanisms in anthracycline therapy.

2.2.1 Statins as a Cardioprotectant in Anthracycline Therapy

3-hydroxy-3-methylglutaryl-coenzyme A (HMG-CoA) reductase inhibitors, commonly known and further referred to as statins, are drugs used in the treatment of hyperlipidemia. The drugs are inhibitors of the enzyme HMG-CoA reductase which reduces HMG-CoA to mevalonate, a rate limiting step in the cholesterol synthesis (2). Statins resultingly gives a decrease in low density lipoprotein (LDL)-cholesterol, which are atherogenic particles. The impaired cholesterol synthesis decreases intracellular cholesterol in the liver, causing higher numbers of liver LDL-receptors, increasing uptake, thus further lowers the LDL-cholesterol in the blood. At the same time there is a reduction in total triglycerides and a rise in high density lipoproteins (HDL). HDL transport cholesterol away from the arteries and are not atherogenic, and considered beneficial to prevent CVD (35).

The statins are a widely used drug group. In 2019 more than ten percent of the Norwegian population were prescribed a statin, and 3.3 percent were prescribed simvastatin (SIM), according to the Norwegian prescription register (36). The drugs have been in use for decades, and protect against CVD by preventing the formation of atherosclerotic plaque and clotting of the coronary arteries (37).The half-life of SIM is approximately five hours, causing the drug to preferably be administrated in the evening to inhibit cholesterol synthesis, which peaks early in the morning (2). SIM is a prodrug, and after absorption, the lactone ring of SIM is hydrolyzed in the liver to yield the active component (see Figure 2.2 for chemical structure of the prodrug and the active form of SIM) (38, 39). SIM undergoes high first pass hepatic metabolism, and less than five percent of the drug is found in plasma after oral dosage (39). Ester groups are

commonly used as prodrugs to increase lipophilicity and membrane permeability of drugs (40). However, for SIM, because of the high first pass metabolism in the liver, which also is the primary cite of action for SIM, the prodrug show higher tissue selectivity as prodrug than the drug administered in active form (38).

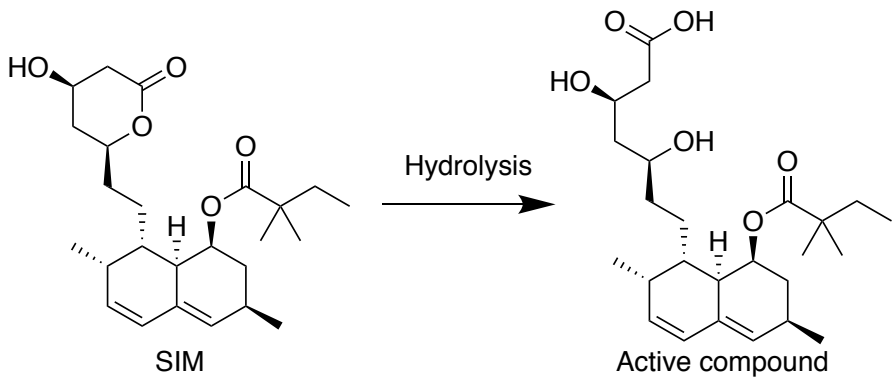

Figure 2.2: Conversion of simvastatin (SIM) into active drug*. The chemical structure of SIM as prodrug (left) and the hydrolyzed form of the drug after enzymatic conversion in the body. Hydrolyzation opens the lactone ring and yields the active form which is a lipid lowering drug (38).*

In addition to the cholesterol lowering effects, statins are shown to possess several other actions unrelated to LDL-lowering effects, so-called pleiotropic effects. The effects are both related and unrelated to the inhibition of HMG-CoA reductase and include improved endothelial function, decreased inflammation in vascular tissue, antithrombotic effects and more (2, 31, 41). As mentioned above, statins reduce the risk of CVD. Additionally, statins are shown to reduce cardiotoxic effects of anthracyclines, and are being increasingly explored as cardiovascular protectants in anthracycline therapy (31). One murine study also found the use of the statin lovastatin to improve the anti-cancer effects of doxorubicin, while still reducing the cardiotoxicity (42). The pleiotropic effect of statins may play a part in the cardioprotective effect statins show in anthracycline therapy (31).

2.3 Nanosized Drug Delivery Systems (NDDS)

The word “nano” comes from Greek, and in science the word referrers to a billionth of a base unit and consequently, the size scales in nanotechnology are within billionth of a meter, nanometers (43). In order to be valid as nanosized, 50% or more of the particles must have one or more external dimension within the size distribution 1-100 nm, as defined by the European

Commission (44). NDDS are one of the strategies that are being extensively studied to overcome challenges in cancer therapy by reformulating existing, effective cytostatic drugs. Nanoparticles are able to carry drugs, and possess abilities which can alter the pharmacokinetic properties, reduce toxic effects and target desired tissue (45).

NDDS can be derived from several different materials giving rise to nanoparticles with distinct properties regarding size, drug loading, efficiency and biocompatibility, to mention a few (46). Materials made to create nanoparticles in medicine can be polymers, dendrimers and lipid based such as micelles or liposomes and many more (46, 47). There are several reasons for utilizing NDDS to transport drugs in the body. Nanoparticles can increase solubility of hydrophobic drugs or extend half-life of drugs that are easily eliminated from the body, resulting in a larger area under the curve (2). By increasing the solubility of drugs when using nanoparticles, higher amounts of drug can be delivered by injection without using potential harmful solvents (48). Examples of some toxic solvents are dimethyl sulfoxide (DMSO), which is often used as a solvent in cell assays, and Cremophor EL, a vehicle used to deliver the cytostatic drug paclitaxel and is known to cause several adverse effects, including anaphylactic reactions in some patients (48, 49). In the case of paclitaxel the use of nanoparticle albumin, which is a natural protein and carrier of hydrophobic compounds in the body, became a solution to avoid the toxic effects of Cremophor EL (50). Nanoparticles can be modified to further increase drug circulation. One common approach is to attach hydrophilic polymers onto the liposome surface of liposome drug carriers. Polymers such as polyethylene glycol (PEG), illustrated in Figure 2.3, will mask the exogenous liposomes from being cleared by the reticuloendothelial system (51). However, perhaps most importantly, NDDS are used to decrease drug toxicity (52).

By increasing target specificity NDDS can be used to reduce adverse or toxic effects (53, 54). This has already been demonstrated in the liposomal formulation of DOX, marketed as Doxil® (or Caelyx®). This FDA-approved formulation shows less cardiotoxic effects compared to free DOX (55). A description of the cardioprotective effects of liposomal anthracyclines is given in section 2.3.1. NDDS are also explored to direct the cells by passive or active targeting, thereby minimize exposure to non-cancerous tissues. Passive targeting takes advantage of the enhanced permeability and retention effect. This is a phenomenon arising when a growing tumor has an increasing need for oxygen and nutrients, and the developing neovasculature inside the tumor differ from normal vasculature. One of the characteristics of tumor neovasculature is lack of

integrity between the endothelial cells, which makes it leaky (56). This causes accumulation of macromolecular compounds such as proteins, as well as nanoparticles at the tumor site (56). Active targeting of nanoparticles can be achieved by attaching molecules onto the nanoparticle surface, which for instance has affinity towards molecules on cancer cells or tumor vasculature (52).

2.3.1 Liposomal Formulation of Anthracyclines

As mentioned, liposomes are already used in the clinic as a NDDS, and because of their high biocompatibility they are the starting point for many NDDS (57). Liposomes consist of a lipid bilayer surrounding an aqueous compartment with the possibility to entrap hydrophilic drugs in the aqueous core and lipophilic molecules in the lipid bilayer (Figure 2.3) (58).

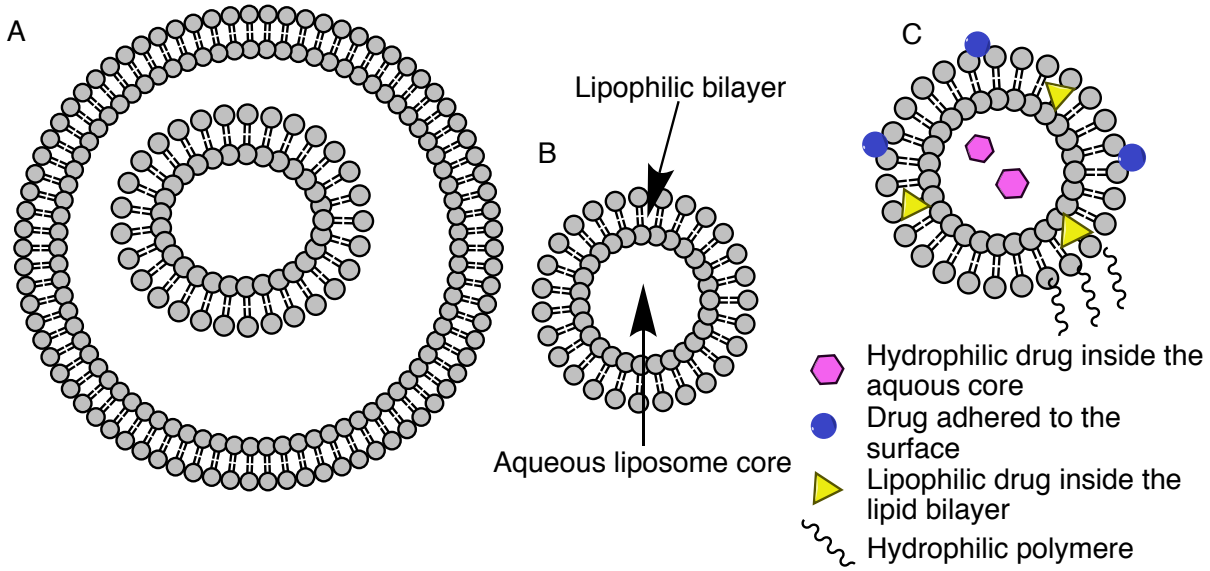

Figure 2.3: Liposome structure. *Liposomes consist of lipid bilayers and can be multilamellar, having multiple lipid bilayers (A) and unilamellar liposomes with only one lipid bilayer (B). The liposomes can be modified by adding hydrophilic polymers to the outer lipid layer or targeting groups to increase favorable pharmacokinetic properties. Drugs or other desired compounds can be trapped inside the aqueous phase, inside the lipid bilayer or adhered to the outside of the liposomes (C). Figure modified from Aulton's Pharmaceutics: The Design and Manufacture of Medicines, fifth edition (59) and Singh et al. (52).*

Loading of DOX into liposomes can be achieved passively by utilizing a pH gradient whereby the non-charged state of DOX in the alkaline suspension medium causes it to diffuse through

the membrane. Once inside the liposomes the DOX molecules becomes protonated in the more acidic environment and the positively charged molecule is unable to diffuse back through the membrane (Figure 2.4) (60). The main goal of liposomal DOX is to reduce toxic side effects associated with DOX treatment (61).

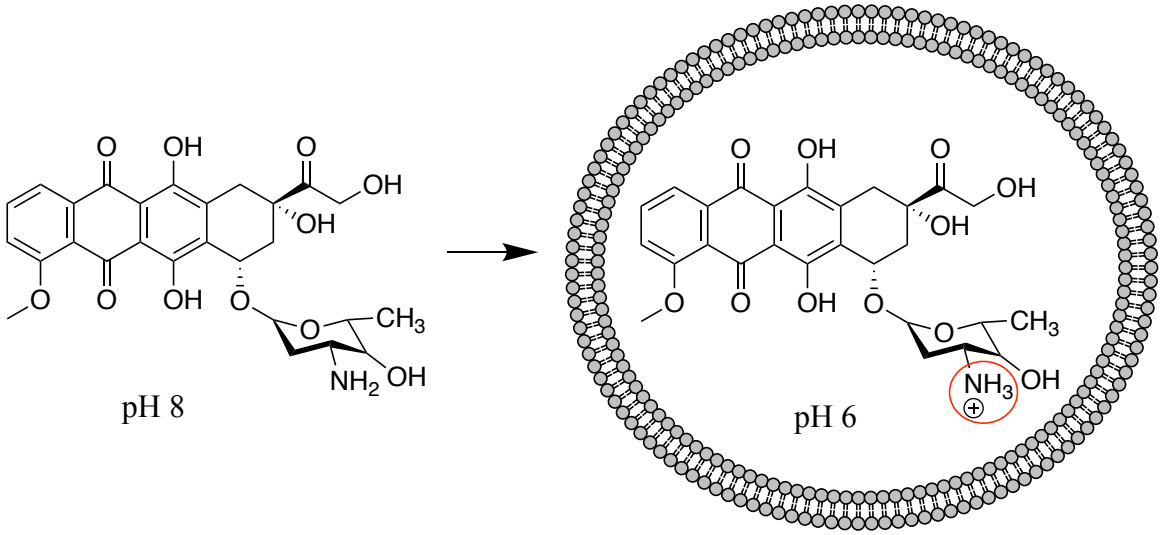

Figure 2.4: Doxorubicin (DOX) encapsulation in liposomes. *Unionized DOX diffuses into the liposome and becomes ionized at the amine site with pKa 8.15 (40) when introduced to pH 6 inside the liposomes (red circle), preventing the DOX molecules from diffusing back out through the membrane.*

2.4 Zebrafish as a Research Model for Human Cancer

Zebrafish (*Danio rerio*) has the last decades emerged as an important model to study several human diseases and in toxicology research (62, 63). Approximately 70% of the human genome has a zebrafish ortholog, and even epigenetic features are conserved between at orthologous genes (64, 65). The cost of keeping zebrafish is much lower than for small mammals, while still making it possible to observe physiological processes that cannot be achieved when using cells assays (62). Not only the adult zebrafish is used in cancer research. Although not fully developed, the zebrafish larvae have properties making them attractive research models. Zebrafish larvae can be exposed to drugs in embryo water, as they absorb small molecules through the epithelium but drugs can also be administered by injection into the larvae (66). Additionally, the juvenile larvae does not have a developed adaptive immune system, making them attractive as transplantation models (67). The zebrafish can become an important intermediary model between cell assays and clinical studies to observe efficacy and toxicity of

new drugs after cell assays, making it possible to increase the number of *in vivo* tests on new lead compounds.

Besides it being a relevant model for human diseases such as cancer (section 2.4.2), in research of CVD, kidney disorders, central nervous system disorders, muscle disorders and many more (68, 69), the zebrafish is advantageous due to its rapid embryonic development, and that it easily produces between 100-200 eggs per week (70). The zebrafish embryo hatches sporadically between 48 to 72 hours post fertilization (hpf), and not at a specific developmental stage, but the embryos can also develop outside their chorion from 24 hpf without it affecting survival (71-73). The high number of embryos and rate of hatching gives a possibility for higher throughput, while lowering husbandry requirements, time and expenses compared to studies on small mammals. Zebrafish do not require feeding until five days post fertilization (dpf), and prior to this they receive all their nutrition from the yolk sac (74). Larval forms of vertebrates are not considered laboratory animals until they are independently feeding (Directive 2010/63/EU of the European parliament and council), and until five dpf the embryo and larvae allow for very inexpensive *in vivo* studies (75).

Altering the zebrafish genome has become increasingly popular, and many different gene modified zebrafish strains exist (76). These strains can inhabit a range of specific phenotypes such as lack of pigmentations (see paragraphs below), fluorescent tissues, or mutated to spontaneously generate cancers (See section 2.4.2) (77). The ability to genetically modify zebrafish has made it even more relevant in cancer research as cell functions can be observed in a microscope in an intact organism. The zebrafish larvae are optically transparent until approximately 24 hours post fertilization (hpf), when it starts developing pigmentation (78). By adding the chemical 1-phenyl 2-thiourea (PTU) in the embryo water, however, pigmentation can be stopped. PTU inhibits the formation of melanophores but does not reverse pigmentation, and treatment must start prior to pigmentation formation, and continue for as long as optical transparency is desired since the process is reversible at withdrawal of the chemical (78). However, the development of strains that are pigment free throughout life has been important for observation of physiological and cellular processes *in vivo* inside the zebrafish.

The *casper* strain was created by breeding two recessive pigment mutants, *nacre* and *roy orbison* which lacked pigmented melanocytes and reflective iridophores, respectively. The lack

of melanocytes in the *nacre* strain is due to a mutation in the *mitfa* gene, while *roy orbison* harbor a mutation in the *mpv17* gene. The resulting *casper* fish is optically transparent throughout adulthood (79). Figure 2.5 show images of AB wild type strain, *roy orbison* and *casper* zebrafish strains as larvae and adult.

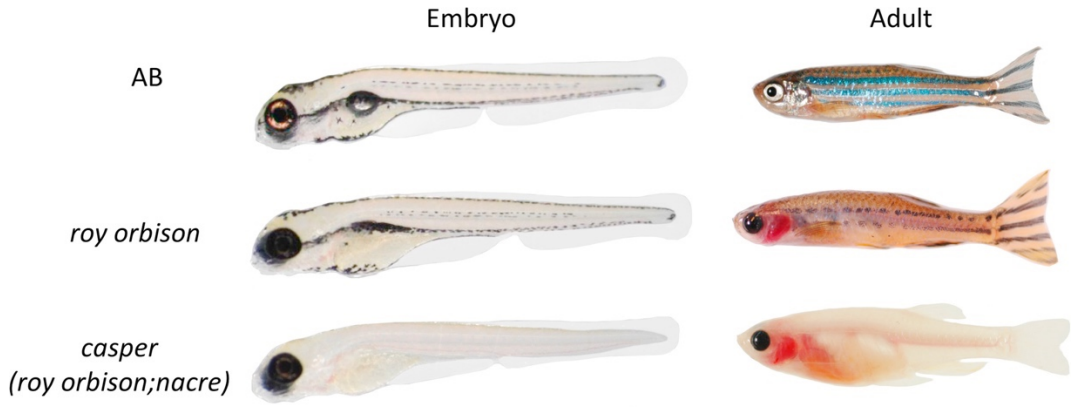

Figure 2.5: Pigmentation of zebrafish strains*. The images (top to bottom) show the AB wild type strain, roy orbison strain which lack reflective iridophores, and casper strain lacking iridophores and melanocytes as larval (left) and adult fish (right). The casper strain is a result of breeding roy orbison and the nacre strain, the latter lacking melanocytes, leaving casper optically transparent. Figure obtained from D'agati et.al. (79). Not to scale.*

2.4.1 Zebrafish in Drug Development

Testing potential drugs on mammals is a requirement in drug development but using zebrafish as a screening tool or as an additional animal model can prove useful. Testing potential drugs and chemicals on zebrafish have shown great potential and have already proven successful in multiple cases (80). One example is the prostaglandin E2 derivative 16,16-dimethyl prostaglandin E2, also referred to as FT1050, which was discovered in a zebrafish larvae screening with 2,500 compounds. This drug entered phase two clinical trials under the name ProHema-CB in 2013 (81, 82). Drug screening using thousands of zebrafish larvae is easy and affordable. Characterization of liver enzymes in zebrafish has also indicated that they metabolize drugs similar to humans. A total of 93 Cytochrome P450 enzymes (CYPs) have been found in adult zebrafish. CYPs transform several compounds in the body including inactivation and activation of drugs and prodrugs. Many of the enzymes found in zebrafish are orthologs to human CYPs, and likely also have conserved mechanisms. A majority of these enzymes are also present in zebrafish embryos (83).

2.4.2 Zebrafish as a Cancer Model

The use of zebrafish in cancer research have advanced after a study from 1965 where zebrafish neoplasms were found to evolve following the exposure carcinogens (84). Zebrafish have several advantages in cancer research. As mentioned, they have relatively high genetically equivalence to humans, are fast developing and require low husbandry costs, making the species an attractive research model (85). Zebrafish cancer models can be created either by transplantation or as genetically engineered zebrafish to spontaneously develop cancers (86).

Inducing cancers in zebrafish serve the purpose of observing the cancer from the cell of origin, and to study the cancer initiation and tumor progression processes. By observing evolving cancers in zebrafish it is also possible to identify genes involved in the cancer process to discover possible drug targets (86). The transgenic models can be achieved by chemical mutagenesis by exposing the fish to known carcinogens, by irradiation or by using transgenic tools (62). Exposure to carcinogens and irradiation will cause random mutation, but several transgenic tools are now available to create desired mutations regulated both spatially and temporally in the zebrafish (87). As zebrafish possess most of the tissues and organs as mammals apart from some exceptions like lungs and mammary tissue, most cancers can be expressed or mimicked in zebrafish (86). Through observing the initial processes in tumor progression and initiation there are great possibilities to discover the roles of specific genes in cancer processes to identify potential drug targets.

The second way to achieve cancer in zebrafish is by transplantation of cells or tissue. Zebrafish has the advantage of not possessing an adaptive immune system until about three weeks post fertilization, and will prior to this not reject transplanted tumor cells or tissue (67). Adult fish have an adaptive immune system, but treatment with either radiation or dexamethasone can suppress the immune system and prevent rejection of transplants (85). These methods allow for easy and affordable *in vivo* cancer models. For long term studies syngeneic zebrafish clones makes transplantation possible. In this way a cancer induced in one fish can be transplanted into a syngeneic fish without the risk of transplant rejection. The transplanted fish can have a fully developed and active immune system, which makes it possible to observe how immune cells interacts with cancerous tissue (88).

Studying cancers *in vivo* inside the zebrafish enables us to observe cancer activities such as migration, metastasis, tumor angiogenesis and how this can be genetically altered. Manipulation of the zebrafish genome to obtain fluorescent endothelium, has made it possible to visualize tumor angiogenesis after cancer cell transplantations (89). By using fluorescent cancer cells for transplantation, either by genetic approaches or by cell staining, the cells can be monitored over time inside zebrafish. In this study a xenograft approach will be made by transferring cancer cells into zebrafish larvae and observing the movement and development of these cells over time inside the larva.

2.5 Aims

As many drugs are withdrawn from clinical studies and the market after the discovery of cardiotoxic effects, both larvae and adult zebrafish may be used to study this at an early stage of drug development (16). If cardiotoxic, or other toxic effects are discovered early on this can both save pharmaceutical companies for much preclinical research and, most importantly, increase patient safety when being discovered prior to clinical trials and entering the market. The main goals of the study are to explore the zebrafish as a model for efficacy and toxicity of liposomal and free drugs, and as a model for cancer by xenograft transplantation.

In the study, a breast cancer adenocarcinoma cell line (MCF-7) was chosen as the cancer model. Even if breast cancer has a relatively high recovery rate (90), many of the therapies, like DOX, are toxic and can give severe adverse effects. By using nanoformulations and co-injecting statins the goal is to lower the adverse effects, and at the same time target the cancerous tissue.

Firstly, liposomes loaded with SIM, DOX, or both drugs will be produced. These liposomes, together with the drugs in free form, will be used to conduct toxicity assays by using intravenous injection into the posterior cardinal vein (PCV) of the zebrafish larvae. The effects will be studied by observing cardiac changes of the zebrafish larvae prior to injection and at certain time points after injection. The co-therapy of SIM will be tested for possible cardioprotective effects in anthracycline therapy. The liposomes will also be tested on MCF-7 and H9C2 cardiomyoblast cells to observe if toxicity of DOX and cardioprotective effects of liposomal formulation and co-treatment with SIM can be observed in cell assays.

Additionally, MCF-7 breast cancer cells will be injected into the yolk sac and observed inside the zebrafish larvae over time. After establishing a model of how the MCF-7-cells behave inside the zebrafish larvae, free and liposomal anti-cancer drugs will be injected, and how these drugs distribute inside the zebrafish larvae and around the cancer cells will be observed. Inspection by confocal microscopy will be used to determine the effect of the drugs on the cancer cells.

3 Experimental Theory

3.1 Chromatography

Chromatography is a separation method used to separate mixtures of various analytes based on their physical-chemical properties. The methods normally consist of a mobile and a stationary phase. Relative interactions with the mobile and stationary phases determine the separation of compounds as defined by the equilibration distribution. The equilibration distribution is given by the distribution constant (K_c) which is dependent on the concentration of compound in stationary and mobile phase C_S and C_M, respectively as in Equation 1 (91).

$$K_C = \frac{C_S}{C_M} \qquad \text{Equation 1}$$

3.1.1 Size Exclusion Chromatography (SEC)

SEC separates compounds in a mixture based on their molecular size. The method is based on a column material with pores of various sizes. Smaller molecules or particles will enter the pores to a larger extent than larger particles and will thereby be retained by the column. This results in the largest compounds eluting first, and the smaller compounds eluting later (Figure 3.1) (92). In the present study SEC is used to separate free from liposomal DOX and SIM and used to quantify the amount of DOX encapsulated into liposomes.

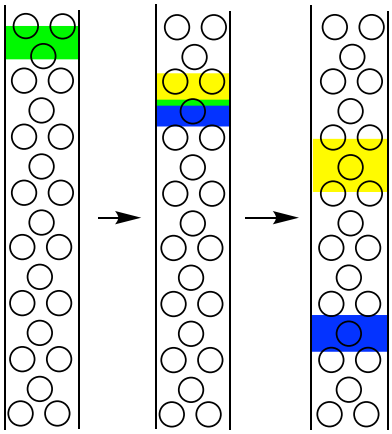

***Figure 3.1: Size exclusion chromatography**. The packing material of the column, illustrated as circles, contains pores where the largest molecules, illustrated by blue colour, fit only into the largest pores or do not fit into the pores at all, and will quite freely follow the solvent through the column. The smaller molecules, illustrated by yellow colour, will enter the pores more easily, and be retained by the column, thereby eluting later.*

3.1.2 High Performance Liquid Chromatography (HPLC)

HPLC is an improved variant of liquid chromatography. Constant flow against high pressure, up to 400 times atmospheric pressure, forces the mobile phase through the column containing the stationary phase much faster than chromatographic principles based on gravity. The basic HPLC system consists of a pump, a sample injector system or an injection loop, a column and a detector illustrated in Figure 3.2 (91).

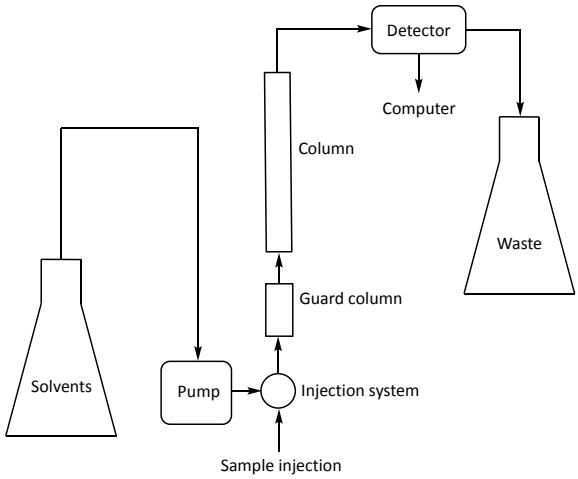

***Figure 3.2: High performance liquid chromatography (HPLC) system**. The HPLC system consist of a solvent reservoir containing one or more solvents which are pulled into the pump generating high pressure. Further along is the injection system, where samples for analysis enter the system and are separated in the column. After separation in the column the sample is analyzed by a detector.*

In normal phase HPLC the stationary phase is polar, while the mobile phase is non-polar. In reversed phase HPLC, the stationary phase is non-polar, and the column is normally packed with silica bound to hydrophobic chains. Reverse phase HPLC is suitable for separation of molecules dispersed in aqueous solvents and is more frequently used in drug analysis. The pump delivers mobile phases into the system at a constant flow. Samples are injected into the system via manual injection or an autosampler and depending on the affinity for the stationary

and the mobile phases are separated in the column. After passing through the column, compounds are measured by detectors (91). In this study a UV-Vis diode array detector is used, described in section 3.2, to identify and quantify DOX and SIM in liposomes.

3.2 UV-Vis Spectroscopy

UV-Vis light is light in the ultraviolet (UV) to visible region with wavelengths between 190 to 800 nm. Different wavelengths of light possess specific amounts of energy. Photons with the same energy level as the difference between two energy states of electrons in a molecule can be absorbed and bring the electrons to an excited stage (Figure 3.3). The molecular structure and functional groups of a compound will determine which wavelength the electrons will absorb, and UV-Vis spectroscopy can be used for compound identification and quantification (93).

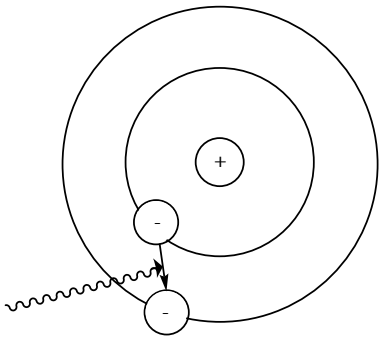

Figure 3.3: Excitation of electron. *Photons with equal energy to the difference of two electron energy states can be absorbed and the electron enter an exited state. The electron will eventually return to the ground state and emit the energy as heat and/or radiation (93).*

There are several different detectors used to measure absorbed light. In this study a photodiode array detector is utilized. This detector works by a light source sending polydisperse light onto the sample. The wavelengths that are not absorbed by the sample will then be dispersed onto the photodiode detector measuring different wavelengths. The light absorbed at specific wavelengths can then be calculated (Figure 3.4) (93).

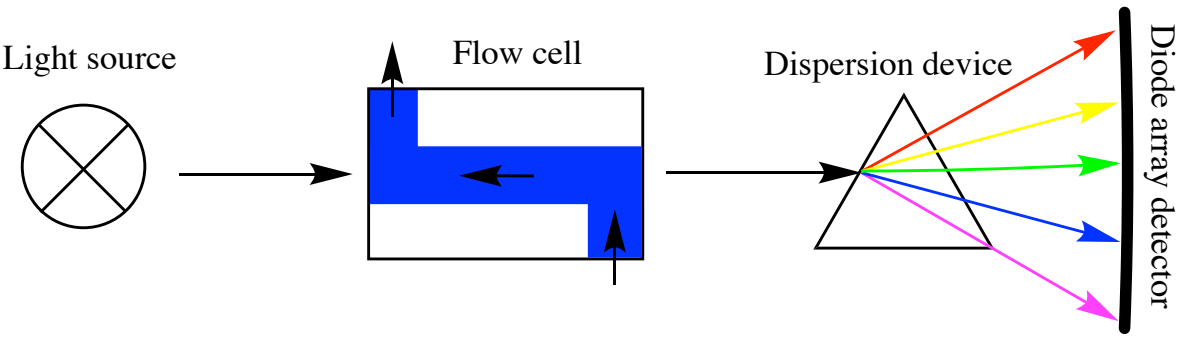

***Figure 3.4: Photodiode array detector**. A photodiode detector used in UV-Vis spectroscopy is composed of a light source sending polydisperse light towards the sample where certain wavelengths of light are absorbed. The light is then sent to a dispersion device that separates the light into different wavelengths which intensities are measured at the diode array detector. Figure modified from Analytical Techniques in the Pharmaceutical Sciences, 2016 (93).*

As the chemical structure of a compound will determine absorption of light in the UV-Vis spectrophotometer and separation in the HPLC column, these methods will together be used to create absorption spectrums to identify and quantify SIM and DOX in various samples.

3.3 Infrared Spectroscopy

Mid Infrared (IR) spectroscopy measures absorption of wavelengths in the IR spectra between 2500 nm to 25 μm. Absorption in this range is due to molecular vibrations, illustrated in Figure 3.5. As specific functional groups absorb different wavelengths, the techniques are often used to recognize functional groups in compounds (94).

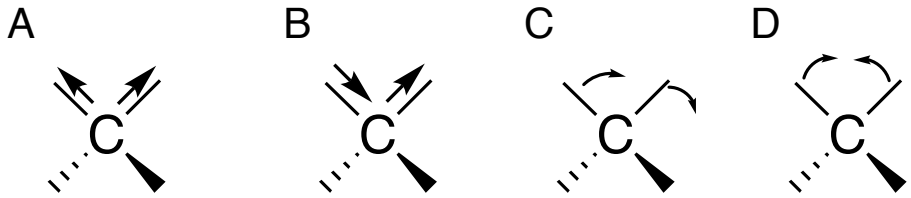

***Figure 3.5: Molecular vibrations with absorption in the infrared spectra**. Molecular vibrations, i.e. stretching (A and B) and bending (C and D), absorb infrared radiation, and enables the technique to be used to identify functional groups in compounds.*

Lipids commonly have distinct groups like their long aliphatic chains and ester carbonyls that can be recognized by IR absorption. This makes it possible to quantify lipid content in a sample by first creating a standard curve with known concentrations. In this study a Direct Detect® spectrophotometer was used to rapidly quantify lipid content in liposomes by adding a few microliters of liposome suspension onto the Direct Detect® assay free cards. This method gives an easy and fast determination of lipid content (95).

3.4 Dynamic Light Scattering

Dynamic light scattering (DLS) is a technique used to measure size and polydispersity of colloidal particles in a medium (96). The method utilizes the Brownian motion of particles, which are the random and irregular movements of particles in a medium caused by the particles collisions with the molecules in the medium, for instance water molecules (97). Light sent at the particles at a set position will scatter the light at the detector where it is measured. Due to Brownian motions, the light scattering will change over time (96). As Brownian motion of particles are related to their size, the detected signal can then be converted into particle size and size distribution (97, 98). The technique requires the particles to be spherical and the refractive index of the particles and medium as well as the viscosity of the dispersion medium to be known in order to achieve the correct correlation between the detected signal and particle size (99).

3.5 Confocal Microscopy

A confocal microscope is based on the same principles as a conventional microscope but with pinholes which should reject out-of-focus planes. This gives clearer images without interfering signals from other z-planes above or below focus illustrated in Figure 3.6 (100).

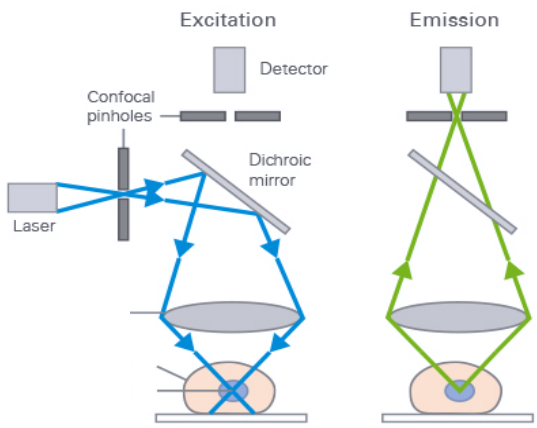

Figure 3.6: Principles of confocal microscopy. *The simplified image of a confocal microscope illustrates how the confocal pinholes reject the out-of-focus planes in z-direction in a three-dimensional sample. This result in clear images without interfering signals from other z-planes. Figure obtained from (101).*

Spinning disc confocal microscopy (SDCM) contains a rotating pinhole disc splitting the laser into multiple laser beams. One of the advantages of SDCM is that this method enables faster imaging, as the image is acquired using multiple beams and pinholes. At the same time the method gives lower phototoxicity when imaging live specimens. The specimens are both exposed to the laser for a shorter amount of time, and the laser beam is weakened after being split by the pinhole disc (102). When observing objects in a confocal microscope, fluorescence is utilized by an energetic beam, most often laser, bringing atoms to an excited state. When the

atoms go back to their ground state they can emit light at different wavelengths which are possible to observe in the microscope (103, 104).

3.6 Cell Lines

Cell lines are clonal population of immortalized cells often used in research as a replacement of primary cells. These cells have several advantages including low cost and an unlimited number of cells available providing high reproducibility of studies (105). Continuous cell lines are produced by primary cells, which either spontaneously or induced, undergo transformation and after this obtain the feature of dividing indefinitely (106).

In this study two cell lines will be used. The first is MCF-7, an adenocarcinoma breast cancer cell line derived from a 69-year old woman (107). This cell line will be used to test the effect of liposomes loaded with DOX and SIM and will also be transplanted into zebrafish larvae to mimic and observe breast cancer in zebrafish. The second cell line used in the study is H9C2, cardiomyoblast cells derived from the heart of rat embryo (108).

3.7 Cell Proliferation and Viability Assays

Cell proliferation and viability assays are used to determine viability and proliferation of cells. One way to measure cell viability and proliferation is by using the compound 4-[3-(4-Iodophenyl)-2-(4-nitro-phenyl)-2H-5-tetrazolio]-1,3-benzene sulfonate (WST-1). The mitochondrial succinate-tetrazolium-reductase system is able to open the tetrazole ring of WST-1, creating a dark red formazan compound (Figure 3.7). More viable, or a higher number of cells has a higher total enzyme activity, and more WST-1 will be reduced. The amount of the WST-1 reduced can be measured by a spectrophotometer (109).

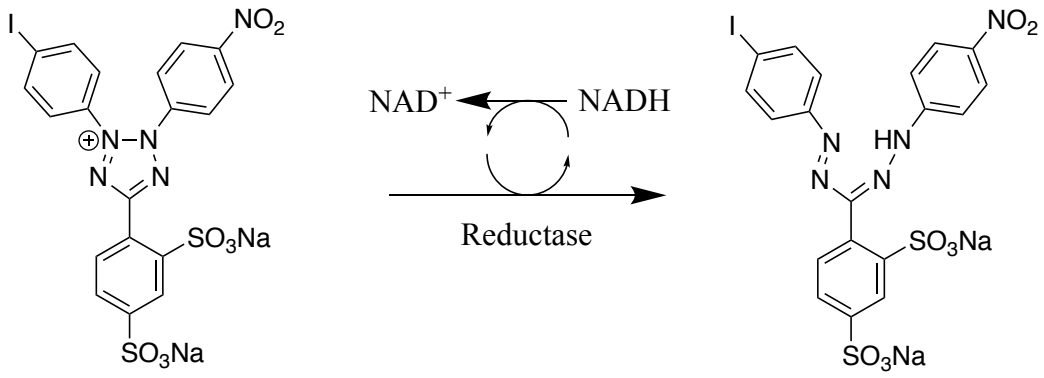

WST-1 Formazan

Figure 3.7: WST-1 formation into formazan*. The light red colored WST-1 molecule is inside the mitochondrial succinate-tetrazolium-reductase system converted into the dark red formazan compound by reducing and cleaving the tetrazole ring of the molecule. An increased number of viable cells will be able to reduce more WST-1, creating a darker red color which can be measured. Figure adapted from Merck Life Sciences (109).*

3.8 Cell Staining

For red fluorescent cells the cell stain 1,1'-Dioctadecyl-3,3,3',3'-Tetramethylindocarbocyanine Perchlorate (DiI) was used. The lipophilic dye stains the cell membrane and diffuses throughout the entire membrane to stain the whole cell. DiI does not exchange between neighboring cells, but will be transferred to daughter cells during mitosis, and can be used to trace cell migration and proliferation after transplantation (110).

CellTracker™ Green CMFDA (5-chloromethylfluorescein diacetate) hereby referred to as CTG, is a green fluorescent cell stain used in the study. The stain diffuses freely into cells where intracellular esterases transforms the stain into a lipophilic, fluorescent product which is unable to exit the cell (Figure 3.8). The stain should be visible for no less than 72 hours, and does not transfer to surrounding cells, but is transferred to daughter cells (111, 112).

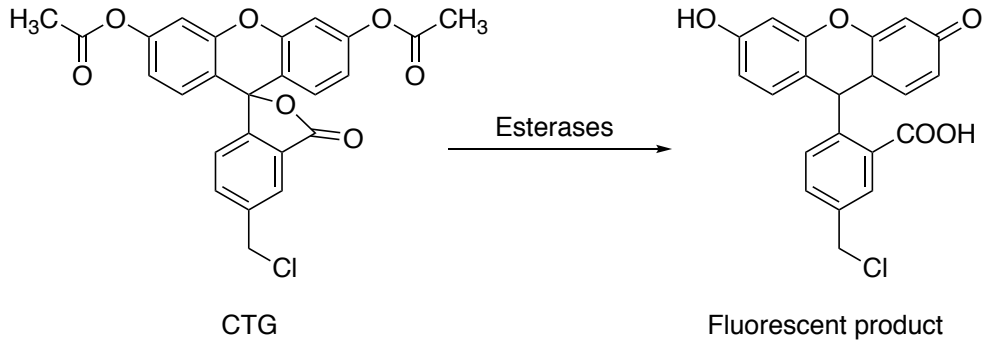

Figure 3.8: Removal of acetate groups on CellTracker™ Green CMFDA (CTG)*. CTG is a non-fluorescent compound before it enters cells. Intracellular esterases cleave the ester groups on the molecule and thereby creates a fluorescent, lipophilic product unable to exit the cells (right) (113).*

4 Materials and Methods

4.1 Materials

Hydrogenated Egg Phosphatidylcholine (HEPC) was from Lipoid GmbH (Ludwigshafen, Germany). 1,2-Distearoyl-sn-Glycero-3-Phosphoethanolamine-N-[Methoxy (Polyethylene glycol)-2000] (Ammonium salt) (PEG-PE) was from Avanti Polar Lipids (Alabaster, USA). ATTO-488 DPPE was from Atto-Tec (Siegen, Germany). Acetonitrile (ACN) was from Merck Millipore (Darmstadt, Germany). Doxorubicin (DOX) was from Accord Healthcare (London, GB). SephadexTM G-50 was from GF Healthcare (Chicago, USA). Microcapillaries were from Clark Electromedical Instruments (Holliston, USA). Hoechst33342 DNA stain, CellTracker Green CMFDA and 1,1'-Dioctadecyl-3,3,3',3'-Tetramethylindo-carbocyanine Perchlorate ('DiI'; DiIC18(3)) (DiI) was from ThermoFisher Scientific (CA, USA). WST-1 cell proliferation agent was from Roche Diagnostics GmbH (Mannheim, Germany). Milli-Q water (MQ) was produced at the laboratory by a Merck Millipore Q-POD (Darmstadt, Germany). All remaining materials were from Sigma-Aldrich (St. Louis, Missouri, USA) and were of analysis grade.

Zebrafish embryos and embryo water were provided from the zebrafish facility at the Department of Bioscience, University of Bergen

4.2 Liposome Production and Quantification

4.2.1 Production Procedure

4.2.1.1 General procedure

Lipids dissolved in chloroform were added to a round bottom flask. The flask was fit on a rotary evaporator in a room tempered water bath and the chloroform evaporated at mild vacuum at 225 mbar for 30 minutes, 175 mbar until dry, followed by full pump capacity for 30 minutes to remove any residual chloroform. The resulting film was rehydrated by adding either 225 mM ammonium sulphate buffer (ASB) or phosphate buffered saline (PBS) preheated to 70 °C and alternating vortexing and heating the flask in a 70 °C water bath until there was no trace of the film left in the flask. The suspension was extruded eleven times each through 0.8, 0.4, 0.2, and 0.1 μm filters, the latter size repeated twice, using an Avanti Polar Lipids Mini Extruder (Alabaster, US) preheated to 70 °C and fitted with Whatman® Nuclepore™ Track-Etched membrane filters (Maidstone, GB) and filter supports from Avanti Polar Lipids Inc.

4.2.1.2 Production of ATTO-488 DPPE Fluorescent Liposomes

For production of fluorescent liposomes, the lipid film was made using 2.40 mg HEPC, 0.62 mg cholesterol and 0.70 mg PEG-PE, and 12 μg ATTO-488 DPPE, a green fluorescent phospholipid, to the flask. The film was rehydrated using two mL PBS pH 7.4.

4.2.1.3 Production of DOX Filled Liposomes

The lipid film was made using exactly 4.80 mg HEPC, 1.23 mg cholesterol and 1.39 mg PEG-PE and rehydrated by adding one mL ASB (pH 6.0). Following extrusion, the suspension was gel filtered through a SEC column (1 cm diameter, 20 cm length) packed with sepharose beads (Sephadex™ G-50) and equilibrated with PBS pH 8. The liposomes were collected, and the lipid concentration measured as defined in section 4.2.2.1. Two mg/mL DOX dissolved in DMSO was added up to 20% w/w of the lipid concentration and incubated for one hour at 70°C followed by refrigerator overnight.

4.2.1.4 Production of SIM liposomes

A lipid film was made from exactly 54.5 mg HEPC, 0.32 mg cholesterol and 0.35 mg PEG-PE and 3.25 mg SIM in the flask. The film was rehydrated in one mL ASB (pH 6.0). After extrusion, the suspension was centrifuged at 10 000 relative centrifugal force (RCF) at 4° C for 15 minutes. The supernatant containing liposomes was collected and filtered through the SEC

column as described in section 4.2.1.3. If the liposomes were to be loaded with DOX in addition to SIM, DOX was added at desired concentrations up to 20% of the lipid concentration, incubated for one hour at 70° C, followed by refrigerator overnight.

4.2.2 Quantitative Analysis of Liposomes

4.2.2.1 Liposome characterization

The lipid concentration of the liposome suspension was measured by using a Merck Millipore Direct Detect® infrared spectrometer (Darmstadt, Germany). Two µL of the liposome suspension was added to the sample cards using PBS as blank. Using a previously made standard curve the w/v concentration was calculated using Equation 2 where y is the absorbance, and x is the lipid concentration (114).

$$y = 0{,}0147x \qquad \text{Equation 2}$$

The liposome size was found by using a Malvern Panalytical Zetasizer nano ZS (Malvern, GB) DLS device. Twenty µL of the liposome samples diluted in one mL PBS pH 8 were added to disposable cuvettes. Refractive indexes of the sample and dispersion media were set to 1.450 and 1.330, respectively and absorption of the sample was set to 0.001. Temperature was set to 25 °C. Each test consisted of twelve ten-second scans, which was repeated three times for each sample. Automatic mode was used to find optimal laser position, measurement duration and number of scans.

4.2.2.2 Quantification of DOX concentration in liposomes

HPLC was used for quantifying the concentrations of DOX and SIM in the liposomes. The HPLC system used was a HITACHI Chromaster 5160 pump, 5260 autosampler and 5430 diode array detector (Tokyo, Japan) and a Merck L-7614 degasser (Darmstadt, Germany).

For DOX quantification, a volume of 50 µL DOX-liposome suspension were filtered through the SEC column and collected in 20 fractions of 719 µL each. From each fraction, 50 µL were added first 50 µL ACN followed by 50 µL MQ, and from this, ten µL samples was injected onto a reversed phase column (Kromasil C18, 100-5 4.6x150 mm fitted with a 4.6x10 mm guard column with the same solid phase). The mobile phases were 0.05% TFA in MQ (mobile phase A) and 0.05% TFA in ACN (mobile phase B) with the gradient is described in Table 4.1.

The duration for each sample was 8 minutes with a flow rate at 1.4 mL/min. A standard curve was made by linear regression of seven standard solutions of DOX in 3:7 ACN:MQ ranging from 0.005 to 0.12 mg/mL DOX.

Table 4.1: HPLC gradient for doxorubicin (DOX) quantification in liposomes*. Mobile phase A is 0.05% trifluoroacetic acid in Milli-Q water and B is 0.05% trifluoroacetic acid in acetonitrile for DOX quantification on a C18 column.*

Time (minutes)	0	1	3	4	5	6	8
A (%)	70	70	30	0	0	70	70
B (%)	30	30	70	100	100	30	30

The elution of DOX in liposomes was compared to elution of ATTO-488 DPPE fluorescent liposomes through the same SEC column used for the DOX liposomes equilibrated with PBS pH 7. The liposomes were collected in 19 fractions of 360 µL each. The fluorescence was measured using a Wallac EnVision™ 2103 Multilabel reader (PerkinElmer, Massachusetts, U.S.) fitted with excitation and emission filters of FITC 485 and FITC 527 nm, respectively.

For encapsulation efficiency of DOX in the SIM-DOX liposomes, 40 µL 0.4 mg/mL DOX in SIM-DOX liposomes and free DOX was added in two separate runs to the SEC column. The liposomal DOX was collected into 45 fractions of 381 µL each. Free DOX was collected into 20 fractions of 952 µL each. From each of these samples, 100 µL was added to a black 96-well plate and fluorescence measured using the Wallac EnVision™ 2103 Multilabel reader with excitation and emission filters at FITC 485 nm and rhodamine 590 nm, respectively, to identify the DOX containing fractions. This was then used to determine the elution volume of free DOX and DOX in SIM-DOX liposomes.

4.2.2.3 Quantifying SIM concentration in liposomes

Three different HPLC methods were tried to quantify SIM content. The first method was based on a previous study (114), and utilized the same C18 column described in section 4.2.2.2 with mobile phases A and B, being 0.05% TFA in MQ and 0.05% TFA in ACN, respectively with the gradient described in Table 4.2 A. The method had a flow rate of 1.4 mL/min, 13 minutes sample duration and 10 µL sample injections. The second method used an Agilent poroshell 120 phenyl-hexyl column 2.7 um, dimensions 4.6 mm x 150 mm fitted with a guard column.

The mobile phases were MQ, ACN and methanol with gradient as described in Table 4.2 B, a flow rate of 0.350 mL/min. The last test was done using the same phenyl-hexyl column and mobile phases as above, but with a flow rate of 0.400 mL/min and a gradient as described in Table 4.2 C.

Table 4.2: HPLC mobile phase gradients for simvastatin (SIM) quantification. *1: Mobile phase gradient for SIM quantification test one using a C18 column. The test was conducted using mobile phases A (Milli-Q water (MQ) with 0.05% trifluoroacetic acid) and B (acetonitrile (ACN) with 0.05% trifluoroacetic acid). 2: Mobile phase gradient used for the first method with a phenyl-hexyl column with the mobile phases C, D and E being MQ, ACN and methanol, respectively. 3: The mobile phase gradients for the second test using a phenyl-hexyl column to quantify SIM with mobile phases C, D and E.*

1:

Time (min)	0	1	7	8	10	13
A (%)	70	70	0	0	70	70
B (%)	30	30	100	100	30	30

2:

Time (min)	0	3	8	24	26	30
C (%)	20	20	0	0	20	20
D (%)	0	0	0	100	0	0
E (%)	80	80	100	0	80	80

3:

Time (min)	0	1	17	20	21	23	31
C (%)	20	20	0	0	0	20	20
D (%)	0	0	40	100	100	0	0
E (%)	80	80	60	0	0	80	80

To analyze the content of SIM in the liposomes, 50 µL of the liposome suspension was evaporated at room temperature using an Eppendorf Concentrator Plus vacuumed centrifuge (Hamburg, Germany) until dry. The remaining pellet was rehydrated by adding 112 µL

methanol, followed by 28 µL MQ and mixed with the pipette to dissolve the pellet before HPLC analyses.

4.3 Maintenance of Cell Lines

The cells used in the study were H9C2 (ATCC® CRL-1446™) and MCF-7 (ATCC® HTC-22™), described in Section 3.6. The MCF-7 and H9C2 cells were cultured in Minimum Essentials Medium Eagle (MEM) and Dulbecco's Modified Eagle Medium (DMEM), respectively. Both media were added 10% v/v fetal bovine serum, 100 IU/mL penicillin and 100 µg/mL streptomycin, 2 mM L-glutamate and the MEM medium was also added 1% non-essential amino acids. All cell culturing medium, serum and additives were from Sigma-Aldrich (St. Louis, MO, USA). Both lines were cultured in 75 cm^2 tissue flasks and split 1:4 after reaching 70-85% confluence (115, 116). To detach the cells, the medium was removed, and the cells washed twice with sterile PBS. The cells were added 1.5 mL trypsin, incubating for 5-15 minutes at 37 °C until cells were observed to detach from the flask. After trypsinization, ten mL medium was added to the flask and the cells further detached by gentle pipetting. The cell suspension was centrifuged at 150 RCF for five minutes, the supernatant was removed, and the cells resuspended in one mL medium.

For further culturing, new flasks were filled with 30 mL fresh medium and added ¼ of the cell suspension harvested from one flask.

4.4 Labeling Cells with Fluorescent Cell Stains

4.4.1 Labeling Adhered MCF-7 Cells with DiI Stain

A one mg/mL stock solution of DiI was prepared in ethanol (110). MCF-7 cells were cultured to 70-85% confluence in 25 cm^2 tissue flasks for staining. The cell medium in the flask was removed and the cells washed once with sterile PBS. DiI in MEM medium at a concentration of 0.005 mg/mL was added to the cells and incubated at 37 °C for one to two hours (110). The medium was removed, and the cells washed twice with sterile PBS. The cells were next trypsinated as described in section 4.3 and counted using a Bürker counting chamber and the amount of medium adjusted to reach a concentration of two million cells per mL.

4.4.2 Labeling Suspended MCF-7 Cells with CTG Stain

CTG was dissolved to ten mM solution in DMSO, and further diluted to ten μM in serum free MEM medium (111). The cells were detached as described in section 4.3, washed twice with PBS, and mixed with one mL medium. The suspension was centrifuged at 150 RCF for five minutes, the supernatant removed and two mL of the ten μM staining solution added, mixed with the cells and incubated for 30 minutes at 37 °C (111). The cells were counted, the medium removed, and the cells washed and added fresh medium to obtain a cell concentration of two million cells per mL.

4.4.3 Co-Labeling of Adherent MCF-7 Cells with CTG and DiI Stain

CTG was dissolved to 10 mM solution in DMSO, and further diluted to 10 μM in serum free MEM medium. The medium was added DiI stock solution from section 4.4.1 to a concentration of 0.005 mg/mL and mixed. The cell medium was removed, and cells washed twice with sterile PBS before being added ten mL of the CTG-DiI medium solution. The cells were incubated for one hour at 37 °C. The medium was removed, and the cells trypsinated as described in section 4.3. The cells were counted, and volume adjusted to a cell count of five million cells per mL.

4.5 Cell Viability Assays

Ten thousand MCF-7 or H9C2 cells were added per well to 96-well cell culture plates and incubated for 24 hours. The medium was then removed and 100 μL of fresh medium containing drugs or liposomes was added. Table 4.3 show the experimental conditions. After 24 or 48 hours each well was added 10 μL WST-1 cell proliferation agent and incubated for two hours. Following this, a Wallac EnVision™ 2103 Multilabel reader fitted with 450 nm filter, with the reference filter at 620 nm was used to measure absorbance of the wells. After measuring metabolic activity, 100 μL 4% buffered formaldehyde solution with Hoechst 33342 (0.01 mg/mL) was added to each well. The plates were stored at 4 °C in the dark until observation in a Nikon Diaphot 300 inverted microscope fitted with a Nikon DS-Fi3 microscope camera and DS-L4 camera control unit (Tokyo, Japan). Three images were obtained from each condition using a DAPI filter to detect Hoechst 33342-stained cells or a rhodamine filter to visualize DOX stained cells.

Table 4.3: Cell viability assay conditions*. Free doxorubicin (DOX), simvastatin (SIM) and SIM-DOX liposomes were diluted in cell medium adequate for the respective cells. From the solutions, 100 μL were added to MCF-7 or H9C2 cells in 96-well plates. All conditions were tested in triplets.*

Conditions	**Concentrations**
Control A	Medium
Control B	Medium and 10% PBS
SIM-DOX liposomes	15 μM DOX + 4.67 μM SIM
	5 μM DOX + 1.51 μM SIM
	2.5 μM DOX + 0.71 μM SIM
	0.5 μM DOX + 0.15 μM SIM
Free DOX	15 μM DOX
	5 μM DOX
	2.5 μM DOX
	0.5 μM DOX
Free SIM	4.67 μM SIM
	1.51 μM SIM
	0.71 μM SIM
	0.15 μM SIM
Free SIM and DOX	15 μM DOX + 4.67 μM SIM
	5 μM DOX + 1.51 μM SIM
	2.5 μM DOX + 0.71 μM SIM
	0.5 μM DOX + 0.15 μM SIM

4.6 Zebrafish Handling and Experimental Conditions

4.6.1 Zebrafish Embryo and Larvae Care

Zebrafish embryos were obtained from the zebrafish facility at the Department of Bioscience, University of Bergen. The zebrafish used were of the strain *Casper*. A maximum of ten adult zebrafish (approximately equal amount of male and female fish) were put in breeding tanks overnight, which contained a mesh that separated the adult fish from the eggs. Embryos were

collected the next morning and kept in an incubator at 28.5°C in petri dishes containing embryo water blue (117, 118). The petri dishes were cleaned for debris and dead embryos daily.

As zebrafish embryos hatch between 48 to 72 hpf, they were in some cases dechorionated between 24 and 48 hpf to be used before hatching. This was done using two syringe needles and carefully gripping separate ends of the chorion. The chorion was then pulled apart by the needles causing the zebrafish larvae to escape into the embryo water (119).

4.6.2 General Methods for Injections

Micropipettes were pulled from microcapillaries using a P-1000 Micropipette puller by Sutter Instruments (Novato, CA, US). The capillaries were of thin walled borosilicate glass with outer diameter of 1.0 mm, inner diameter of 0.78 mm and length of 10 cm (Clark description GC100TF-10) and pulled with the settings given in Table 4.4. The micropipettes were retrograde filled with injection solution, then fitted on a Femtojet 4x by Eppendorf (Hamburg, Germany) and the micropipette tip was emerged in a thin layer of groundnut oil in a petri dish on top of a one mm grid with 0.1 mm intervals. The tip was cut using a scalpel after the micropipette was fully emerged in the oil. The size of the drop was measured, with an acceptable diameter being between 0.1- and 0.2 mm. Equation 3, the equation for the volume of a sphere, was used to calculate injection volume. In Equation 3, V is volume and r is the radius of the drop. To adjust injection volume, injection time (0.1-0.4 seconds) and injection pressure (400-1200 hPa) was adjusted. The maximum injection volume was 4.18 nL.

$$V = \frac{4}{3}\pi r^3 \qquad \text{Equation 3}$$

Table 4.4: Micropipette production settings*. Settings on the Sutter Instruments P-1000 Micropipette puller for production of micropipettes from borosilicate glass capillaries with inner diameter 0.78 mm, outer diameter 1.0 mm and length 10 cm for microinjections into zebrafish posterior cardinal vein and yolk sac.*

Heat	Pull	Velocity	Delay	Pressure
482	80	70	150	200

Tricaine (Ethyl 3-aminobenzoate methanesulfonate) was used for sedation of the zebrafish larva before observation or injection. A stock solution was prepared from 200 mg tricaine, 48.95 mL

MQ and 1.05 mL Tris-HCl (pH 9). The stock solution was diluted further in Embryo Water Blue (E3) to a 0.2 mg/mL solution (120). The larvae were placed into the solution at least 10 minutes prior to visualization or injection.

Injections were performed intravenously into the posterior cardinal vein (PCV) or into the yolk sac (Figure 4.1). Cancer cells were injected intravenously or the yolk sac, and drugs were injected into the PCV or dissolved in embryo water. Cells for xenograft transplantation were stained as described in section 4.4 and kept on ice until injection.

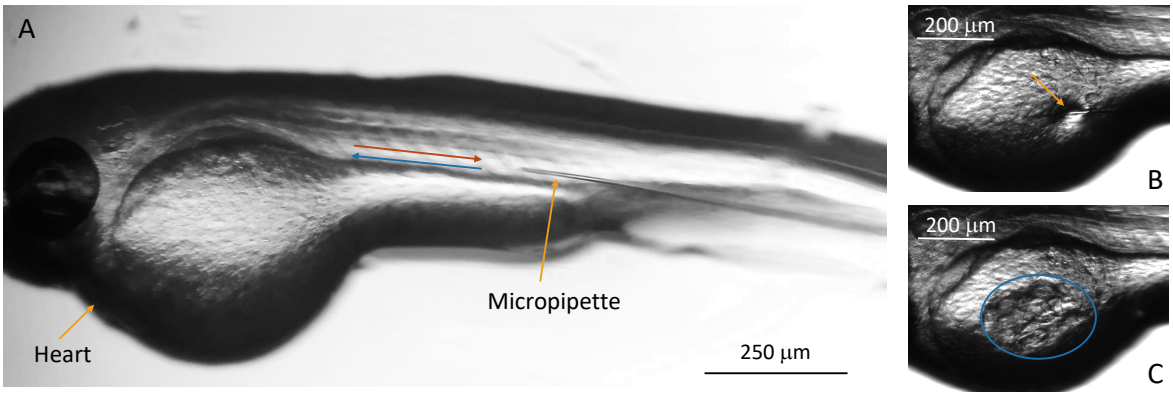

***Figure 4.1*: Intravenous and yolk sac injections in zebrafish larva**. *A: A zebrafish larva with the micropipette placed in position for injection in the posterior cardinal vein (PCV). PCV (blue arrow) can easily be distinguished from the dorsal aorta (red arrow) in the microscope by the direction of blood flow. Orange arrows point to the micropipette and the heart of the larva. B: The micropipette inserted into the yolk sac with arrow pointing towards the micropipette. C: The yolk sac directly after injection of the cell suspension with the blue circle surrounding the injected volume of cell suspension. Images obtained using a Leica M205 stereo microscope. Scale bar: A: 250 µm, B: 200 µm.*

When observing HR and other physiologic effects of drugs on zebrafish, a Leica M205 stereo microscope and a Leica DFC3000 G camera combined with the Leica Application Suite X software was used to obtain movies and still images. The HR was found by filming each larva for 10 seconds and calculating beats per minute (bpm). See Appendix, Supplementary Figure 1 and 2 for illustrations of zebrafish heart beats in zebrafish larvae.

Injected cancer cells and blood distribution of liposomes were visualized using an Andor Dragonfly 505 confocal with cameras iXon 888 Life EMCCD and Zyla 4.2 PLUS sCMOS (Andor Technology Ltd, Belfast, GB) fitted with a Nikon inverted Ti-E microscope (Tokyo, Japan). The zebrafish larvae were placed individually in 96-well plates containing embryo water and sedated in tricaine solution at observations. The iXon camera was used to image the cancer cells or liposomes inside the zebrafish using 10x and 20x dry objectives and green (laser line 405 nm) and red (laser line 561 nm) fluorescent filters. Imaris (Oxford Instruments) was used to observe and analyze confocal images and FIJI software was used to analyze area and number of fluorescent events in cell injected zebrafish larvae by using the Analyze Particle function in images with maximum intensity from the z-stack.

4.7 Statistics

Graphs were created and Students t-test performed in Microsoft Excel for Mac version 16.37 (Microsoft). One-way analysis of variance (ANOVA) and least significant difference (LSD) post hoc tests were performed in SPSS Statistics version 26 for Mac (IBM Corporation). Significance level was set at $P < 0.05$ for all tests.

5 Results

5.1 Liposome Characterization

5.1.1 Drug Content in Liposomes

From HPLC, Figure 5.1 show the chromatogram for the 0.12 mg/mL DOX standard solution and illustrates DOX eluting as one single peak with maximum absorbance at 2.31 minutes retention time, where there were low levels of or interferences from the gradient. The inset shows the standard curve obtained with a linear relationship between DOX concentration and peak area giving the equation further used to calculate encapsulation of DOX. A small disturbance in the baseline is observed immediate left of the DOX peak, seen to be the same size in all chromatograms, and was not included in the quantification of DOX concentrations.

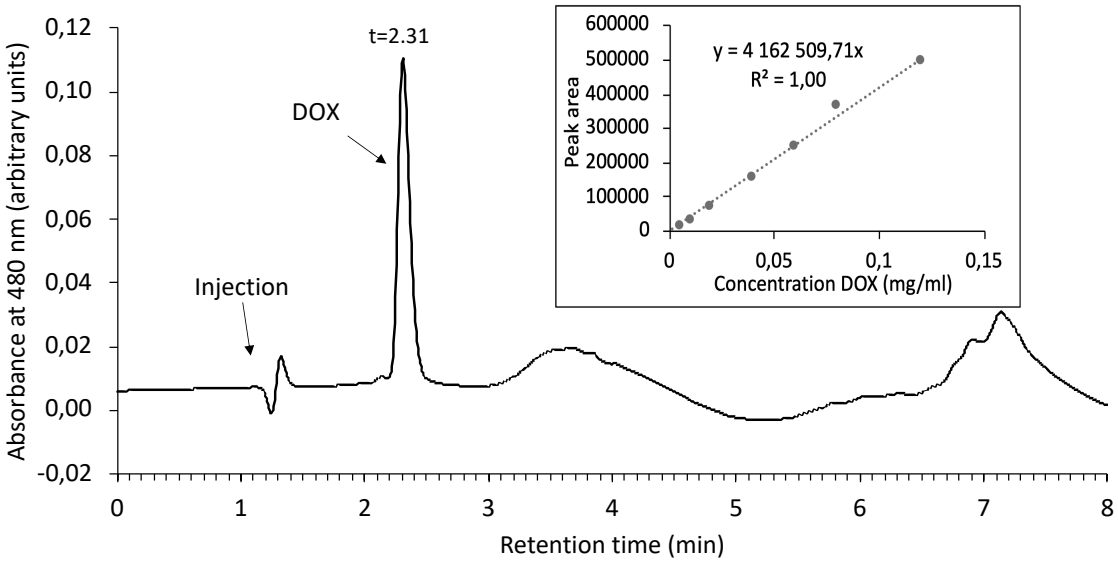

Figure 5.1: HPLC chromatogram and standard curve of doxorubicin (DOX). *HPLC chromatogram for a 0.12 mg/mL standard solution of DOX obtained with a C18 column and mobile phases Milli-Q water and acetonitrile, both added 0.05% trifluoroacetic acid. Injection and DOX detection peaks are marked with arrows. The inset shows the standard curve obtained with DOX standard solutions with concentrations from 0.05 to 0.12 mg/mL DOX. See methods section for details on instrumentation and experimental set-up.*

The first SIM quantification test on HPLC was performed using the same C18 column used for the DOX analysis and the mobile phase gradient from Table 4.2 A and resulted in the chromatogram illustrated in Figure 5.2. The SIM peak eluted at 9.93 minutes, at the same time as the wash and equilibration of the column with ACN, which causes the baseline to be noisy, and also giving a risk of impurities to elute with the sample.

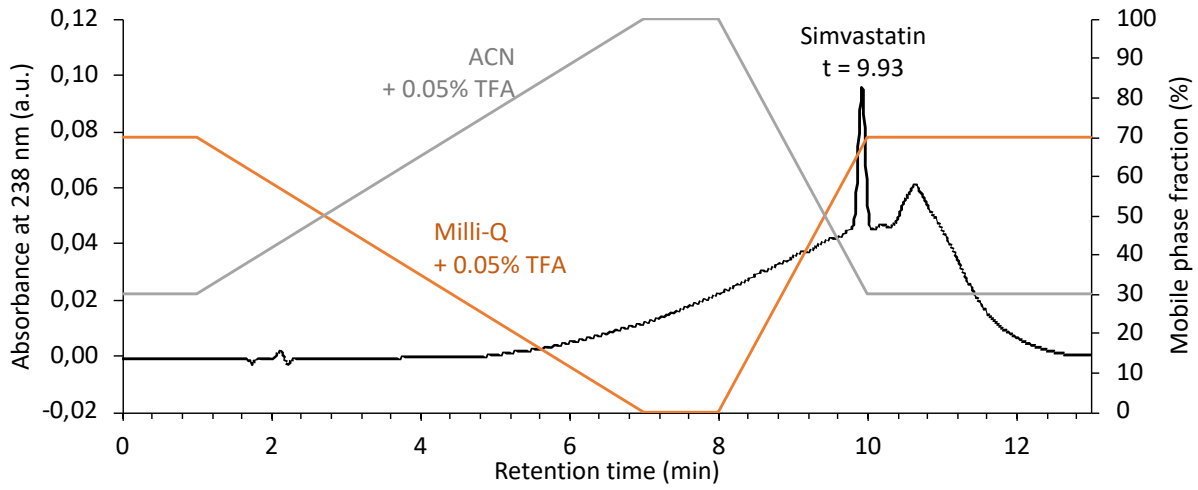

Figure 5.2: HPLC chromatogram for analysis of simvastatin (SIM) on a C18 column*. The chromatogram for SIM injected onto a C18 column and mobile phase gradient for Milli-Q water and acetonitrile (ACN), both with 0.05% trifluoroacetic acid (TFA). Chromatogram of SIM illustrated as a black line, and mobile phase fractions as orange and grey lines for Milli-Q water and ACN, respectively.*

Next, a phenyl-hexyl column was used with the mobile phases from Table 4.2 B in Methods section. However, this also gave a chromatogram with a noisy baseline, where it was hard to distinguish the SIM peak (chromatogram not illustrated). The gradient in Table 4.2 C, using the same phenyl-hexyl column, but methanol as the main eluting mobile phase produced the chromatogram displayed in Figure 5.3. With this method, the baseline had low noise levels, and SIM eluted as a narrow peak with a retention time of 14.6 minutes (Figure 5.3 A). The standard solutions provided a linear relationship between peak area and SIM concentrations giving the standard curve and equation used to calculate SIM content in liposomes (Figure 5.3 B).

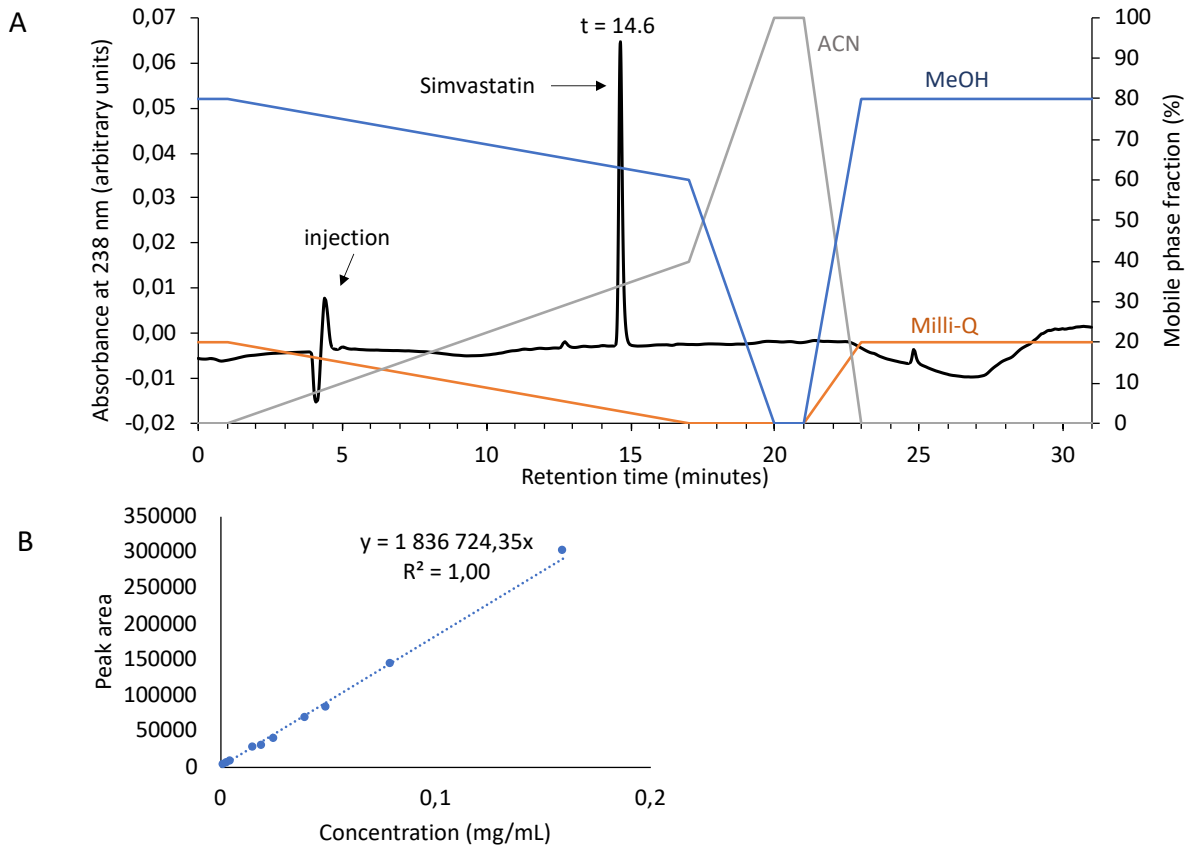

Figure 5.3: HPLC chromatogram and standard curve for simvastatin (SIM). *A: Chromatogram of a five µL injection of 0.16 mg/mL SIM standard solution analyzed on a phenyl-hexyl column with mobile phases acetonitrile (ACN), Milli-Q water and methanol (MeOH). The chromatogram is illustrated as a black line, while mobile phase gradient fractions for ACN, Milli-Q and MeOH are showed as grey, orange and blue lines, respectively. The sample injection and SIM signal are marked with arrows. B: The standard curve obtained by analyses of SIM standard solutions ranging from 0.0016-0.16 mg/mL. See the methods section for instrumentation and experimental setup.*

To separate encapsulated from free DOX in liposomes, they were gel filtered on a SEC column and compared to the elution of a batch ATTO-488 DPPE liposomes or free DOX. The drug in DOX liposomes and in SIM-DOX liposomes were found to have an elution volume between three to eight mL and four to eight mL, respectively. The peaks overlapped with the elution of the ATTO-488 DPPE liposomes, confirming that the DOX in the peaks was encapsulated (Figure 5.4). Only trace amounts of DOX was detected after the main peak. Calculations of area under the curve showed that more than 90% of DOX eluted in the major peak area between

3.60 and 7.19 mL in the DOX liposomes (Figure 5.4 A). For the SIM-DOX liposomes as well, no peak was observed after the main liposomal peak (Figure 5.4 B). Free DOX began to elute after approximately 9.5 mL with a broad peak that was still not fully eluted after 19 mL at the last fraction and did not overlap with the elution of the liposomes (Figure 5.4 B).

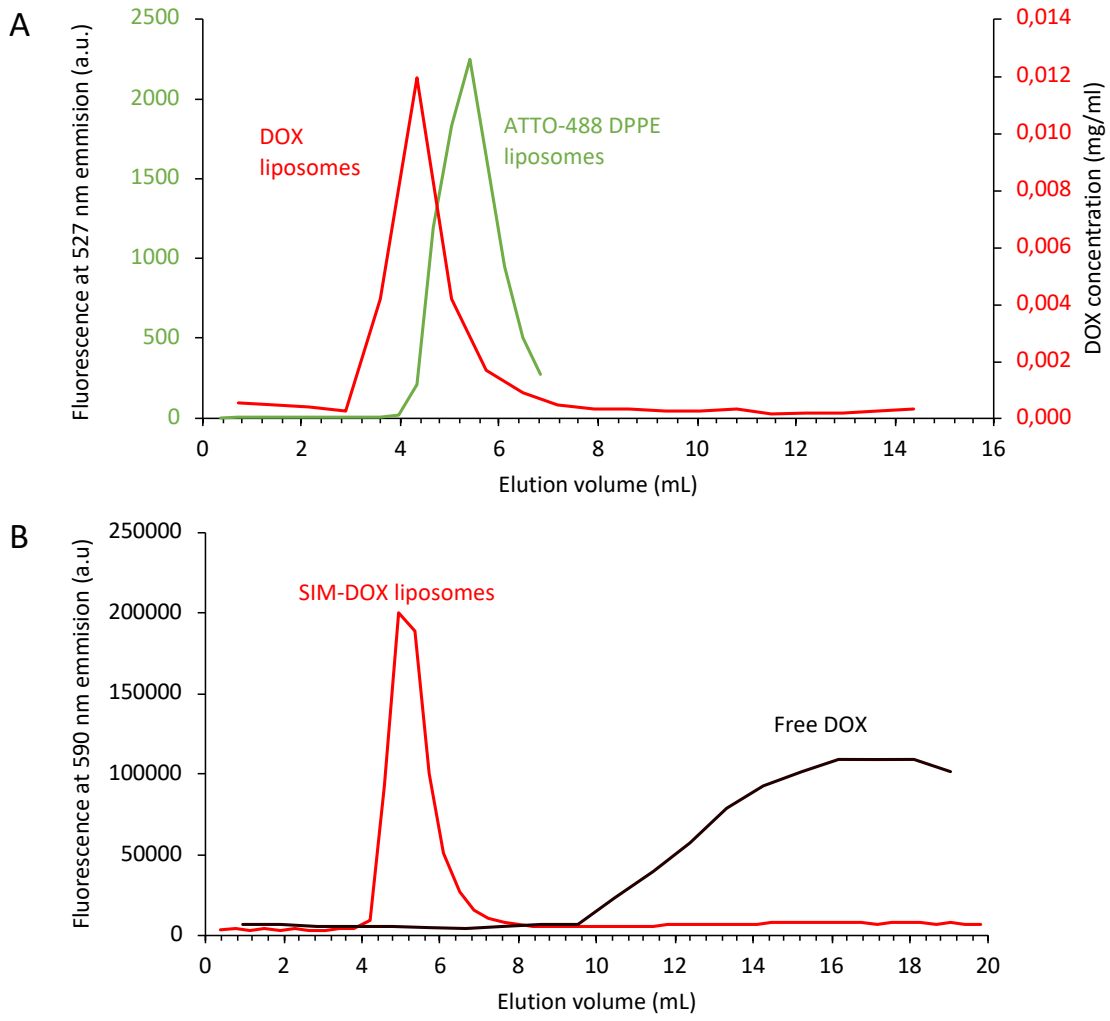

Figure 5.4: Size exclusion chromatography (SEC) of drug-loaded liposomes*. A: Doxorubicin (DOX) liposomes and ATTO-488 DPPE labeled liposomes were separately added to a SEC column packed with Sephadex beads, and fractions collected. The concentration of DOX in the fractions were measured using HPLC, and the ATTO-488 DPPE liposome fractions measured with a Wallac EnVision™ plate reader (excitation: 485 nm, emission: 527 nm) to quantify fluorescent marker. B: Simvastatin-DOX liposomes and free DOX was separately added to a SEC column and fractions collected. The fractions were analyzed for DOX content by measuring fluorescence in the Wallac EnVision™ plate reader (excitation 485 nm, emission: 590 nm).*

5.1.2 Size and Lipid Concentration of Liposomes

The empty liposomes were found to be 130 nm in diameter with a polydispersity index of 0.021 using DLS. The lipid concentration in the liposomes was calculated to be between 2.5 and 3.0 mg/mL. The SIM liposomes had a lipid concentration between 5.3 and 7.4 mg/mL, a diameter of 128 nm and a polydispersity index of 0.056. The liposome size was not measured after addition of DOX, but Knudsen (114) and Myhren et al. (121) found that encapsulation of anthracyclines did not alter liposome size.

Table 5.1: Size, lipid concentration and drug loading of liposomes in the study.

Liposomes	Size (nm)	Lipid concentration (mg/mL)	DOX content (mg/mL)	SIM content (mg/mL)
Empty	130	2.5-3.0	-	-
DOX	-*	1.9-2.25	0.45-0.50	-
SIM	128	5.3-7.4	-	0.3
SIM-DOX	-*	2.24	0.45	0.09

*Size was not measured after addition of DOX in liposomes.

5.2 Cytotoxic Activity of Free and Liposomal Drugs

Two methods were used to measure cell viability, but because of poor correlation between the two methods, counting the fractions of viable cells in a microscope was chosen as the most reliable method. The viability calculated from the WST-1 proliferation assay is illustrated in Supplementary Figure 3. In a microscope, cells with normal morphology and apoptotic or necrotic cells were counted to estimate cell viability following incubation with drugs. Necrotic or apoptotic nuclei were observed as pyknotic, condensed and sometimes fragmented when observed in the microscope, while normal nuclei were seen as larger and less intensely stained as observed in Figure 5.6 A and B (122).

In Figure 5.5, MCF-7 cells from the 24-hour incubation assay are displayed. Cells treated with 4.67 μM free SIM (Figure 5.5 D) appears similar to the control (Figure 5.5 A), as does SIM-DOX liposomes, however, the latter has lower contrast in the image (Figure 5.5 E), indicating less Hoechst in the nuclei. In Figure 5.5 B the cells are detached from the well, many cells are smaller relative to untreated cells and have clustered together in the medium. This is also the case for free SIM and DOX in image C, but here a few cells are also observed to be adhered to

the well with weaker fluorescence. See Figure 5.6 A to observe how normal MCF-7 cells would look in bright field.

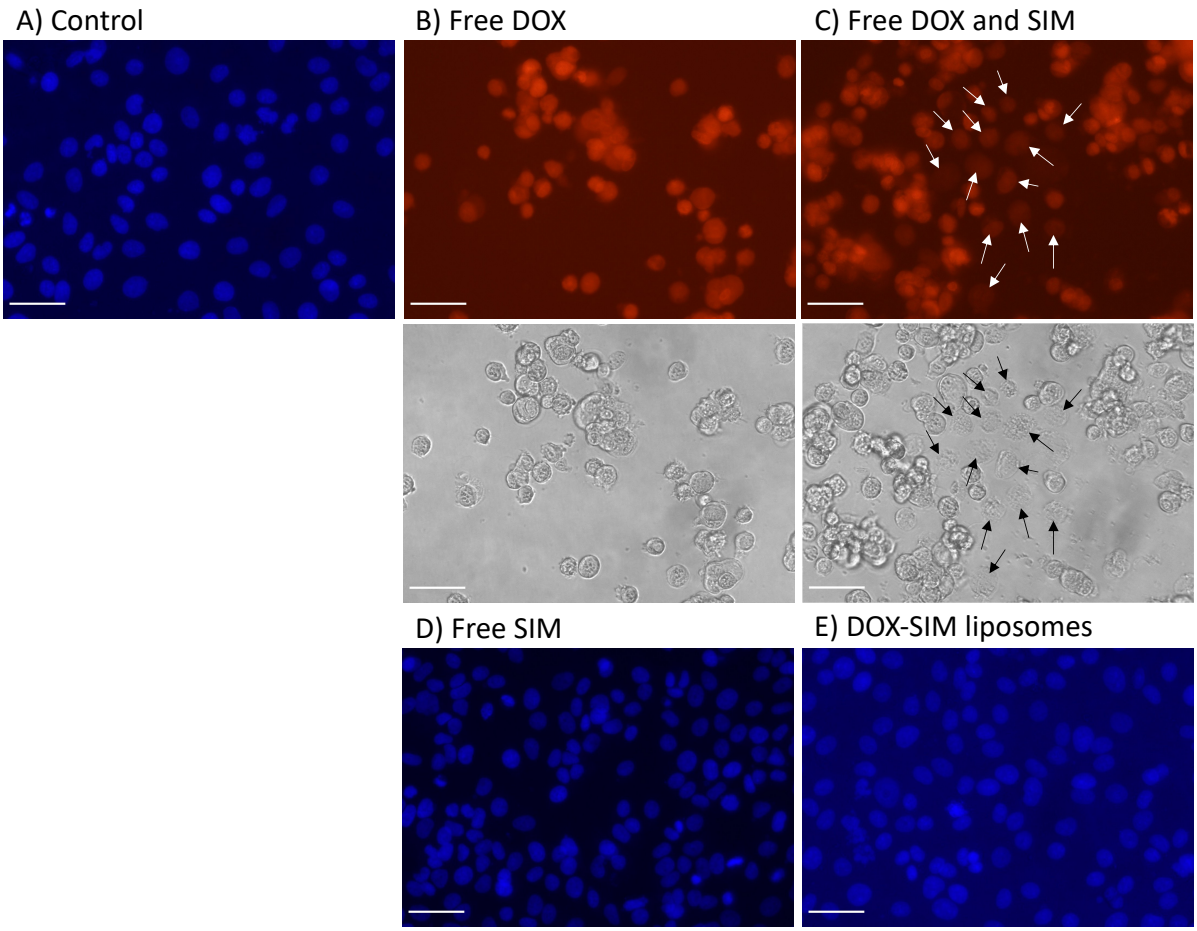

Figure 5.5: Morphology of MCF-7 cells after 24 hours of exposure to drug formulations. *MCF-7 cells were incubated for 24 hours with doxorubicin (DOX), simvastatin (SIM) or a combination, free and liposomal, before being fixed in 2% formaldehyde solution with Hoechst33342. A: Control cells incubated with cell medium. B: Cells incubated with 15 μM free DOX. C: Cells incubated with 15 μM free DOX and 4.67 μM free SIM. The arrows point to cells with normal morphology in the images. D: Cells incubated with 4.67 μM free SIM. E: Cells incubated with DOX-SIM liposomes. Images were obtained in a Nikon Diaphot 300 inverted microscope at 20x magnification with a rhodamine filter (red), a DAPI filter (blue) or in bright field (grey). Scale bar: 50 μm.*

Figure 5.6 illustrates MCF-7 cells incubated for 48 hours with the highest drug concentrations. Free SIM did not appear to affect viability and nuclear morphology resembled that of the control wells (Figure 5.6 D and A). All cells treated with 15 μM free DOX were apoptotic or necrotic,

and no longer adhered to the surface. Co-treatment with SIM did not affect viability compared to treatment with DOX alone (Figure 5.6 B and C). The image from the cells treated with SIM-DOX liposomes for 48 hours showed several apoptotic cells (Figure 5.6 E).

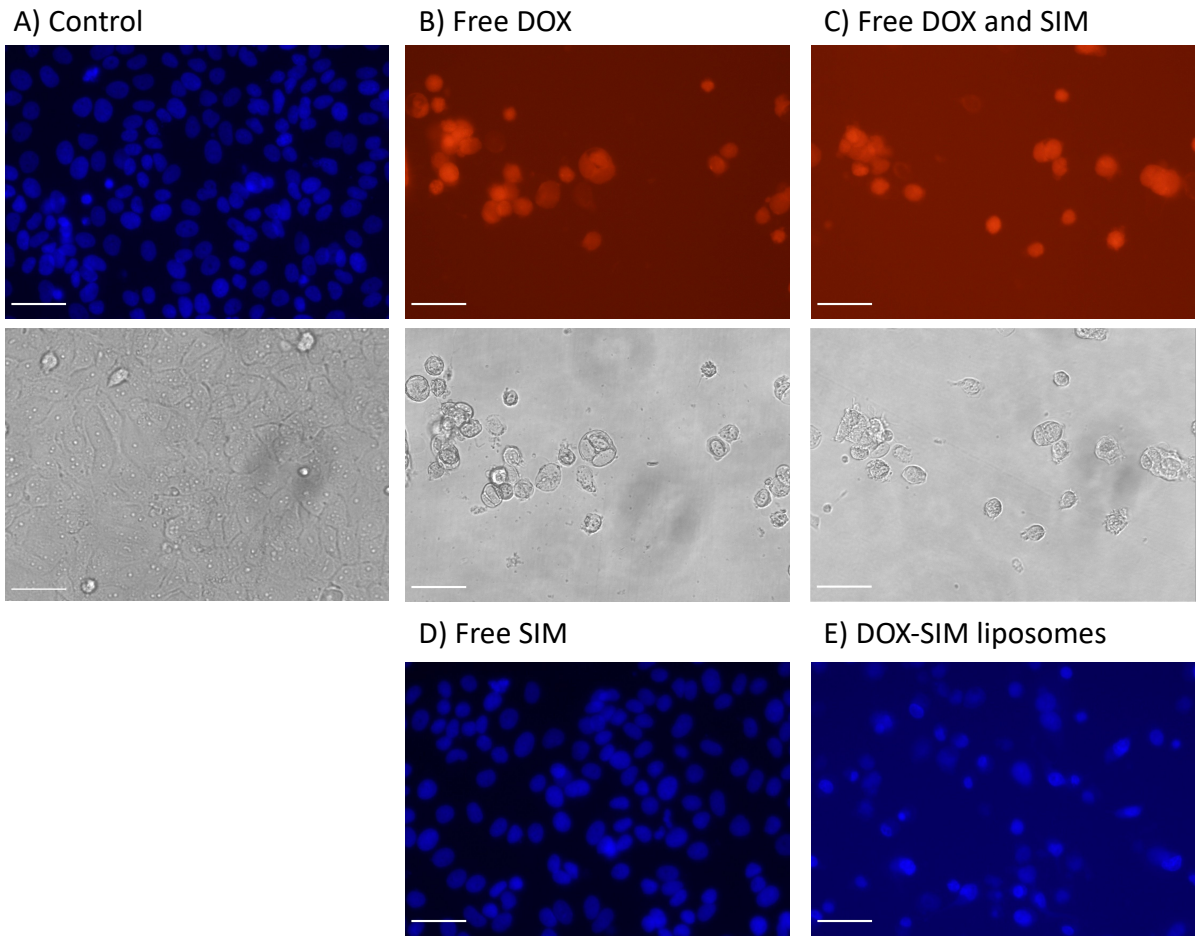

Figure 5.6: Morphology of MCF-7 cells after 48 hours exposure to drug formulations. *MCF-7 cells were incubated for 48 hours with doxorubicin (DOX), simvastatin (SIM) or both, free and liposomal before being fixed in 2% formaldehyde solution with Hoechst33342. A: Control cells. B: Cells incubated with 15 μM free DOX. C: Cells incubated with 15 μM free DOX and 4.67 μM free SIM. D: Cells incubated with 4.67 μM free SIM. E: Cells incubated with DOX-SIM liposomes. Images were obtained in a Nikon Diaphot 300 inverted microscope at 20x magnification with a rhodamine filter (red), a DAPI filter (blue) or in bright field (grey). Scale bar: 50 μm.*

The H9C2 cells were incubated for 24 hours with the same drug combinations are displayed in Figure 5.7. In both Figure 5.7 B and C there are cells still attached to the well. However, the cells in Figure 5.7 B have fluorescent signal equally distributed in cells, while DOX normally

concentrates in the nuclei, and the cells were therefore considered as necrotic. The cells still attached in Figure 5.7 C, are observed to have higher fluorescent signal in the nucleus and are therefore considered as viable. The H9C2 cell wells treated with DOX-SIM liposomes also gave a lower contrast using the DAPI filter, as observed for MCF-7, but no decreased viability was observed (Figure 5.7 E).

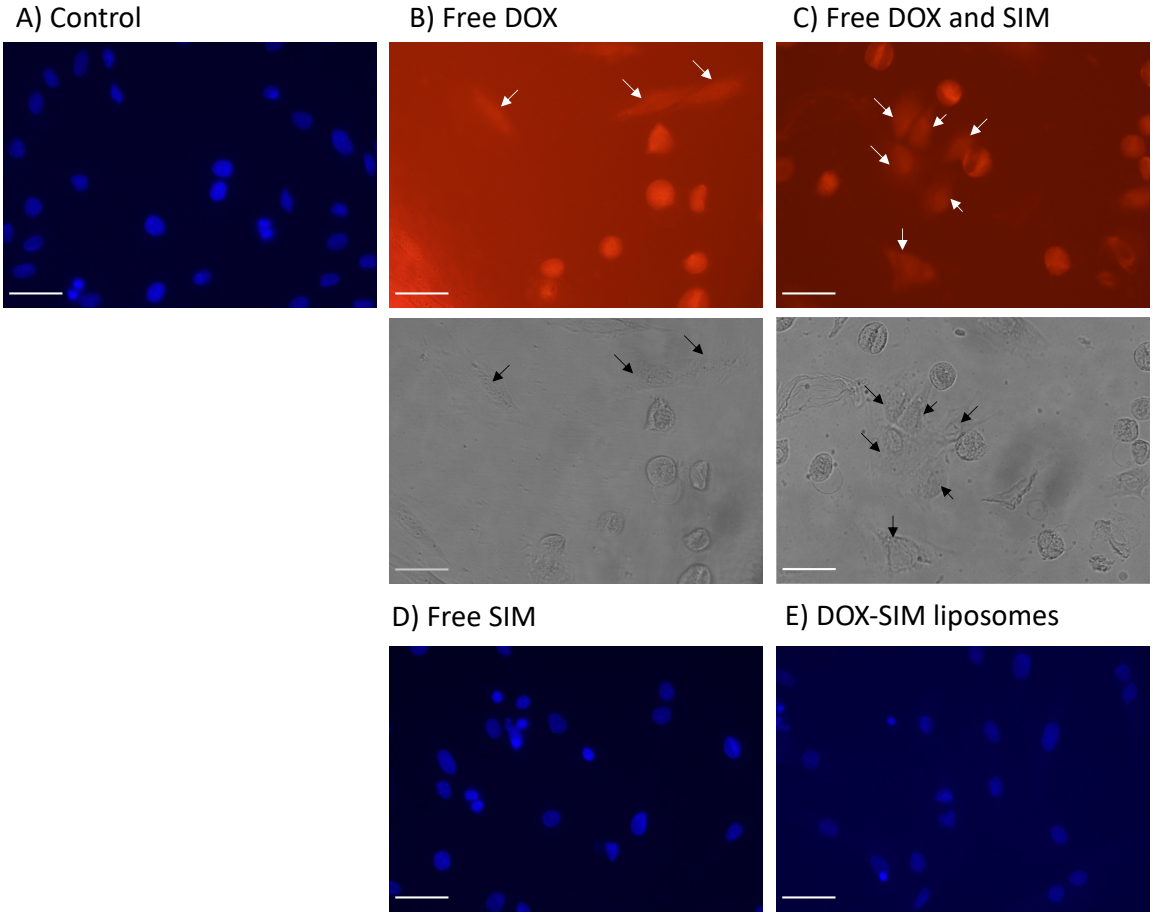

Figure 5.7: Morphology of H9C2 cells incubated for 24 hours with drugs formulations. *H9C2 cells were incubated for 24 hours with doxorubicin (DOX), simvastatin (SIM) or both, free and liposomal before being fixed in 2% formaldehyde solution with Hoechst33342. A: Control cells incubated with cell medium. B: Cells incubated with 15 µM free DOX with arrows pointing to adherent cells in the well. C: Cells incubated with 15 µM DOX and 4.67 µM SIM and arrows pointing to adherent cells in the image. D: Cells incubated with 4.67 µM SIM. E: Cells incubated with DOX-SIM liposomes. Images were obtained in a Nikon Diaphot 300 inverted microscope at 20x magnification with a rhodamine filter (red), a DAPI filter (blue) or in bright field (grey). Scale bar: 50 µm.*

Neither control B, SIM, nor SIM-DOX liposomes in any concentration altered MCF-7 cell viability compared to control after 24 hours (Figure 5.8 A). There was a dose-dependent increase in cell death in cells treated with DOX, both alone and in co-treatment with SIM (Figure 5.8 A). There were, however, differences between the cells depending on SIM co-therapy (Table 5.2 A). For the cells receiving 2.5 μM free DOX, co-therapy with SIM gave a significant decrease in viability ($P < 0.05$) compared to those receiving DOX alone (Figure 5.8 A and Table 5.2 A). The remaining concentrations of DOX gave no change in viability between those receiving free DOX alone and those receiving free DOX and SIM (Figure 5.8 A and Table 5.2 A).

MCF-7 cells treated with drugs for 48 hours had a significant decrease in viability when treated with the highest concentration of SIM-DOX liposomes with $P < 0.001$ compared to control A. The viability of these cells was still significantly higher than cells treated with equal concentrations of free DOX ($P < 0.001$, Figure 5.8 B and Table 5.2 B). There was also a decrease in viable cells treated with 2.5 μM DOX and 0.71 μM SIM compared to those treated with 2.5 μM free DOX alone ($P < 0.005$) while no significant change in the higher concentrations (Figure 5.8 B and Table 5.2 B). After 48 hours of incubation, SIM alone did still not cause any change in viability relative to control in MCF-7. Neither did 0.5 μM free DOX nor the SIM-DOX liposomes in concentrations 5 μM or lower (Figure 5.8 B).

For H9C2 cells, co-treatment with DOX and SIM gave significant less cell death compared to treatment with DOX alone in the 15 μM DOX concentrations (Figure 5.8 C and Table 5.2 C). There was, however, a significant decrease in viability for 0.5 and 2.5 μM free DOX when in co-treatment with free SIM, with $P < 0.005$ and < 0.001, respectively (Figure 5.8 C and Table 5.2 C). There was not observed any change in viability for cells treated with Control B, SIM-DOX liposomes nor free SIM in any concentration.

In general, H9C2 cells appeared to tolerate higher concentrations of DOX (5 and 15 μM) relative to MCF-7 over 24 hours, both with and without co-treatment of SIM. SIM treatment alone did not show toxicity in any concentration for whether MCF-7 or H9C2. The SIM-DOX liposomes did not show cytotoxicity in either cell line after 24 hours of incubation, but some toxicity was observed in the highest concentration after 48 hours incubation in MCF-7 cells

(Figure 5.8 and Table 5.2). For all of the cell assays, there was a significant decrease in viability for the 2.5 µM free DOX concentration when in co-treatment with SIM (Table 5.2).

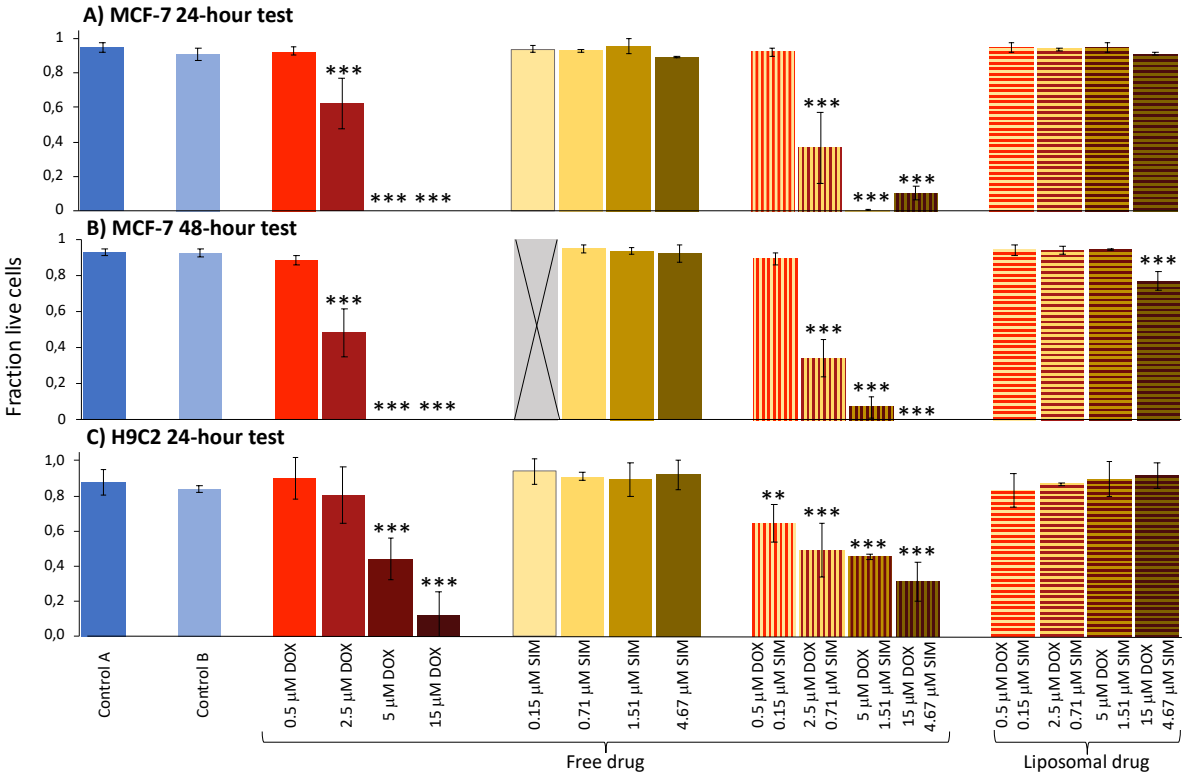

Figure 5.8: Cytotoxic response in MCF-7 and H9C2 cells treated with doxorubicin (DOX) and simvastatin (SIM) as free drugs and in liposomes. *Cell lines were treated with various concentrations of SIM, DOX or both drugs, as free or liposomal drugs for 24 or 48 hours. Between 30 and 400 cells were counted for each concentration to find the fraction of live cells. A: MCF-7 cells incubated for 24 hours. B: MCF-7 cells incubated for 48 hours. This group did not receive treatment with the lowest SIM concentration, which is marked with an X. C: H9C2 cells incubated for 24 hours. Control A is cells in medium and control B is cells in medium diluted with 10% PBS. ***: P<0.001 and **: P<0.005 significance relative to control A. Significance is found using one-way ANOVA with LSD post hoc tests.*

Table 5.2: Statistics from cell viability assays. *Statistics comparing the fraction of live MCF-7 and H9C2 cells in the cell viability assays after incubation for 24 or 48 hours with free or liposomal doxorubicin (DOX), simvastatin (SIM) or both drugs. The concentration of conditions are in µM and grey condition background are liposomal drugs, while the conditions with white background are free drugs. Ctrl A is cell medium and Ctrl B is medium diluted in 10% PBS. Significance levels are obtained by doing one-way ANOVAs with LSD post hoc test. *: P<0.05, **: P<0.005 and ***: P<0.001, n.s.: not significant.*

A) MCF-7 24 hour test

Condition	Ctrl A	Ctrl B	15 DOX 4.67 SIM	5 DOX 1.51 SIM	2.5 DOX 0.71 SIM	0.5DOX 0.15 SIM	15 DOX	5 DOX	2.5 DOX	0.5 DOX	4.67 SIM	1.51 SIM	0.71 SIM	0.15 SIM	15 DOX 4.67SIM	5 DOX 1.517SIM	2.5 DOX 0.71SIM	0.5 DOX 0.15 SIM
Ctrl A		n.s.	n.s.	n.s.	n.s.	n.s.	***	***	***	n.s.	n.s.	n.s.	n.s.	n.s.	***	***	***	n.s.
Ctrl B	n.s.		n.s.	n.s.	n.s.	n.s.	***	***	***	n.s.	n.s.	n.s.	n.s.	n.s.	***	***	***	n.s.
15 DOX 4.67 SIM	n.s.	n.s.		n.s.	n.s.	n.s.	***	***	***	n.s.	n.s.	n.s.	n.s.	n.s.	***	***	***	n.s.
5 DOX 1.51 SIM	n.s	n.s	n.s		n.s.	n.s.	***	***	***	n.s.	n.s.	n.s.	n.s.	n.s.	***	***	***	n.s.
2.5 DOX 0.71 SIM	n.s	n.s	n.s	n.s		n.s.	***	***	***	n.s.	n.s.	n.s.	n.s.	n.s.	***	***	***	n.s.
0.5 DOX 0.15 SIM	n.s	n.s	n.s	n.s	n.s		***	***	***	n.s.	n.s.	n.s.	n.s.	n.s.	***	***	***	n.s.
15 DOX	***	***	***	***	***	***		n.s.	***	***	***	***	***	***	n.s.	n.s.	***	***
5 DOX	***	***	***	***	***	***	n.s.		***	***	***	***	***	***	n.s.	n.s.	***	***
2.5 DOX	***	***	***	***	***	***	***	***		***	***	***	***	***	***	***	***	***
0.5 DOX	n.s	n.s	n.s	n.s	n.s	n.s.	***	***	***		n.s.	n.s.	n.s.	n.s.	***	***	***	n.s.
4.67 SIM	n.s	n.s	n.s	n.s	n.s	n.s.	***	***	***	n.s.		n.s.	n.s.	n.s.	***	***	***	n.s.
1.51 SIM	n.s	n.s	n.s	n.s	n.s	n.s.	***	***	***	n.s.	n.s.		n.s.	n.s.	***	***	***	n.s.
0.71 SIM	n.s	n.s	n.s	n.s	n.s	n.s.	***	***	***	n.s.	n.s.	n.s.		n.s.	***	***	***	n.s.
0.15 SIM	n.s	n.s	n.s	n.s	n.s	n.s.	***	***	***	n.s.	n.s.	n.s.	n.s		***	***	***	n.s.
15 DOX 4.67 SIM	***	***	***	***	***	***	n.s	n.s.	***	***	***	***	***	***		*	***	***
5 DOX 1.51 SIM	***	***	***	***	***	***	n.s.	n.s.	***	***	***	***	***	***	*		***	***
2.5 DOX 0.71 SIM	***	***	***	***	***	***	***	***	***	***	***	***	***	***	***	***		***
0.5 DOX 0.15 SIM	n.s.	n.s.	n.s.	n.s.	n.s.	n.s.	***	***	***	n.s.	n.s.	n.s.	n.s.	n.s.	***	***	***	

B) MCF-7 48 hour test

Condition	Ctrl A	Ctrl B	15 DOX 4.67SIM	5 DOX 1.51SIM	2.5 DOX 0.71 SIM	0.5DOX 0.15SIM	15 DOX	5 DOX	2.5 DOX	0.5 DOX	4.67 SIM	1.51 SIM	0.71 SIM	15 DOX 4.67SIM	5 DOX 1.517SIM	2.5 DOX 0.71SIM	0.5 DOX 0.15SIM
Ctrl A		n.s.	***	n.s.	n.s.	n.s.	***	***	***	n.s.	n.s.	n.s.	n.s.	***	***	***	n.s.
Ctrl B	n.s.		***	n.s.	n.s.	n.s.	***	***	***	n.s.	n.s.	n.s.	n.s.	***	***	***	n.s.
15 DOX 4.67 SIM	***	***		***	***	***	***	***	***	**	***	***	***	***	***	***	**
5 DOX 1.51 SIM	n.s	n.s	***		n.s.	n.s.	***	***	***	n.s.	n.s.	n.s.	n.s.	***	***	***	n.s.
2.5 DOX 0.71 SIM	n.s	n.s	***	n.s		n.s.	***	***	***	n.s.	n.s.	n.s.	n.s.	***	***	***	n.s.
0.5 DOX 0.15 SIM	n.s	n.s	***	n.s	n.s		***	***	***	n.s.	n.s.	n.s.	n.s.	***	***	***	n.s.
15 DOX	***	***	***	***	***	***		n.s.	***	***	***	***	***	n.s.	n.s.	***	***
5 DOX	***	***	***	***	***	***	n.s.		***	***	***	***	***	n.s.	n.s.	***	***
2.5 DOX	***	***	***	***	***	***	***	***		***	***	***	***	***	***	**	***
0.5 DOX	n.s.	n.s	**	n.s	n.s	n.s.	***	***	***		n.s.	n.s.	n.s.	***	***	***	n.s.
4.67 SIM	n.s.	n.s	***	n.s	n.s	n.s.	***	***	***	n.s.		n.s.	n.s.	***	***	***	n.s.
1.51 SIM	n.s.	n.s	***	n.s	n.s	n.s.	***	***	***	n.s.	n.s.		n.s.	***	***	***	n.s.
0.71 SIM	n.s.	n.s	***	n.s	n.s	n.s.	***	***	***	n.s.	n.s.	n.s		***	***	***	n.s.
15 DOX 4.67 SIM	***	***	***	***	***	***	n.s.	n.s.	***	***	***	***	***		n.s.	***	***
5 DOX 1.51 SIM	***	***	***	***	***	***	n.s.	n.s.	***	***	***	***	***	n.s.		***	***
2.5 DOX 0.71 SIM	***	***	***	***	***	***	***	***	**	***	***	***	***	***	***		***
0.5 DOX 0.15 SIM	n.s.	n.s.	**	n.s.	n.s.	n.s.	***	***	***	n.s.	n.s.	n.s.	n.s.	***	***	***	

C) H9C2 24 hour test

Condition	Ctrl A	Ctrl B	15 DOX 4.67 SIM	5 DOX 1.51 SIM	2.5 DOX 0.71 SIM	0.5 DOX 0.15 SIM	15 DOX	5 DOX	2.5 DOX	0.5 DOX	4.67 SIM	1.51 SIM	0.71 SIM	0.15 SIM	15 DOX 4.67 SIM	5 DOX 1.51 SIM	2.5 DOX 0.71 SIM	0.5 DOX 0.15 SIM
Ctrl A		n.s.	n.s.	n.s.	n.s.	n.s.	***	***	n.s.	n.s.	n.s.	n.s.	n.s.	n.s.	***	***	***	**
Ctrl B	n.s.		n.s.	n.s.	n.s.	n.s.	***	***	n.s.	n.s.	n.s.	n.s.	n.s.	n.s.	***	***	***	*
15DOX 4.67SIM	n.s.	n.s.		n.s.	n.s.	n.s.	***	***	n.s.	n.s.	n.s.	n.s.	n.s.	n.s.	***	***	***	***
5DOX 1.51SIM	n.s	n.s	n.s		n.s.	n.s.	***	***	n.s.	n.s.	n.s.	n.s.	n.s.	n.s.	***	***	***	***
2.5DOX 0.71SIM	n.s	n.s	n.s	n.s		n.s.	***	***	n.s.	n.s.	n.s.	n.s.	n.s.	n.s.	***	***	***	**
0.5DOX 0.15SIM	n.s	n.s	n.s	n.s	n.s		***	***	n.s.	n.s.	n.s.	n.s.	n.s.	n.s.	***	***	***	*
15DOX	***	***	***	***	***	***		***	***	***	***	***	***	***	*	***	***	***
5DOX	***	***	***	***	***	***	***		***	***	***	***	***	***	n.s.	n.s.	n.s.	*
2.5DOX	n.s.	n.s.	n.s.	n.s.	n.s.	n.s.	***	***		n.s.	n.s.	n.s.	n.s.	n.s.	***	***	***	n.s.
0.5DOX	n.s	n.s	n.s	n.s	n.s	n.s.	***	***	n.s.		n.s.	n.s.	n.s.	n.s.	***	***	***	**
4.67SIM	n.s	n.s	n.s	n.s	n.s	n.s.	***	***	n.s.	n.s.		n.s.	n.s.	n.s.	***	***	***	***
1.51SIM	n.s	n.s	n.s	n.s	n.s	n.s.	***	***	n.s.	n.s.	n.s.		n.s.	n.s.	***	***	***	***
0.71SIM	n.s	n.s	n.s	n.s	n.s	n.s.	***	***	n.s.	n.s.	n.s.	n.s.		n.s.	***	***	***	***
0.15SIM	n.s	n.s	n.s	n.s	n.s	n.s.	***	***	n.s.	n.s.	n.s.	n.s.	n.s		***	***	***	***
15DOX 4.67SIM	***	***	***	***	***	***	*	n.s.	***	***	***	***	***	***		*	*	***
5DOX 1.51SIM	***	***	***	***	***	***	***	n.s	***	***	***	***	***	***	*		n.s.	*
2.5DOX 0.71SIM	***	***	***	***	***	***	***	n.s.	***	***	***	***	***	***	*	n.s.		*
0.5DOX 0.15SIM	**	*	***	***	**	*	***	*	n.s.	**	***	***	***	***	***	*	*	

5.3 Monitoring Toxic Effects on Zebrafish Larvae After Drug Exposure

5.3.1 The Anesthetic Drug Tricaine does not Affect Heartrate in Zebrafish Larvae

To exclude the possibility that the handling and sedation of the larvae affected the heart rate (HR), the HR of zebrafish larvae exposed to tricaine was measured. There was no significant change HR in three dpf zebrafish larvae exposed to 0.2 mg/mL tricaine for 10- or 40-minutes (students t-test, Figure 5.9).

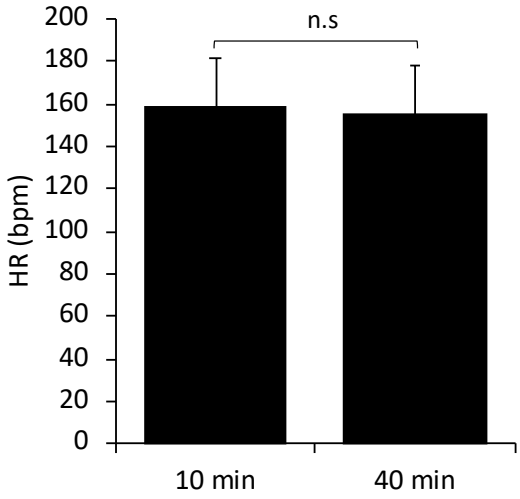

Figure 5.9: The effect of the anesthetic drug tricaine on zebrafish larvae HR. *Zebrafish larvae at three days post fertilization were placed in 0.2 mg/mL tricaine dissolved in embryo water (n=12). HR of the zebrafish larvae was observed after 10- and 40-minutes and calculated to beats per minute (bpm). n.s.: not significant change using paired-sample students t-test, significance level 0.05.*

5.3.2 Cardiotoxicity of Free and Liposomal DOX on Zebrafish Larvae

To see whether a cardiotoxic effect of DOX could be observed in zebrafish larvae, they were intravenously injected with 1.9 ng free or liposomal DOX, their HR examined and compared with larvae injected with empty liposomes and PBS. In addition to HR, physical observations as pericardial effusion (PCE) were observed. Figure 5.10 B and C illustrates how these injections caused a decrease in HR in the recipients of free DOX ($P < 0.001$) and empty liposomes ($P < 0.005$). In the recipients of PBS and DOX liposomes, no change in HR was observed (Figure 5.10 A and D). In addition, PCE was observed in five out of 11 recipients of free DOX. This effect is illustrated in Figure 5.10 E-G. For DOX liposomes, two out of nine larvae were observed with PCE and for the control groups one of ten in the PBS group and two out of 21 in the empty liposome group were observed with PCE (Figure 5.10 H).

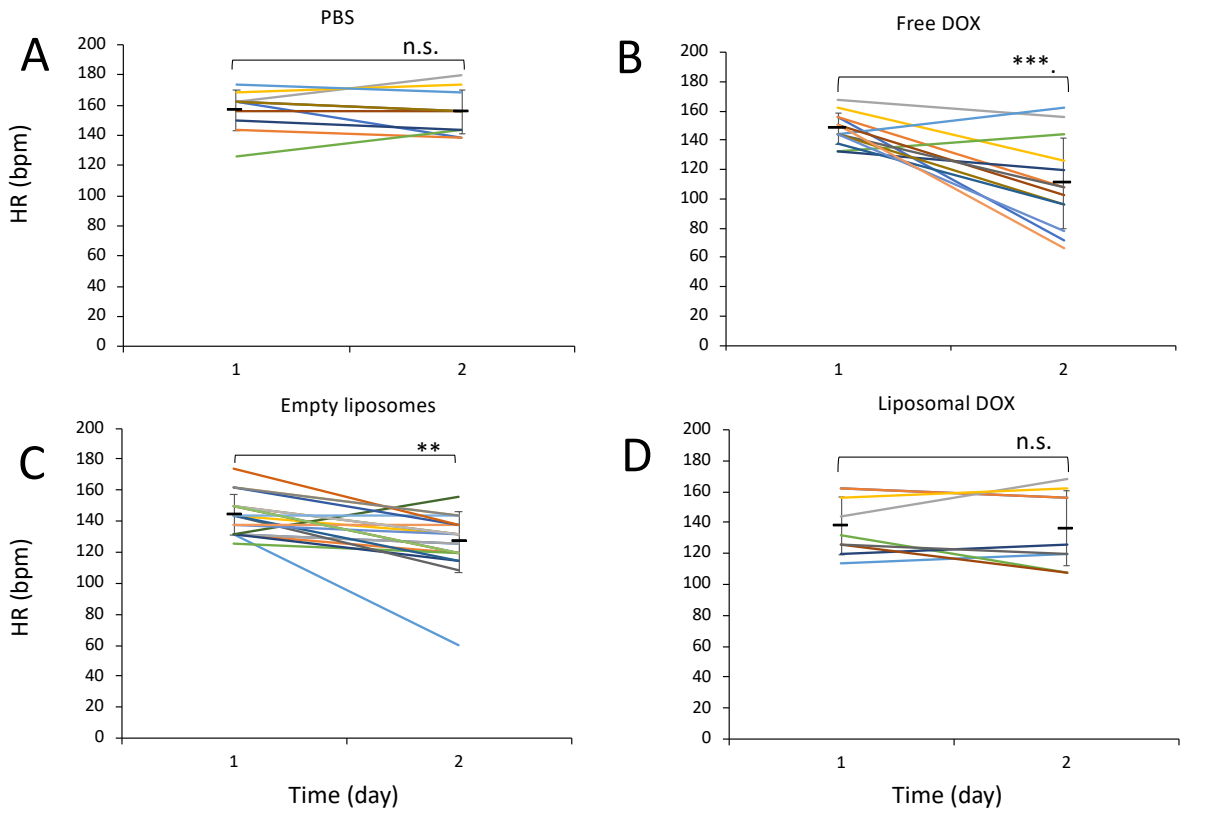
A
PBS
n.s.
HR (bpm)
B
Free DOX
***.
C
Empty liposomes
**
D
Liposomal DOX
n.s.
Time (day)

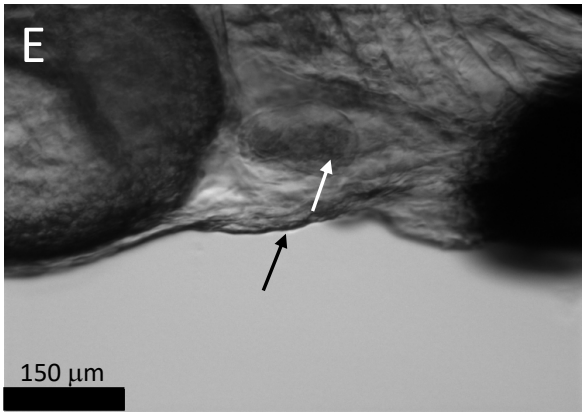
E
150 µm

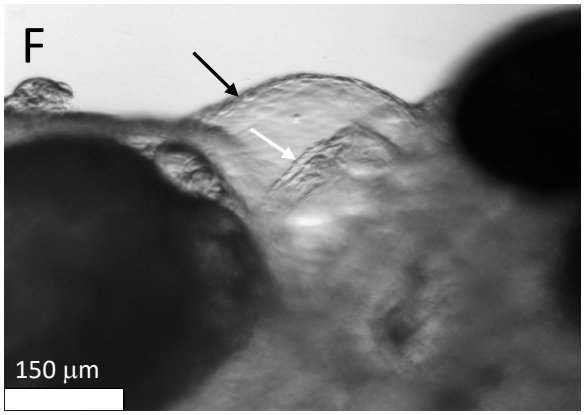
F
150 µm

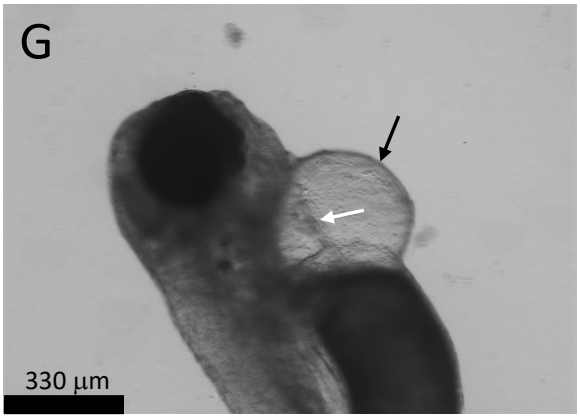
G
330 µm

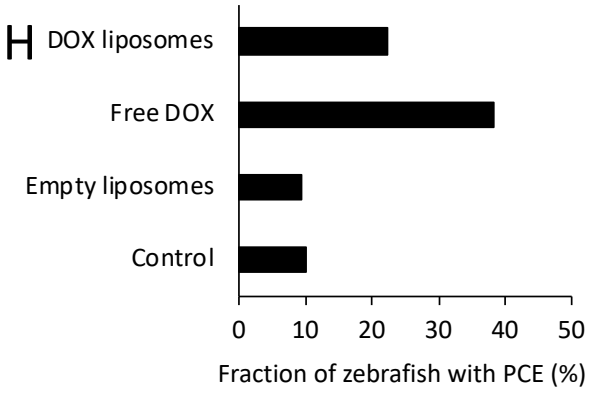
H
DOX liposomes
Free DOX
Empty liposomes
Control
0
10
20
30
40
50
Fraction of zebrafish with PCE (%)

Figure 5.10: The effect of doxorubicin (DOX) on zebrafish larvae heart*. PBS (n=10), empty liposomes (n=21), 1.9 ng free DOX (n=11) or 1.9 ng liposomal DOX (n=9) was injected into the posterior cardinal vein (PCV) of 72 hpf zebrafish larvae. All larvae were sedated in 0.2 mg/mL tricaine prior to injection and observation. The larvae HR was observed prior to injection and after 24 hours. A: HR of zebrafish larvae injected with PBS. No significant (n.s.) change after 24 hours. B: HR of zebrafish larvae injected with empty liposomes without DOX. Significant decrease at P < 0.005 (**) in HR after 24 hours C: HR of zebrafish larvae injected with free DOX. Significant decrease at P < 0.001 (***) in HR after 24 hours. D: HR of zebrafish larvae injected with DOX liposomes, with n.s. decrease after 24 hours. Statistical significance calculated using paired-sample t-test. E-G illustrate pericardial effusion (PCE) in zebrafish larvae treated with 1.9 ng free DOX. E: No visible PCE. F: A mild PCE. G: A more advanced PCE. White arrows point to the heart of the zebrafish larvae while black arrow point to the pericardial sac. H: Fraction of recipients with PCE in each treatment. The images were obtained using a Leica M205 stereo microscope.*

5.3.3 The Effects of SIM on Zebrafish Embryo and Larvae

As SIM was to be tested as a cardioprotective drug in DOX-treatment, effects of SIM on zebrafish embryo and larvae was examined. First, lethality of the drug dissolved in embryo water was determined. Zebrafish embryos at 30 hpf were exposed to SIM-concentrations from 9.56 nM to 9.56 μM for 24 and 48 hours and observed. Larvae exposed to 0.96 and 9.56 μM SIM were all dead and still inside their chorions after 24 hours. For the larvae exposed to 95.6 nM SIM, five of ten larvae were dead after 24 hours, the dead larvae were still in their chorions. Following 48 hours of exposure, all ten larvae in 95.6 nM SIM-group were dead. With the lowest concentration of 9.56 nM SIM, no lethality was observed after 24 hours, and all larvae were hatched. However, after 48 hours, three out of nine larvae were dead. In the control group, exposed only to embryo water, all larvae were alive after 48 hours (Figure 5.11).

In a second test, older zebrafish larvae at 48 hpf were exposed to the same concentrations as in the section above for 48 hours. In this test the only group that showed increased lethality was the group receiving 9.56 μM SIM, where 50% of the larvae were dead following 48 hours incubation. For the larvae that received 0.96 μM SIM, no lethality was observed, but PCE was observed in one larva. Neither PCE nor death was observed in the group exposed to 95.6 nM SIM or lower (Figure 5.11). Only one test was conducted, and statistics not calculated.

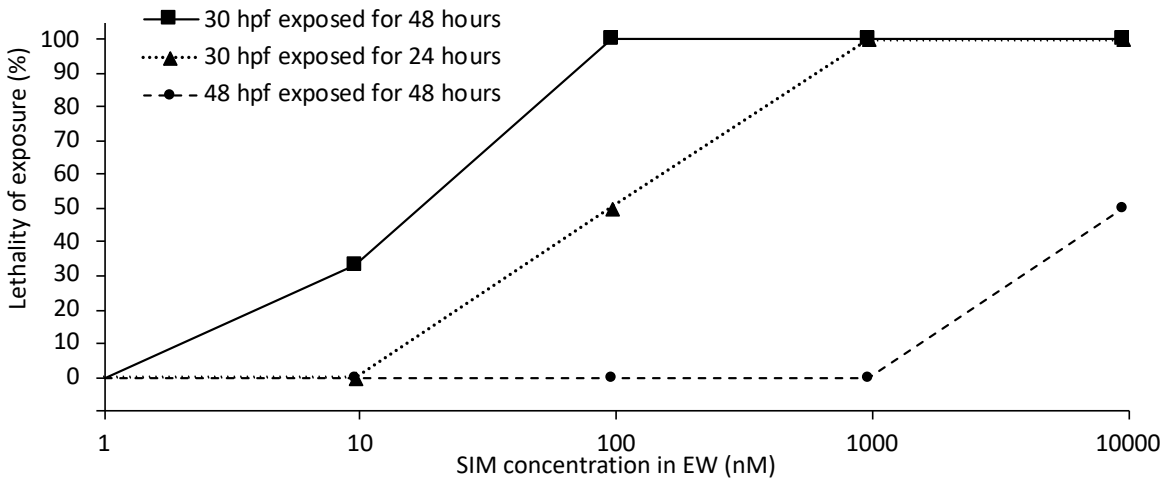

Figure 5.11: Lethality of zebrafish larvae exposed to simvastatin (SIM) dissolved in embryo water. *SIM was dissolved in embryo water in concentrations from 9.56 nM to 9.56 μM. Zebrafish embryos at 30 hours post fertilization (hpf), n=9-10, were exposed and lethality observed after 24 and 48 hours. Zebrafish larvae at 48 hpf (n=10) were exposed to the same concentrations and exposed for 48 hours before observation. No zebrafish larvae in the control groups were dead after 48 hours.*

Next, 72 hpf zebrafish larvae were exposed to SIM in embryo water and HR examined after 24 hours. The larvae were placed in SIM concentrations ranging from 4.78 nM to 95.6 nM in embryo water, and the control group in embryo water. SIM concentrations up to 38.4 nM did not affect HR after 24 hours, but the zebrafish larvae exposed to 95.6 nM SIM had a decreased HR to 87.5% ($P < 0.001$) relative to control (Figure 5.12). PCE was observed in eight out of ten zebrafish larvae in the group receiving 95.6 nM SIM, while in one of ten zebrafish larvae exposed to 38.4 nM SIM.

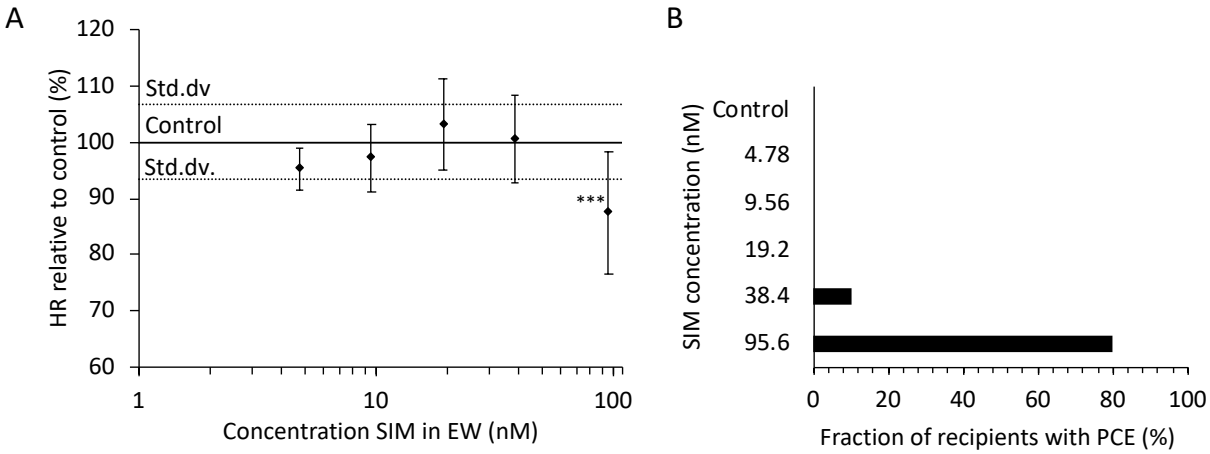

Figure 5.12: Cardiac effects of simvastatin (SIM) on zebrafish larvae. *A:Heart rate (HR) of 96 hpf zebrafish larvae treated for 24 hours with 4.78 to 95.6 nM SIM dissolved in embryo water. Control group were in pure embryo water, and their HR is illustrated as a horizontal line with standard deviation (std.dv.) as dotted lines. ANOVA with LSD post hoc tests was used to find significant change in HR of the treated zebrafish larvae (***: P<0.001). B: Percentage of zebrafish larvae with pericardial effusion (PCE) for each concentration after 24 hours. n=10 for all groups.*

Statins are known to cause adverse effects affecting the muscles, causing for instance muscle pain or rhabdomyolysis (37). Therefore, a preliminary test on the possible effect of SIM on zebrafish larvae muscle fiber was investigated. Zebrafish larvae at 48 hpf were exposed to SIM concentrations ranging from 9.56 nM to 9.56 μM for 24 hours before muscle fibers in the ventral and dorsal parts of the tail were observed. Figure 5.13 shows images of the muscles after exposure to SIM. More tests are necessary but note that in images D and E in Figure 5.13 has a higher contrast in the muscle fiber as well as the tail being less transparent relative to the zebrafish larvae receiving lower SIM concentrations where the muscle is smoother and more translucent.

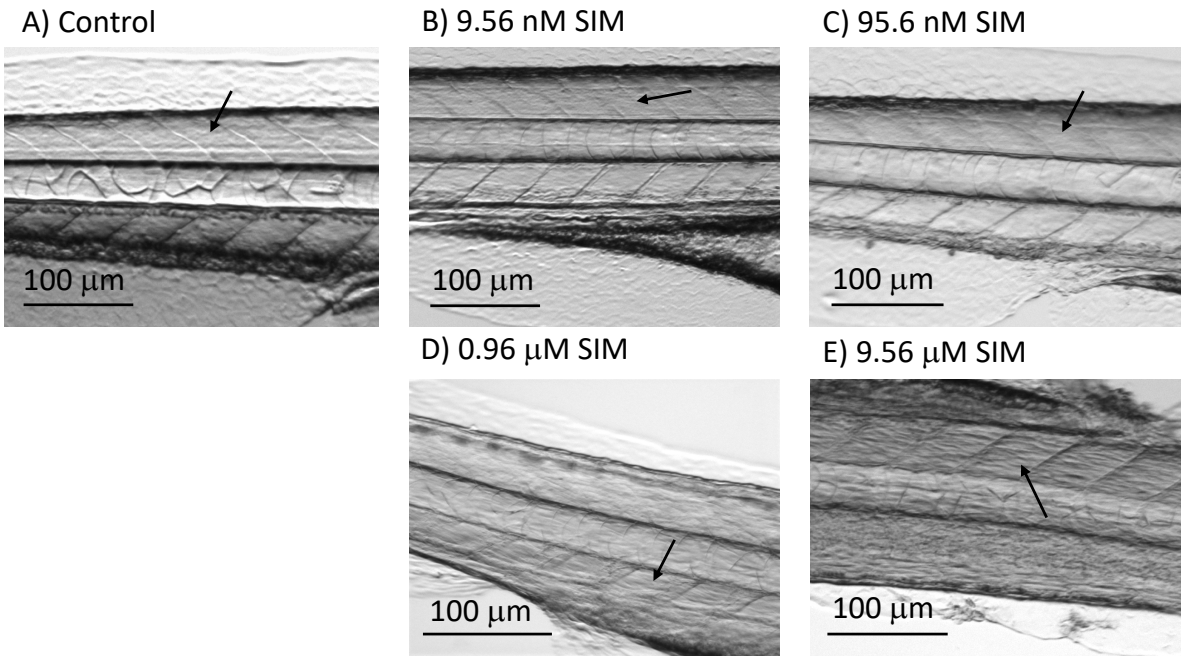

Figure 5.13: Zebrafish tail muscle fibers after treatment with simvastatin (SIM) in embryo water*. Images of 72 hours post fertilization zebrafish larvae after 24 hours of treatment with SIM dissolved in embryo water. A: Control, only exposed to embryo water. B: 9.56 nM SIM exposure. C: 95.6 nM SIM exposure. D: 0.96 µM SIM exposure. E: 9.56 µM SIM exposure. The arrows point to either dorsal or ventral skeletal muscles to indicate changes in muscle fibers. Images obtained using a Leica M205 stereo microscope. Scale bar: 100 nm.*

5.3.4 Exploring SIM as a Cardioprotective Agent in DOX Treatment

In the first experiments conducted to find whether SIM offered cardioprotective effect in DOX treatment of zebrafish larvae, the larvae were injected with 1.9 ng DOX and placed in embryo water with or without 9.56 nM SIM. Reduced HR was observed in DOX injected larvae both with and without being exposed to SIM, $P<0.01$ and $P<0.005$, respectively (Figure 5.14 A). In the group receiving only DOX, there was a higher fraction of zebrafish larvae dead and with PCE after 24 hours relative to those treated with SIM post injection. No zebrafish larvae were dead nor had PCE in the control or the SIM group (Figure 5.14 B).

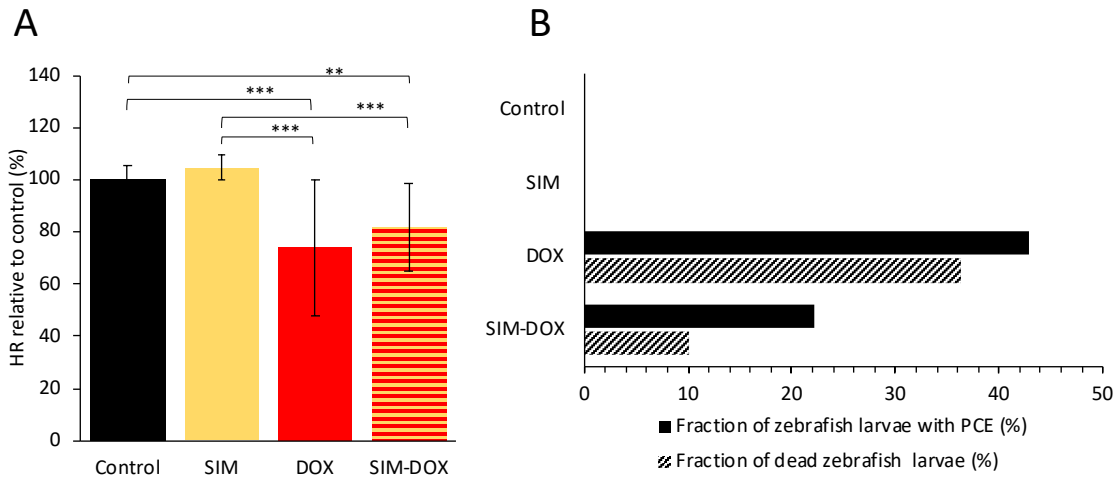

Figure 5.14: Toxic effects of doxorubicin (DOX) and simvastatin (SIM) on zebrafish larvae heartrate and survival. *A: Heartrate of 72 hours post fertilization zebrafish larvae observed 24 hours post injection with 1.9 ng DOX and/or being placed in 9.56 nM SIM dissolved in embryo water post injection. The control group was placed in embryo water. n=10-11 for all groups. Significance **: P<0.01, ***: P<0.005 found by one-way ANOVA with LSD post hoc test. Unless otherwise mentioned, no significance was observed. B: Percentage of dead zebrafish larvae and zebrafish larvae with pericardial effusion 24 hours post injection and/or SIM exposure.*

Next, three dpf zebrafish larvae were injected with PBS, free DOX, DOX liposomes, SIM liposomes or SIM-DOX liposomes and the toxic effects were observed after 24 hours. Two zebrafish larvae were observed to have PCE in the group receiving free DOX, and one in the SIM-DOX liposome group.While there was a significant decrease in HR for the DOX injected larvae relative to control ($P < 0.001$), there was an increase for those injected with SIM liposomes ($P < 0.001$). For the zebrafish larvae injected with DOX liposomes or DOX-SIM liposomes no change in HR was observed after 24 hours (Figure 5.15 A).

Two dpf zebrafish larvae were also injected with PBS, DOX, DOX liposomes or SIM-DOX liposomes and observed after 48 hours. After 48 hours a decrease in HR was observed in the larvae injected with free DOX, DOX liposomes and SIM-DOX liposomes (Figure 5.15). One larvae was dead in the DOX liposome group, while all larvae that recieved free DOX, PBS and SIM-DOX liposomes were alive. PCE was observed in one of the zebrafish that was injected with free DOX and one injected with DOX liposomes.

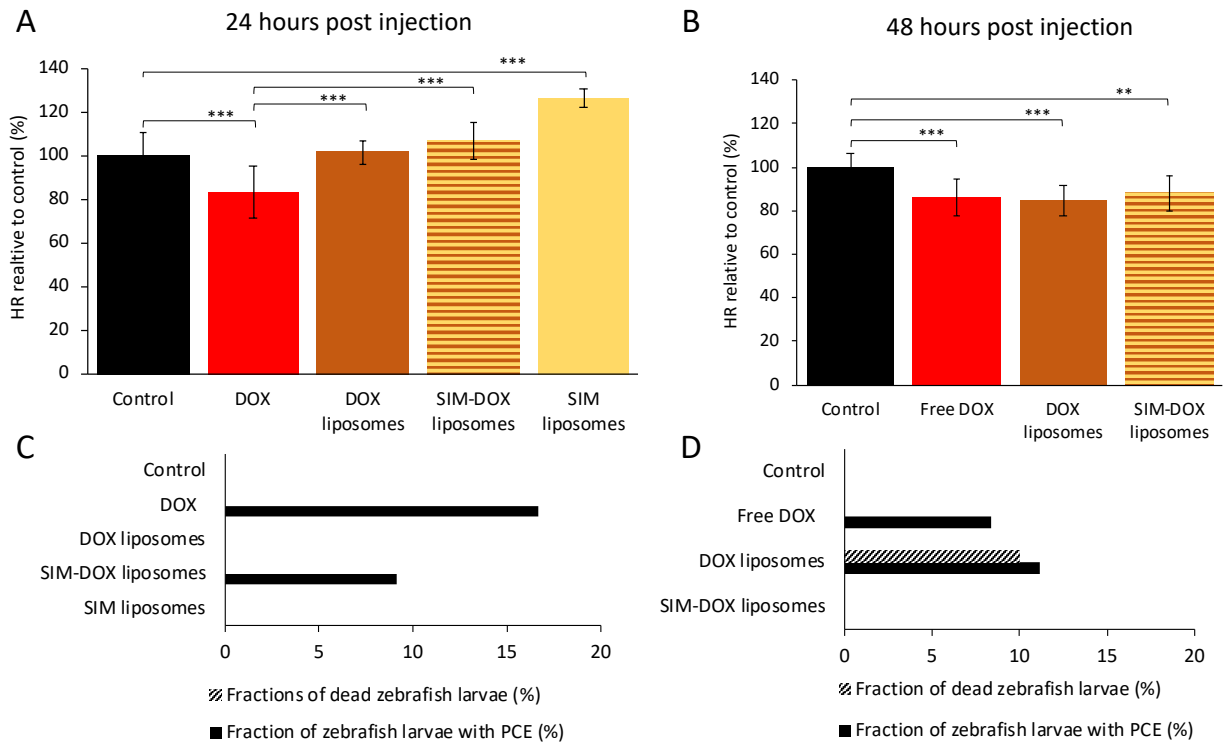

Figure: 5.15: Cardiac and lethal effects on zebrafish larvae after injections with doxorubicin (DOX) and simvastatin (SIM) as free drug and liposomes. *Heartrate (HR), pericardial effusion (PCE) and death in zebrafish larvae after injection with PBS, free DOX, DOX liposomes, SIM liposomes or SIM-DOX liposomes (n=10-12). The drug doses were 1.9 ng DOX and 0.38 ng SIM. A: The HR of four days post fertilization (dpf) zebrafish larvae observed 24 hours post injection (hpi), B: The HR of four dpf zebrafish larvae injected and observed 48 hpi. One-way ANOVA with LSD post hoc test was used and significance being **: P<0.005 or ***: P<0.001. There was no significant change unless otherwise is mentioned. C: Fractions of dead zebrafish larvae or zebrafish larvae with PCE 24 hpi D: Fractions of dead zebrafish larvae or zebrafish larvae with PCE 48 hpi.*

5.4 Distribution of Liposomes in Zebrafish Larvae Circulation

The green fluorescent phospholipid ATTO-488 DPPE was incorporated into DOX liposomes which was injected into the PCV of two dpf zebrafish larvae. This made it possible to visualize and inspect how the fluorescent liposomes was distributed in the zebrafish larvae over the course of two days (Figure 5.16). Two to four hours post injection, the liposomes were observed in the entire zebrafish larvae vasculature, including the smaller vessels in the head and along the tail of the larvae (Figure 5.16 A). The vascular fluorescence became less clear one- and two

days post injection (dpi) as more of the fluorescence was observed extravascular and seemed to accumulate in spots, but there was still fluorescence present in the vasculature (Figure 5.16).

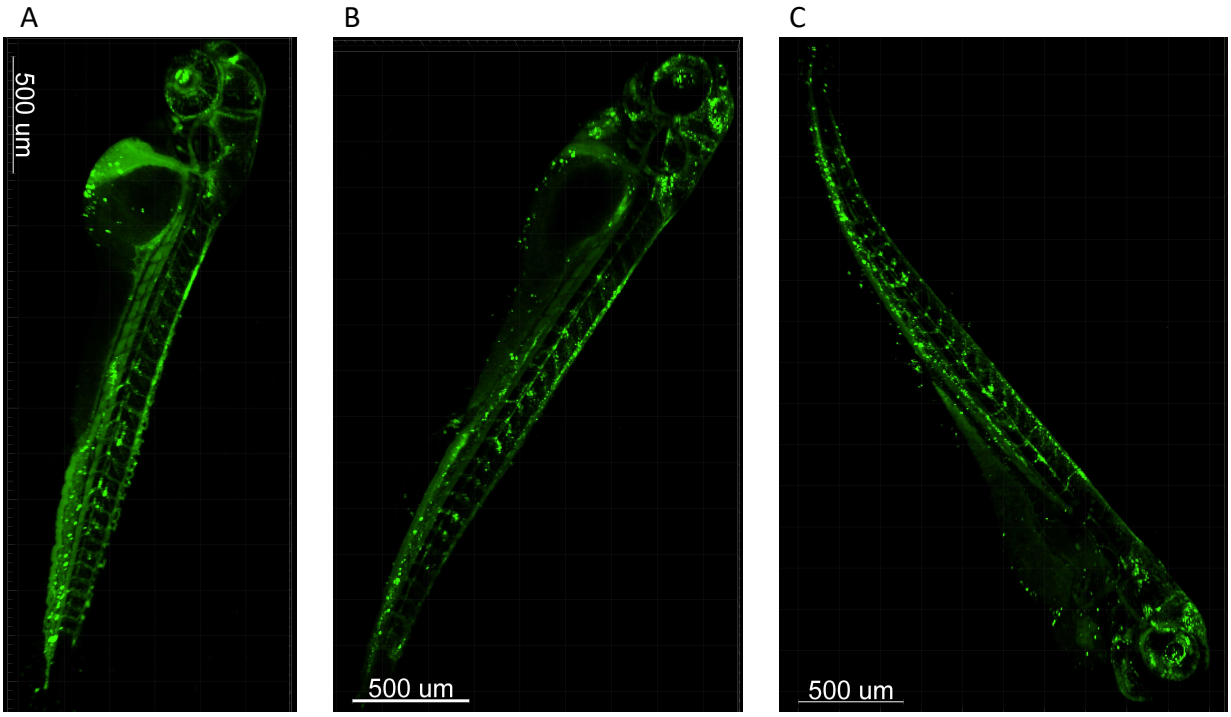

Figure 5.16: Zebrafish larvae injected with fluorescent liposomes*. ATTO-488 DPPE labeled liposomes with doxorubicin were injected in the posterior cardinal vein of two days post fertilization zebrafish larvae. The figure displays representative images of one injected larva. A: The larva two to four hours post injection. B: One day post injection (dpi). C: Two dpi. Images obtained as z-scans in an Andor Dragonfly 505 confocal microscope. Scale bar: 500 µm.*

5.5 Injections of MCF-7 Cells in Zebrafish Larvae

To observe how MCF-7 cancer cells acted inside the zebrafish larvae, the cells were stained with the cell stains, injected in the yolk sac or in PCV of zebrafish larvae and observed once daily over one to two days. The first cell stain tested on MCF-7 was CTG. Figure 5.17 show the clearest images obtained with CTG at a few hours post injection. However, the fluorescence disappeared and was no longer visible at one and two dpi.

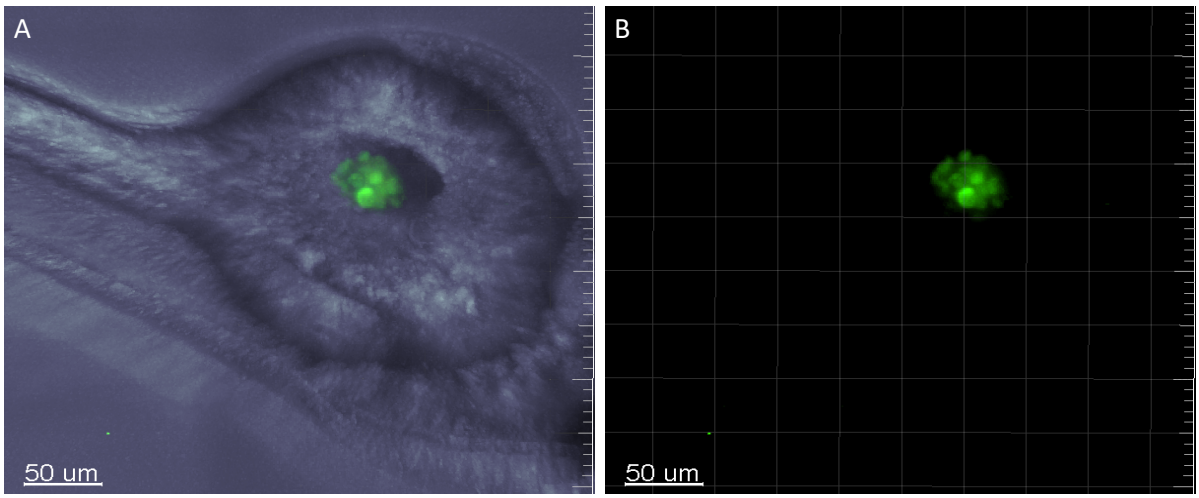

Figure 5.17: CellTracker™ green (CTG) stained MCF-7 cells in zebrafish yolk sac*. Zebrafish larvae at one day post fertilization were dechorionated and injected with CTG stained MCF-7 cells in the yolk sac. The images were obtained as z-scans at the day of injection. A: The zebrafish yolk sac and injected cells. B: The injected cells in the yolk sac. The images were obtained in an Andor Dragonfly 505 confocal at 20x magnification. Scale bar: 50 µm.*

Previously, another cell tracker, DiI, gave good results when injecting human acute myeloid leukemia cells MOLM-13 into zebrafish larvae (see Appendix, Supplementary Figure 4). Staining of MCF-7 cells with DiI stain was therefore tested.

Figure 5.18 shows a zebrafish larva injected in the yolk sac with DiI stained MCF-7 cells from between two- and four hpi, and one- and two dpi. At two to four hpi, the fluorescent signal was only visible in the yolk sac, but after one- and two- dpi, the signal also had spread to the tail of the zebrafish larvae (Figure 5.18). In this experiment three out of nine total yolk sac injected zebrafish larvae had signal redistributed to the tail at one day post injection (Zebrafish larvae with MCF-7 cells in the yolk sac over two days without spreading is illustrated in Supplementary Figure 5). Table 5.3 show the number and area of fluorescent events observed in Figure 5.18. Both the area and number of events were seen to increase from hours post injection, to one and two dpi.

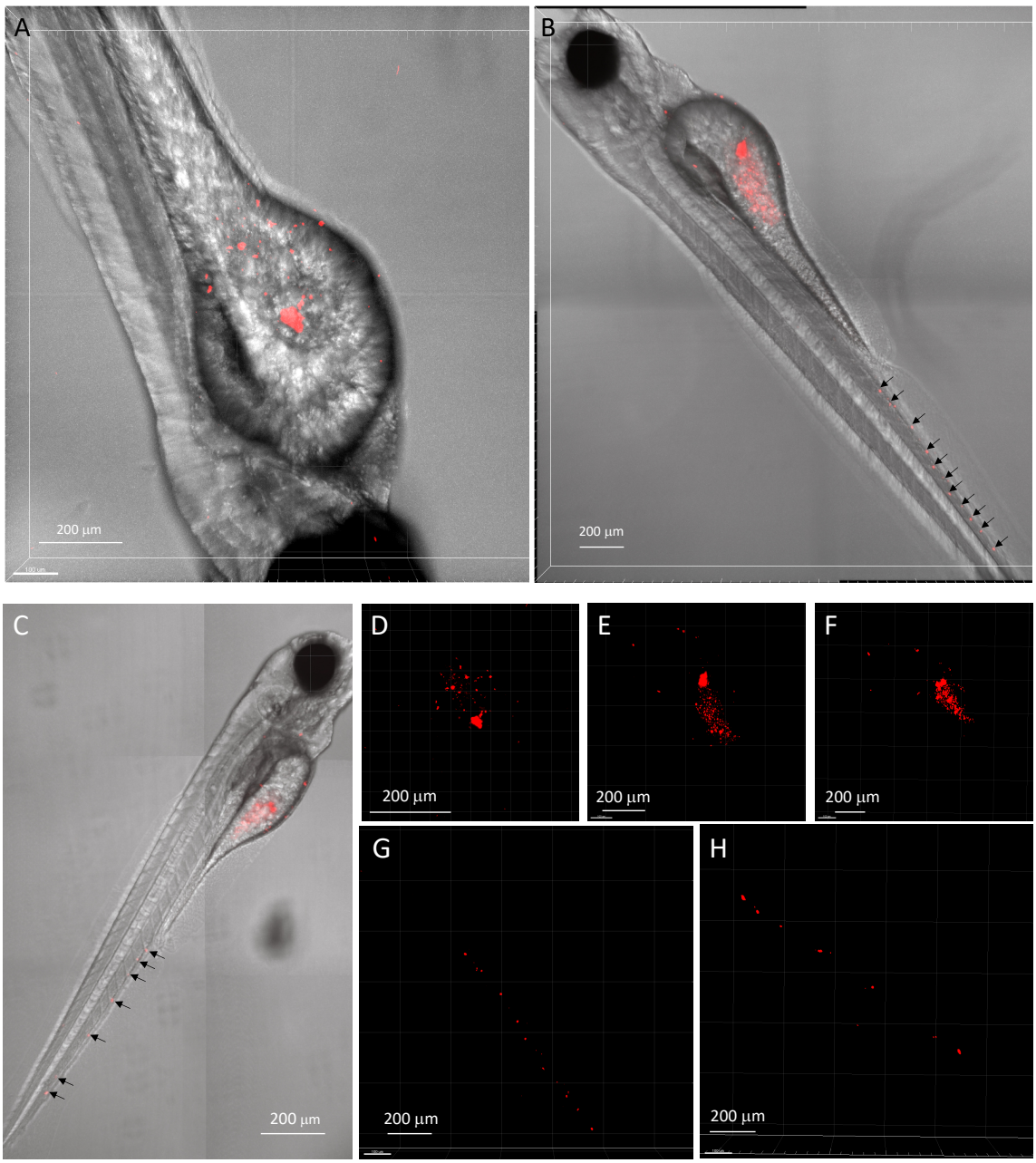

Figure 5.18: Zebrafish larvae injected into the yolk sac with DiI stained MCF-7 cells*. Representative images of a two days post fertilization zebrafish larva injected with DiI stained MCF-7 cells into the yolk sac with signal spreading to the tail at one day post injection (dpi). A: The zebrafish larva yolk sac imaged between two to four hours post injection (hpi). B: One dpi, with arrows pointing to fluorescent signal in tail. C: Two dpi with arrows illustrating fluorescent signal in the tail. D: Fluorescence in the yolk sac two to four hpi. E: Fluorescence in the yolk sac one dpi. F: Fluorescence in the yolk sac two dpi. G: Fluorescence in tail one dpi. H: Fluorescence in tail two dpi. The z-scans were obtained at 10x magnification in an Andor Dragonfly 505 confocal. Scale bar: 200 µm.*

***Table 5.3: Fluorescence in the Figure 5.18 zebrafish larva**. Fluorescent events as number and area in the zebrafish larva at zero, one- and two days post injection of MCF-7 cells into the yolk sac. Analyzed using FIJI software.*

Days post injection	**0**	**1**	**2**
Fluorescent events	18	47	56
Area of fluorescence (μm^2)	3401	3542	8754

Next, two dpf zebrafish larvae were injected intravenously into the PCV with DiI stained MCF-7. Two to four hpi, the fluorescent signal could be observed in most parts of the zebrafish vascular system. After one and two days the signal was mainly observed in the area of the dorsal aorta (DA) and PCV, as well as the ventral parts of the yolk sac, and was observed to be more condensed compared to the image from the day of injection (Figure 5.19). These observations were done for all three PCV injected larvae in the experiment. Quantification of fluorescent events and area showed a decrease over the two days following injection (Table 5.4).

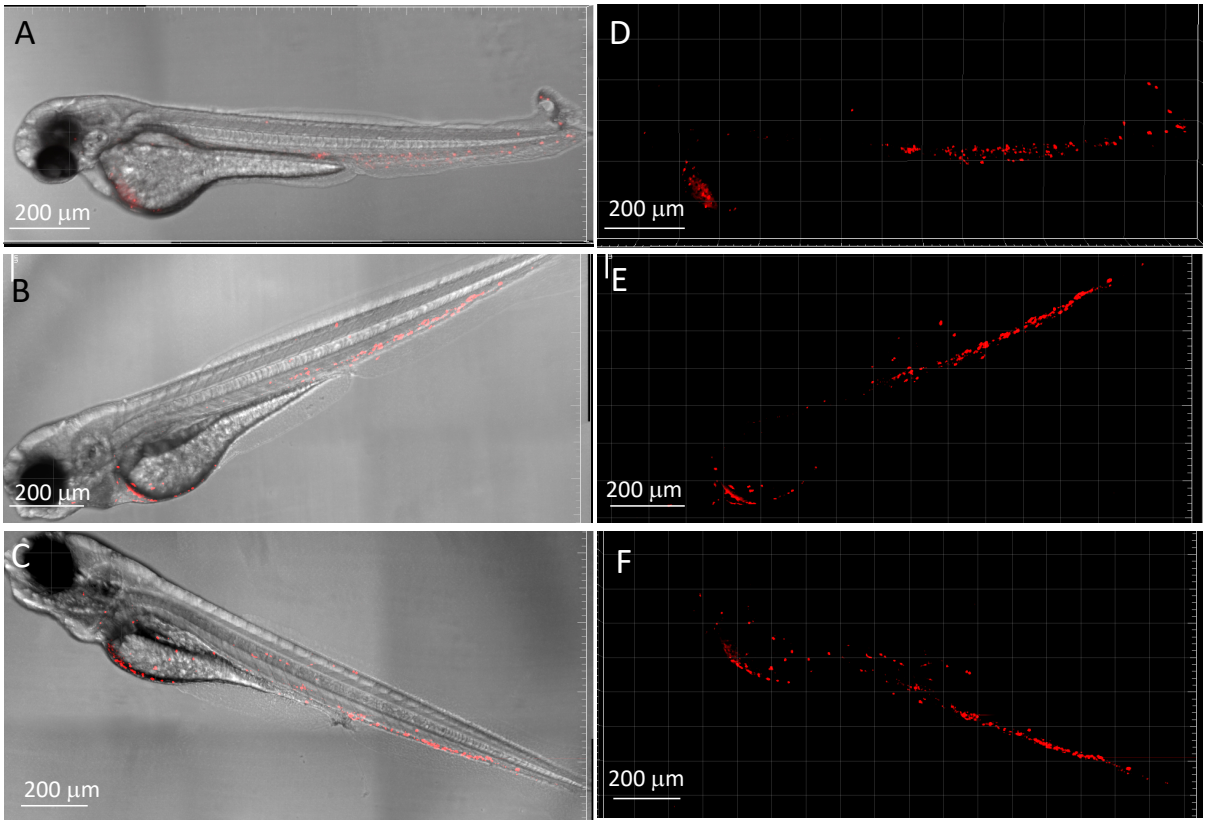

***Figure 5.19: Intravenously injected MCF-7 cells in a zebrafish larva**. Representative images of a zebrafish larva injected with DiI stained MCF-7 into the posterior cardinal vein at two days post fertilization. A and D: The zebrafish larva two to four hours post injection. B and E: The zebrafish larva one day post injection (dpi). C and F: The zebrafish larva two dpi. The images were obtained as z-scans at 10x magnification with an Andor Dragonfly 505 confocal. Scale bar: 200 µm.*

***Table 5.4: Number of fluorescent events in the zebrafish larvae from Figure 5.19.** Fluorescent events at zero, one- and two days post injection into the posterior cardinal vein of MCF-7 cells stained with DiI. Particles analyzed using FIJI software.*

Days post injection	**0**	**1**	**2**
Fluorescent events	251	123	55
Area of fluorescence (µm^2)	4000	3654	2024

In another experiment, two 48 hpf zebrafish larvae were injected intravenously with DiI stained MCF-7 and observed to have a much higher number of fluorescent signals at one dpi relative to two to four hours post injection. One of these zebrafish larva is visualized in Figure 5.20. In Table 5.5 it is illustrated that more than 20 times as many fluorescent events were observed at one dpi relative to two to four hpi, and more than eight times as large area is covered by the fluorescence in the zebrafish larvae. These larvae were unfortunately not visualized at two dpi because the university was closed down due to the covid-19 pandemic.

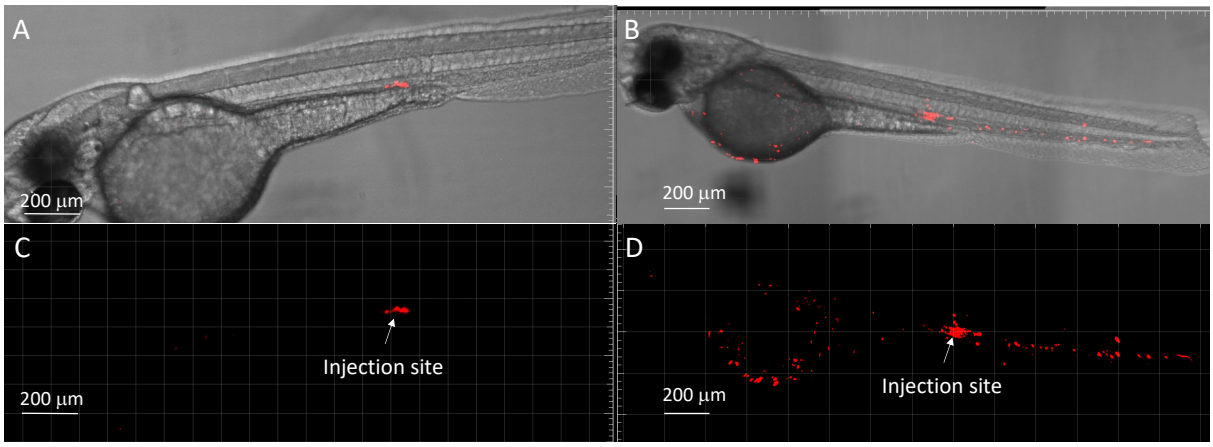

Figure 5.20: Zebrafish larva injected intravenously with DiI stained MCF-7*. A zebrafish larva injected into the posterior cardinal vein with DiI stained MCF-7 cells at two days post fertilization. A and C: The zebrafish larva two to four hours post injection with the injected cells visualized only at the injection site. B and D: The zebrafish larva one day post injection where the fluorescent signal has spread to both tail and yolk sac region of the larva. Arrows point to the injection site. Images obtained as z-scans at 10x magnification in an Andor dragonfly 505 confocal microscope. Scale bar: 200 μm.*

Table 5.5: Fluorescent events from Figure 5.20. *The number and area of fluorescent events in the zebrafish larva in Figure 5.20 at the day of injection and one day post injection. Particles analyzed using FIJI software.*

Days post injection	**0**	**1**
Fluorescent events	4	98
Area of fluorescence (μm^2)	1261	10170

Next, the zebrafish larvae were injected with both DiI and CTG stained MCF-7 cells in the PCV. Longer incubation time for cells with the CTG stain was attempted to see whether the staining remained visible for longer after injection. However, while the DiI stain was clearly visible after two days, CTG was visible at two to four hours post injection and barely visible in a few larvae at one dpi (Figure 5.21 and Figure 5.22). In Figure 5.21, at the day the of injection, eleven fluorescent events are seen with both green and red fluorescence and three are seen with only green fluorescence. At one dpi, only one spot is seen with both green and red fluorescence, and one with only green fluorescence. In Figure 5.22, 14 events are seen with both fluorescent stains at a two to four hpi, while only two events are seen with both DiI and CTG stains at one dpi. One particle is observed with only CTG stain in the image, but this is outside the zebrafish, probably adhered to the bottom of the well. The zebrafish larva in Figure 5.22 was not imaged at two dpi. In Figure 5.21 A, a larger green fluorescent signal is observed dorsal to the yolk sac. This was only observed in the one larva at the day of injection, and likely a reflection or autofluorescence.

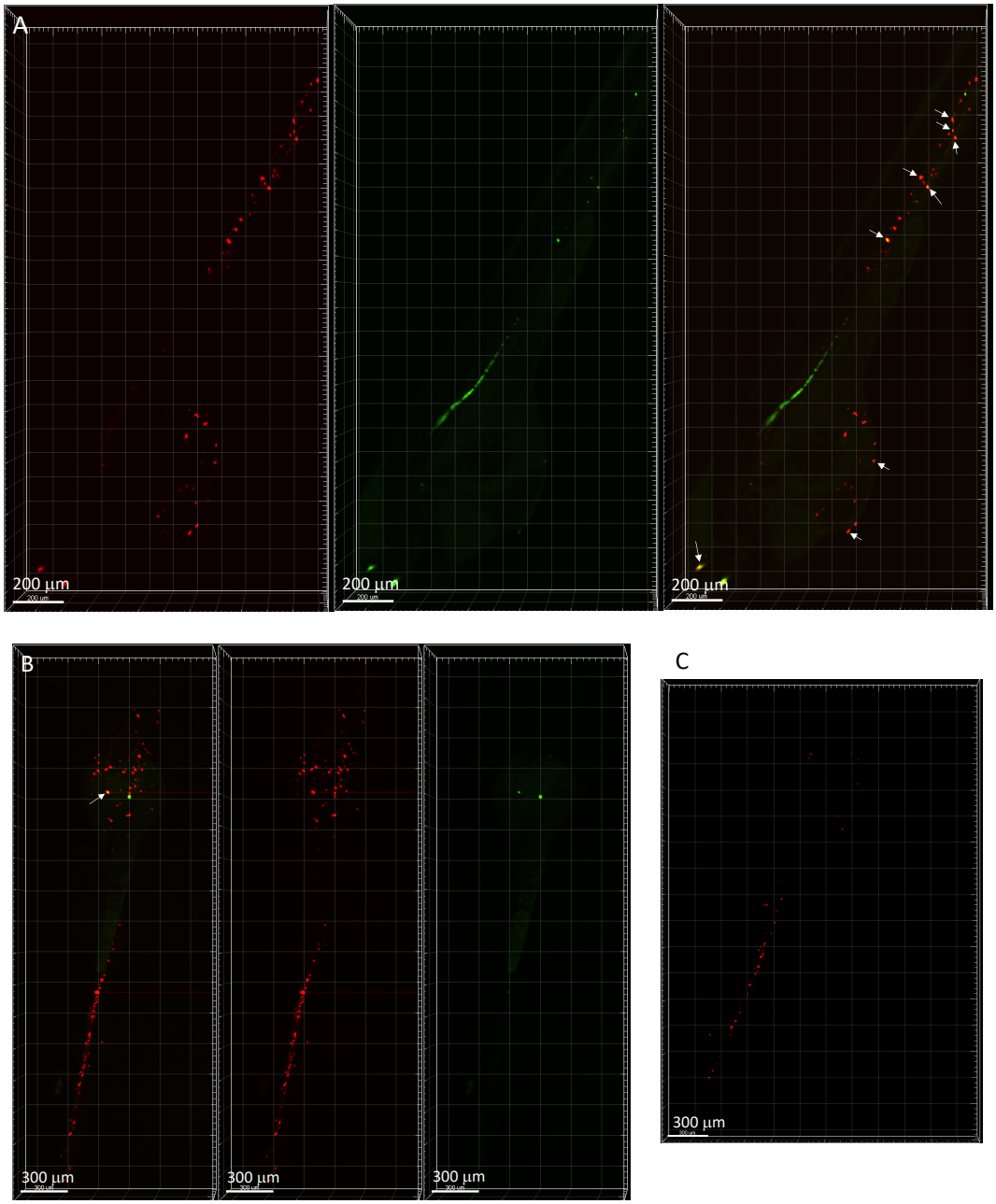

Figure 5.21: Zebrafish larva injected with CellTracker Green CMFDA (CTG) and DiI labeled MCF-7*. MCF-7 cells stained with both DiI and CTG was injected into the posterior cardinal vein of two days post fertilization zebrafish larvae. The figure shows representative images of one of the injected larvae. A: The larva visualized two to four hours post injection with both red DiI and green CTG signal present. B: One day post injection where two cells are still visible with green fluorescence. C: Two days post injection with just the red fluorescence still visible. Arrows point to cells inhabiting both green and red fluorescence. Images obtained as z-scan with an Andor Dragonfly 505 confocal at 10x magnification. Scale bar: A: 200 µm, B and C: 300 µm.*

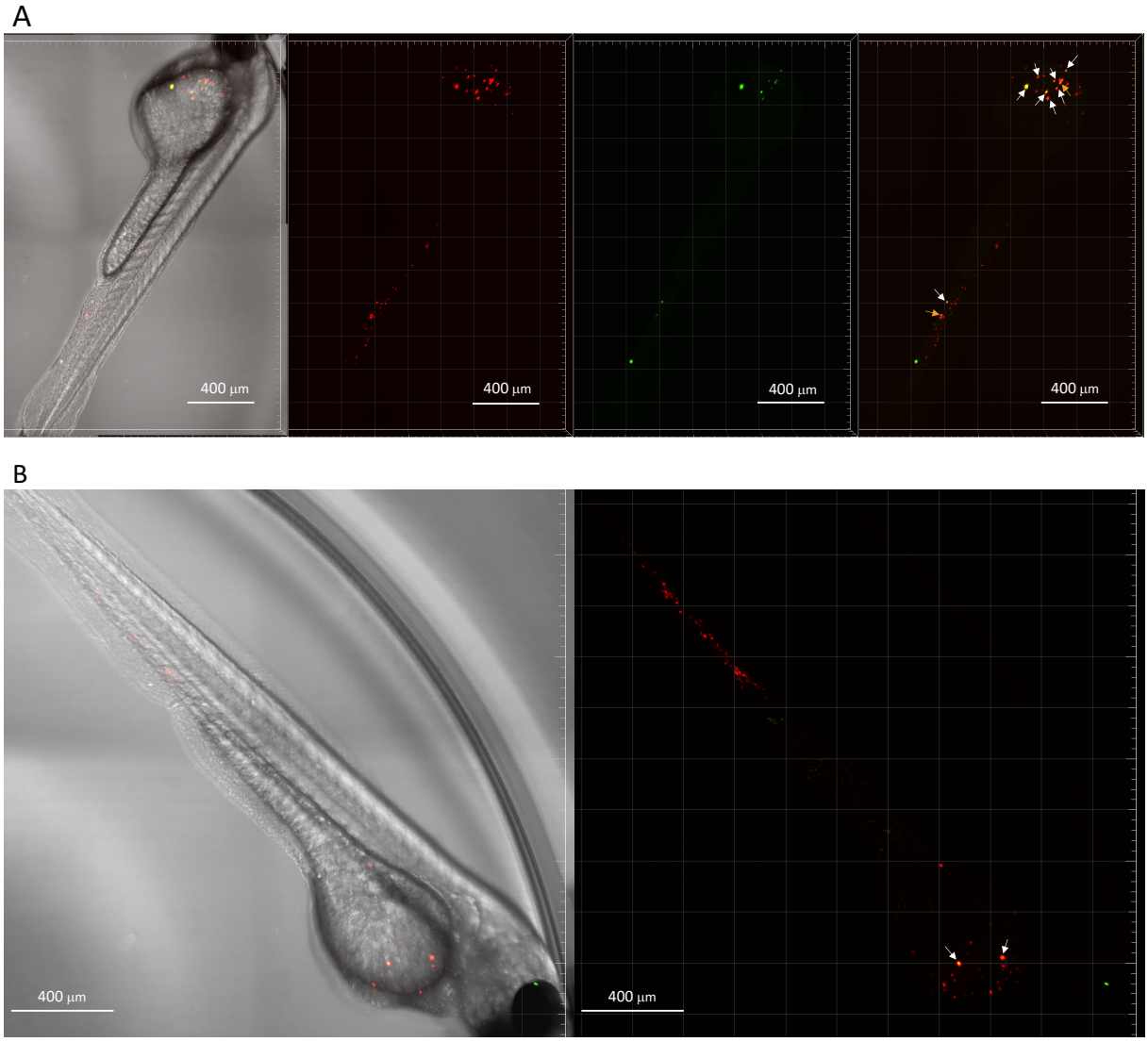

Figure 5.22: Zebrafish larva injected with CellTracker Green CMFDA (CTG) and DiI labeled MCF-7*. MCF-7 cells stained with both DiI and CTG and injected into the posterior cardinal vein of two days post fertilization zebrafish larvae. A: The larva visualized two to four hours post injection with both red DiI and green CTG signal present. B: Zebrafish larva visualized at one day post injection where two cells are still visible with green fluorescence. Yellow arrows point to clusters of three cells with both cell stains. White arrows point to single cells with both cell stains. Images obtained as z-scan in an Andor Dragonfly 505 confocal at 10x magnification. Scale bar: 400 µm.*

In order to see if intravenously injected liposomes interacted with cancer cells, zebrafish larvae at two dpf was injected with DiI stained MCF-7 cells in the yolk sac and ATTO-488 DPPE labeled DOX liposomes in PCV. Both cells and liposomes were observed in the confocal microscope, but the liposomes did not accumulate to the area of the cancer cells in the yolk. When counting the area and number of fluorescent events, both were seen to approximately double over after one day (Figure 5.23 and Table 5.6).

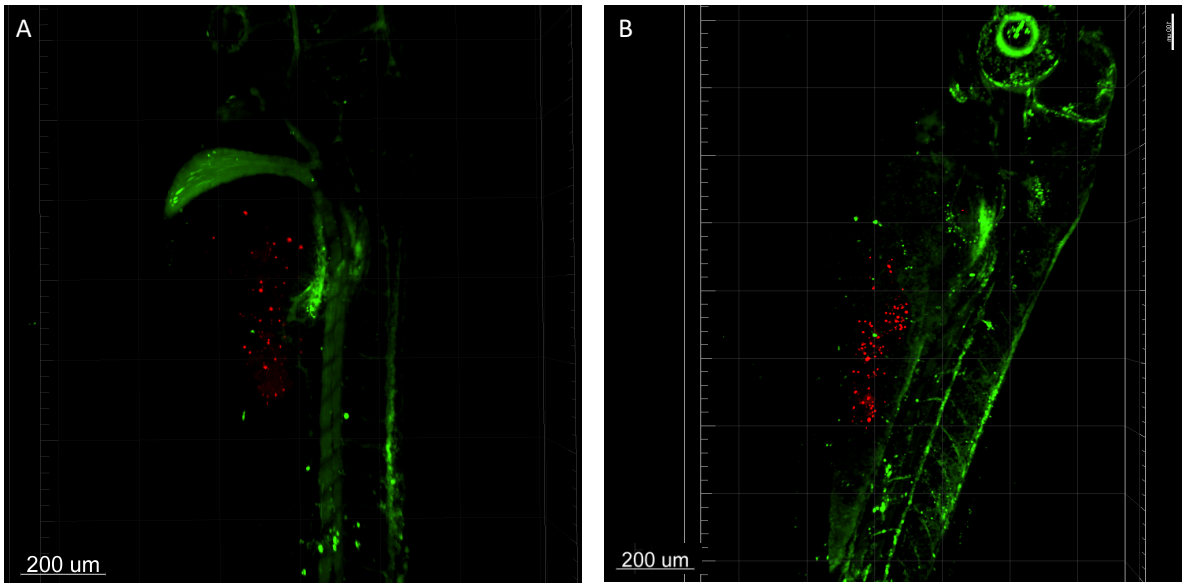

Figure 5.23: Zebrafish injected with doxorubicin (DOX) liposomes and MCF-7. *Representative images of a zebrafish larva injected with DiI stained MCF-7 cells in the yolk sac and green fluorescent ATTO-488 DPPE labeled DOX liposomes in the posterior cardinal vein at two days post fertilization. A: Zebrafish larva between two to four hours post injection. B: Zebrafish larva one day post injection. Images obtained as z-scan with an Andor Dragonfly 505 confocal at 10x magnification. Scale bar: 200 µm.*

Table 5.6: Fluorescent events from DiI stained MCF-7 cells in zebrafish larvae injected with DOX liposomes. *The observed DiI fluorescence in the yolk sac from the zebrafish larva in Figure 5.23 injected with both MCF-7 cells and DOX liposomes. Particles analyzed using FIJI software.*

Days post injection	**0**	**1**
Fluorescent events	17	33
Area of fluorescence (μm^2)	601	1176

6 Discussion

In this study, free and liposomal DOX and SIM were tested for toxicity in zebrafish larvae and in cell assays. The liposomal formulations were observed to be less toxic than equivalent doses of free drug, whereas further studies need to be conducted to establish potential cardioprotective effects of SIM. Additionally, injection of the human cancer cell line MCF-7 in zebrafish larvae was conducted to establish a method for cancer cell transplantation in zebrafish larvae, and the fluorescent signal used to stain the cells was observed to grow in number and to redistribute in the zebrafish larvae over two days.

In order to obtain consistent results, it was important that the drug content in the liposomes were measured exactly. This study used HPLC, which is a reliable method for quantification of small organic molecules and drugs. The HPLC chromatogram of DOX showed minor peaks directly prior to the elution of DOX (Figure 5.1). The area of these peaks was the same in all DOX standard concentrations and therefore likely to be an impurity of the mobile phase or solvents used, and not a degradation product from DOX from the stock solution. The standard curve obtained had an R^2 of 1.00 and was considered sufficient to estimate DOX concentration in the liposome samples (Figure 5.1, insert). The first HPLC-test for SIM using the C18 column was developed so it was possible to quantify both DOX and SIM in one run. However, this method gave poor results with SIM eluting on top of a noisy baseline at the wash of the column (Figure 5.2). Using a phenyl-hexyl column took advantage of pi-pi interactions between ring structures of SIM (Figure 2.2) and the phenyl residues in the solid phase (123), and a more predictable elution of SIM was achieved. In these methods, methanol was used as a mobile phase to disrupt the pi-pi interactions which eluted the drug on a baseline with little noise and in a narrow, single peak, before wash of the column with ACN. The standard curve had an R^2 of 1.00 and was determined to be good for calculation of liposomal SIM concentration (Figure 5.3).

The DOX loading in both DOX- and SIM-DOX liposomes was 20% w/w DOX loading relative to lipid concentration and the encapsulation efficiency was high with little DOX outside the liposomes even before SEC. This is demonstrated by no secondary peaks in Figure 5.4 and correlating with other findings (124). Ideally, the liposomes should have been filtered through the SEC column after the addition of DOX to ensure that all unencapsulated drug was eliminated, but this would decrease DOX concentration below what would cause toxic effects

in zebrafish larvae. In Figure 5.4 A, the SEC elution volume of DOX liposomes is compared to that of ATTO-488 DPPE liposomes to determine encapsulation. The DOX liposomes were found to elute approximately one minute before the fluorescent liposomes. This difference in elution volume can be explained by the fact that the column ran dry during the washing process after the filtration of the ATTO-488 DPPE liposomes and needed to be repacked. Repacking of columns will influence the conditions, such as packing density, and thus travelling length and elution volume for the DOX liposomes. However, the DOX liposomes and SIM-DOX liposomes were observed to elute in one, narrow peak, and no peaks were observed to elute at a later point (Figure 5.4). On the other hand, free DOX eluted as a broad peak starting at eight mL, and not fully eluted after 19 mL (Figure 5.4 B). As DOX molecules are much smaller than the liposomes, this difference in elution volume was expected, and no overlap between fluorescent liposomes and free DOX made it possible to conclude that the observed peaks from the SEC of the liposomes were indeed encapsulated drug. Thus, the liposomes were used on the zebrafish larvae without an additional SEC filtration after DOX addition. The highest DOX concentrations achieved in the liposomes were between 0.45 and 0.5 mg/mL liposomal DOX, which allowed for maximum injection dose of 1.9 ng DOX in zebrafish larvae in the study.

In treatment of hyperlipidemia, SIM is administered orally as tablets (37). It was desired to produce a liposomal formulation with SIM, which in many cases are designed to minimize adverse and toxic effects. A known adverse effect of statins in humans is rhabdomyolysis, destruction of skeletal muscle (37). In the study, skeletal muscle in the tail of zebrafish larvae exposed to 0.96 and 9.56 μM SIM for 24 hours was observed to become more irregular and revealed a higher contrast compared to those exposed to 9.56 and 95.6 nM SIM and control (Figure 5.13). However, only a few larvae were observed for each concentration, and more tests must be conducted to observe if this effect is typical to SIM exposure. The encapsulation of SIM together with DOX in liposomes could allow for the zebrafish larvae to tolerate higher concentrations of SIM and achieve cardioprotective effects without risks of rhabdomyolysis. Additionally, orally administered SIM has its main mechanism of action in the liver, and little drug reaches circulation, making it less suitable as a cardioprotective drug in anthracycline therapy (Section 2.1.1). Liposomes with both drugs encapsulated would reach the same cells in the body, ensuring the protective effect at the correct site. Further dose-escalation studies with SIM liposomes should be done to find MTD in zebrafish larvae, which could be used to find the optimal SIM dose to prevent DOX cardiotoxicity.

Liposome size was measured using DLS, an indirect method for determining size of spherical particles. It was considered to use transmission electron microscopy (TEM) to verify the size. However, extrusion is a reliable method for liposome production, and the suspensions were passed through the smallest filters twice. In addition, due to the covid-19 situation, this analysis could not be conducted. Knudsen (114) and Gundersen (125) found, when comparing results from DLS and TEM, that the former resulted in larger liposome size relative to what was visualized in TEM. Nevertheless, DLS is still regarded as a reliable method to measure liposome size. In the present study, the liposomes were found to be approximately 130 nm in diameter by DLS. Upon PCV injection of green fluorescent liposomes in zebrafish larvae, the fluorescence was observed to be distributed in the entire vascular system, and not observed to clog even the small capillaries, as demonstrated in Figure 5.16.

Cell assays were performed to observe toxicity of the produced liposomes and free drugs. The results from the WST-1 assay showed poor correlation between signal and the number of normal cells observed in the microscope (Appendix, Supplementary Figure 1 and Figure 5.8). Several explanations were considered. One possibility was that the cells had extremely high metabolic activity, and even a few cells still alive in the wells would be able to convert all WST-1 to the formazan compound. Another explanation was that there were bacteria growing in the wells that were able to convert WST-1 to formazan. However, no bacteria were observed when studying the wells in light microscope or in fluorescence microscopy after Hoechst-staining. Thus, no good explanation to why the WST-1 assay did not give satisfactory results was found. Consequently, assessment of cytotoxic effects of the treatments was done by visual counting of the cells and nuclei. The counting process has some drawbacks, it is tedious, and it can be difficult to distinguish cells with normal morphology from apoptotic or necrotic cells. Also, DOX and Hoechst 33342 both bind in the minor groove of DNA and compete on binding (126). Higher free DOX concentrations therefore resulted in weak Hoechst-stained cell nuclei, causing difficulties in visualizing the nuclei. Because of this, the nuclei of cells treated with higher concentrations of free DOX were observed using a rhodamine fluorescence filter for red fluorescence. This made it harder to compare the free DOX treated wells to control wells, which were observed using a DAPI filter for blue Hoechst fluorescence. There was a desire to conduct more cell assays to observe reproducibility of the tests, the effects on H9C2 after 48 hours

incubation, as well as including DOX liposomes in the study but because of the limited laboratory time as a result of the covid-19 pandemic this could not be prioritized.

Incubation for 24 hours with SIM-DOX liposomes was found not to affect cell viability for either H9C2 or MCF-7 cells (Figure 5.8). After 48 hours incubation, however, decreased viability was observed for the MCF-7 cells, but these cells were still more viable than those treated with equivalent concentrations of free DOX (Table 5.2). The cells treated with SIM-DOX liposomes for both 24- and 48 hours also had visible Hoechst 33342 fluorescence, indicating that less DOX had entered the nuclei relative to the cells treated free DOX, where the Hoechst fluorescence was not visible in the highest concentrations (Figure 5.5-5.7). The H9C2 cells showed a higher tolerance to DOX than the MCF-7 cells, where incubation with 5 and 15 μM rendered all MCF-7 cells dead, whereas 44 and 12% of H9C2 cells were still viable in these concentrations, respectively. Additionally, H9C2, but not MCF-7, seemed to benefit from co-treatment with SIM in 15 μM DOX concentration since a reduction of death was observed in the H9C2 cells (Figure 5.8 and Table 5.2 A and C). These results could indicate that during high-dose therapy of DOX, co-therapy with SIM can be beneficial to the heart, while not reducing therapeutic response of DOX on cancer cells.

The toxicity of DOX and the potential protective effects of liposomal formulations and SIM were tested on zebrafish larvae. Several zebrafish larvae assays testing the toxicity of nanoparticular anthracyclines are based on adding drugs or nanoparticles in embryo water, like those of Han et al. (16) and Calienni et al. (127). This will not only unnecessarily expose the zebrafish skin and gills to toxic drugs, but more importantly, the zebrafish larvae are only able to absorb small molecules through diffusion, and the absorption of free drug would happen much more efficient compared to liposomal drugs. This would give an overestimated protective effect of the liposomal formulation on zebrafish larvae. Additionally, in the clinic, intravenous infusions are the administration route of DOX, thus microinjections represent a more realistic approach. DOX is, as mentioned in the introduction, known to cause cardiotoxic effects years and even decades after treatment, with young age being a risk factor. As we could not observe larvae after four dpf, when they start to require feeding, in this study, long-term cardiotoxic effects in zebrafish were not investigated. It would have been interesting to observe how DOX treatments on larvae affected the health of the fish during growth.

As tricaine exposure did not affect HR over time (Figure 5.9), sedated larvae were used to study cardiotoxicity in the study (Figure 5.10). Free DOX caused a decrease in HR, and an increased occurrence of PCE in zebrafish larvae 24 hpi, while liposomal DOX did not affect HR, and the incident of PCE was lower. This was to be expected as liposomal DOX is used in the clinic to reduce adverse effects. The reduced HR of zebrafish could be associated with the arrythmias that is seen in humans as an acute cardiotoxicity of DOX (27). Arrythmias, were not examined in the present study, but should possibly be evaluated in further experiments. Additionally, PCE and reduced HR could be a result of cell death in the heart after DOX treatment, as observed for H9C2 in the cytotoxicity assays, causing the heart to lose integrity, and ultimately leading to edema of the pericardium and reduced HR. There were individual differences between the larvae within one treatment, both in regards of HR and PCE (Figure 5.10). This reflects the situation in humans, where the occurrence and rate of adverse effects of drugs are very individual. This also illustrates the power of *in vivo* models compared to cell-based systems for toxicity screenings, and that zebrafish, and especially larvae, can be an inexpensive model for drug toxicity screenings and discovery of rare adverse effects. In the test, injection of PBS did not change HR, but unexpectedly, reduced HR was observed for the larvae injected with empty liposomes (Figure 5.10). These injections were intended as a control for DOX liposomes and giving that DOX liposomes did not decrease HR it seemed strange that liposomes with no drug added would. Damage to the heart could have been caused by too high injection pressure in the test which further could have reduced HR of the larvae in the empty liposome group.

As SIM is practically insoluble in aqueous solutions (38), the drug alone could not be injected. However, the zebrafish larvae were exposed to SIM dissolved in embryo water, or as injections with SIM liposomes. When adding SIM to the embryo water, it was observed that higher concentrations were harmful to the larvae, causing death, PCE and reduced HR (Figure 5.11 and 5.12). Injection of 0.38 ng SIM liposomes increased HR of zebrafish larvae after 24 hours (Figure 5.15 A). Increased HR in humans or in other zebrafish studies due to statin therapy is not observed, and there could be other factors like high injection pressure in the control group causing it to have reduced HR, affecting the results. Campos et al. hypothesized that reduction in HR after SIM treatment could be caused by low cholesterol and found that treatment with LDL cholesterol together with SIM did not alter HR, while SIM alone gave a significant reduction when exposed from 6 to 24 hpf (128). They did not, however, provide further explanation of mechanisms behind this hypothesis. In treatment of hyperlipidemia, withdrawal

of statins are recommended in pregnancy where cholesterol is crucial to development of the fetus (37, 129). Maerz et al. related heart defects in zebrafish larvae treated with atorvastatin from 10 to 48 hpf to those of humans with hypocholesterolemic syndromes. They linked dysfunctional cilia to be caused by low cholesterol, further causing several developmental malformations, including of the heart (130). In addition to decreased HR and PCE after treatment with atorvastatin, Maerz et al. found physical alterations including smaller atrium and ventricles and elongation of the heart in the treated zebrafish larvae. This supported their theory of lowered cholesterol levels in embryogenesis causing defects in the formation of the heart, which further could affect HR and give PCE (130). Campos et al. also observed the effect of SIM treatment early in embryonic development, where treatment from six hpf gave more advanced developmental defects relative to embryos treated from eleven hpf (128). Figure 5.11 shows that larvae exposed to SIM dissolved in embryo water from 48 hpf had a higher survival when exposed to the same concentrations of SIM for 48 hours compared to embryos exposed from 30 hpf. Taken together, SIM is observed to be more toxic in an early developmental stage of zebrafish larvae, likely because of cholesterol-lowering effects, which is also a risk in human embryonic development.

Further, the combination of SIM with DOX was explored, both as free drug dissolved in the embryo water post DOX injection, and by co-injections of both drugs in liposomes. SIM did not provide further protection against decreased HR than what was achieved by liposomal formulation of DOX. However, there was observed lower frequency of PCE and death in the SIM-DOX co-treated larvae, compared to those treated with free DOX alone in the test with SIM dissolved in embryo water post DOX injection (Figure 5.14). H9C2 cells had increased viability in the highest concentration of DOX and SIM together, relative to high dose DOX alone. It might be necessary with higher SIM concentrations to observe cardioprotective effects in DOX treatment in zebrafish. Higher doses of free SIM, however, gave toxic effects when dissolved in embryo water. Therefore, higher concentrations of SIM liposomes should be produced. Escalating doses of SIM liposomes injected in zebrafish larvae could be used to find MTD, and then used in SIM-DOX liposomes to see if this could provide a cardioprotective effect in zebrafish larvae.

When comparing injections of free DOX, DOX liposomes and SIM-DOX liposomes injected in zebrafish larvae, the two latter did not affect HR after 24 hours, but after 48 hours all

treatments gave equal reduction in HR (Figure 5.15 A and B). The HR conserving effect seen at 24 hours could be related to the liposomal formulation alone. Liposomal drugs would not be instantaneously available to cells and tissues like free drugs. This could explain why DOX- and SIM-DOX liposomes also gave reduction in HR and reduced viability of MCF-7 cells in the cell assays following 48 hours incubation, while not after 24 hours (Figure 5.8, 5.15 and Table 5.2). More toxicity assays comparing free and liposomal DOX on zebrafish larvae should have been conducted over a 48-hour period as well as 24 hours since DOX- and SIM-DOX liposomes were observed to be more toxic after 48 hours of incubation (Figure 5.15). SIM is a prodrug, and it is not known whether the cardioprotective effect requires the active component of the drug, which could be a limitation in the drug being encapsulated in liposomes. However, a cardioprotective effect was observed in the H9C2 cardiomyoblast cells upon co-treatment of SIM and DOX, so it is assumed that this active component is not necessary or that SIM also can be converted to its active form in non-hepatic cells.

In order to find whether tissues could be affected by liposomal drugs, it was important to know the fate of the intravenously injected liposomes. When injecting ATTO-488 DPPE labeled DOX liposomes in zebrafish larvae, the liposomes were initially observed to flow free in the vascular system, but already in the first images at a two to four hpi, the green fluorescence tended to accumulate in spots along the vasculature, as likely to be in macrophages. Evensen et al. illustrated this in one study, where pegylated liposomes were seen to be continuously removed from the circulation and entering macrophages over 72 hours (131). The liposomes in that study appeared to be completely cleared from the circulation after 70 hours, while the fluorescence of liposomes was still present in macrophages at this point (131). Following one and two dpi in the present study, the number and intensity of the fluorescent spots increased, but there was still green fluorescence observed intravascularly at two dpi, indicating that intact liposomes were still in circulation after two days. The use of liposomal formulations of DOX will increase plasma circulation and give a larger area under the curve compared to equivalent doses of free DOX (132). At the same time a lower peak concentration of available drug in the body could help avoid adverse effects, since DOX will be slowly released from the liposomes, and not be instantaneously available. In the study, the cardioprotective effect of injected liposomes on HR was seen to decline 48 hpi, following the decline of intravascular green fluorescence observed, and the degradation of liposomes inside the zebrafish larvae.

Both yolk sac and PCV injections of MCF-7 cells were performed in the study, and the distribution of injected cells differed based on injection method (Figure 5.18 and 5.19). In literature, cancer cells are seen to metastasize after yolk sac injection in zebrafish larvae already at 24 hpi, and that cancer cell lines with higher migratory capacity more often metastasize out of the yolk sac (133). In other studies, MCF-7 cells have shown little invasive and metastasizing capacity in zebrafish (134, 135). In the present study, the cells usually remained in the yolk sac over the course of two days after yolk sac injections. However, in three zebrafish larvae the fluorescent signal was in fact observed in the tail region of the zebrafish larvae at one and two dpi (Figure 5.18). In Figure 5.18 the area of fluorescent signal is seen to increase over two days as the cells spread across the yolk sac and tail of the larvae (Table 5.3). In the intravenously injected larvae, the cells were observed to spread throughout the vascular system already two to four hpi, before accumulating ventrally in the duct of Cuvier and along the line of the DA and PCV at one and two dpi with the area of fluorescent signal decreasing as the fluorescence seemed to concentrate (Figure 5.19 and Table 5.4). In the study, PCV injections of cells did more often result in visible fluorescence in the zebrafish larvae compared to yolk sac injections. However, the yolk sac injections were interesting as they allowed for mapping the metastasizing potential of the cancer cells. Further microscopic analyses would have been interesting to observe whether the cells adhered to the vasculature and started to form tumors or migrated out of the vasculature. Additionally, injections of both liposomes and MCF-7 in the PCV could have allowed for observations of cell interactions with liposomes. By observing these features, it can be studied whether cancer cell lines behave in zebrafish larvae after xenograft transplantation as they are expected in humans.

As mentioned in the introduction, zebrafish does not have an adaptive immune system at two to four dpf, but they do have an innate immune system including for instance macrophages (136). One difficulty when injecting cells in zebrafish larvae was to verify if the fluorescent events observed were cells, and not cell stain consumed by macrophages as they ingest debris of dead cancer cells, which then were transported around the zebrafish larvae. Evensen et al. observed that fluorescent liposomes were consumed by macrophages (131), and the fluorescent events in the tail regions of the larvae injected with MCF-7 cells in Figure 5.18 and 5.19 appeared to settle at the same area as the green fluorescent liposomes in Figure 5.16, which likely are taken up by macrophages. The zebrafish larvae visualized in Figure 5.20 has a very high increase in fluorescent events from the day of injection to one dpi. It can be argued that

cell remains being consumed by macrophages, also picking up the fluorescence could explain this. Another explanation is that the fluorescent event observed at two to four hpi in Figure 5.20 consist of more cells than apparent in the microscope, which later will spread along the larvae by the blood. In future studies, it would be interesting to fixate and section the larvae for histological analyzes. By for instance using fluorescent monoclonal antibodies binding specifically to human cells it could be determined whether the spots located in the medial tail region in fact were human MCF-7 breast cancer cells metastasizing in the larvae. This was demonstrated by Lee et al. who labeled human melanoma cells using monoclonal antibodies to distinguish these cells from zebrafish cells (137). Further, the use of genetically manipulated zebrafish with mutations like fluorescent endothelium or macrophages could give better indications of the cancer cells whereabouts relative to the vasculature and interactions with macrophages (131, 134).

Two types of cellular stains, DiI and CTG, were used in the study to visualize injected cells in the zebrafish larvae. One of the main benefits with CTG is that the stain is non-fluorescent until it has entered the cells, where it is converted into the fluorescent product (Section 3.8). Consequently, all fluorescence observed in confocal microscope is intracellular. Additionally, in this study the images obtained with CTG allowed for clearer visualization of single cells (Figure 5.17), while the fluorescent signals obtained with DiI was so strong that it was difficult to distinguish separate cells located close together (Figure 5.18). The DiI stain also caused the injection medium to be lightly fluorescent, giving weak fluorescent signals in the area around the cell injections in the zebrafish larvae. This made quantification of the cell mass inside zebrafish larvae difficult, as this background fluorescence had to be filtered out. One clear disadvantage with CTG however, was the short duration of the signal visible in the microscope. In the first test using CTG stain the cells were only visible at the day of injection (Figure 5.17). In the second test the incubation time of the staining was doubled. That made it possible to observe some cells at one dpi as well, but the signal was very weak (Figure 5.21 and 5.22). The stain could be more light sensitive than the DiI stain, and care had to be taken to protect the larvae from light. Optionally, too few CTG molecules were present in cells after cell division to be detected. Strouse et al. found CTG to be a substrate for both multidrug resistance protein 1 and breast cancer resistance protein (138), and CTG could have been pumped out of the cells by such proteins. This would not be a problem with DiI which is a cell membrane stain, and not present in the cytosol as CTG.

Due to the covid-19 pandemic, some tests had to be terminated before completion as the university was closed, and some tests that were planned could not be conducted. In the present study, the experiments that were most affected by the lock-down were the planned injections of both MCF-7 cells and DOX liposomes to observe therapeutic effect. The plan was to do a larger study with MCF-7 cells injected both in the yolk sac and PCV, and thereafter inject free DOX and DOX liposomes. From this, we could observe whether free DOX and DOX liposomes affected growth and metastasis of the MCF-7 cells in zebrafish larvae, and also whether the liposomes associated, or accumulated close to the cancer cells. The results from the one test that was executed is displayed in Figure 5.23. Here MCF-7 cells were injected in the yolk sac and liposomes into the PCV. No interaction between the liposomes and cells were observed. This was expected since the liposomes will not be able to enter the yolk sac. The cells did not metastasize beyond the yolk sac, but the fluorescent events were observed to approximately double in both number and area (Table 5.6). One last experiment was attempted with yolk sac injections of MCF-7 and further injecting half of the recipients with free DOX in PCV, to study whether a therapeutic effect was observed. However, the test failed as cancer cells only were observed in three of the forty injected larvae, probably because the cancer cells clogged the microinjection pipette. Because of a limited number of recipients of MCF-7 cells in combination with DOX liposomes in the study, it cannot be concluded whether the liposomes affected cancer cell survival or metastasizing activity inside zebrafish larvae.

7 Conclusion and further work

The cardioprotective effect of liposomal drug formulations intended for cancer therapy were tested on zebrafish larvae, and there was a clear cardioprotective effect observed from encapsulating DOX in liposomes. However, over longer periods of time the cardioprotective effect diminished, presumably due to degradation of the liposomes. This must be evaluated further in zebrafish larvae. The cell assays supported the theory of increased liposome toxicity over time, where high-dose SIM-DOX liposomes decreased viability of MCF-7 over 48 hours, while not after 24 hours. Whether this is due to the drug being released from liposomes into the cell medium, prolonged uptake by the cells or a delayed cytotoxic mechanism is not known.

Additionally, the possible cardioprotective effect of SIM co-therapy with DOX treatment was explored. The cell assays showed increased viability of H9C2 cardiomyoblasts following exposure to high doses of free DOX and SIM compared to free DOX alone, indicating a cardioprotective effect of SIM co-treatment. In zebrafish larvae, however, a cardioprotective effect was not observed. The co-treatment appeared to give lower incidence of PCE in zebrafish larvae receiving DOX and SIM. These data can be improved by increasing the number of experiments to better establish the rate of PCE, and also by finding the optimal SIM-DOX ratio to verify this effect. Dose escalation tests of SIM liposomes should be conducted to find the MTD of SIM liposomes and also find the optimum SIM-DOX ratio for observation of a possible cardioprotective effect in zebrafish larvae.

Zebrafish larvae were also tested as a model for cancer by utilizing xenograft transplantations of MCF-7 cells. The fluorescent signal used to stain the cells was observed to be present and to redistribute inside the zebrafish larvae, but more detailed microscopic analysis of the MCF-7 injected recipients should be done to confirm the presence and movements of MCF-7 cells, and that the observed fluorescent signals were in fact viable cells metastasizing in the larvae. The effect of DOX liposomes were to be tested on MCF-7 injected zebrafish larvae, but due to limited laboratory time, no concluding results were achieved. However, during the work with this thesis, the necessary methods have been established, and preliminary experiments conducted of DOX-SIM toxicity and xenograft transplantations in zebrafish larvae, paving the way for more advanced experiments in the near future.

Taken together, this study has demonstrated the power of the zebrafish model in toxicity of DOX and SIM, and as a cancer model for xenograft transplantations of MCF-7. Fluorescent signal from DiI and CTG stained MCF-7 cells was observed after injection of the cells in zebrafish larvae, but further experiments are required to confirm the presence and movement of live cancer cells. Liposomal DOX was observed to give less cardiac adverse effects than free DOX in zebrafish larvae, but the addition of SIM to the treatment did not provide further cardioprotective effects. Zebrafish larvae proves to be a more robust model than cells in revealing adverse effects of drugs, since toxic effects beyond cell death and proliferation can be observed, and experiments of how the drugs affects the entire organs and tissue can be conducted.

8 References

1. Cancer WHO: World Health Organization; 2018 [updated Sep 12. 2018; cited 2020 Feb 19.]. Available from: https://www.who.int/news-room/fact-sheets/detail/cancer.

2. Rang HP, Ritter JM, Flower RJ, Henderson G. Rang & Dale's Pharmacology. 8. ed: Elsevier; 2014.

3. Christiansen J, Rajasekaran AK. Biological impediments to monoclonal antibody–based cancer immunotherapy. Molecular Cancer Therapeutics. 2004;3(11):1493.

4. Singh N, Shi J, June CH, Ruella M. Genome-Editing Technologies in Adoptive T Cell Immunotherapy for Cancer. Curr Hematol Malig Rep. 2017;12(6):522-9.

5. Remesh A. Toxicities of anticancer drugs and its management. International Journal of Basic & Clinical Pharmacology. 2017;1(1):11.

6. Le Tourneau C, Lee JJ, Siu LL. Dose escalation methods in phase I cancer clinical trials. J Natl Cancer Inst. 2009;101(10):708-20.

7. Sleijfer S, Wiemer E. Dose Selection in Phase I Studies: Why We Should Always Go for the Top. Journal of Clinical Oncology. 2008;26(10):1576-8.

8. Chemotherapy Side Effects American Cancer Society: American Cancer Society; [cited 2020 Jun 10.]. Available from: https://www.cancer.org/treatment/treatments-and-side-effects/treatment-types/chemotherapy/chemotherapy-side-effects.html#references.

9. Chakraborty S, Rahman T. The difficulties in cancer treatment. Ecancermedicalscience. 2012;6:ed16-ed.

10. Aslantürk ÖS. In Vitro Cytotoxicity and Cell Viability Assays: Principles, Advantages, and Disadvantages. Genotoxicity - A Predictable Risk to Our Actual World: IntechOpen; 2018. p. 122.

11. Katt ME, Placone AL, Wong AD, Xu ZS, Searson PC. In Vitro Tumor Models: Advantages, Disadvantages, Variables, and Selecting the Right Platform. Frontiers in Bioengineering and Biotechnology. 2016;4(12).

12. Justice BA, Badr NA, Felder RA. 3D cell culture opens new dimensions in cell-based assays. Drug Discov Today. 2009;14(1-2):102-7.

13. Directive 2001/83/EC of the European Parliament and of the Council of 6 November 2001 on the Community code relating to medicinal products for human use, (2001).

14. Arcamone F, Cassinelli G, Fantini G, Grein A, Orezzi P, Pol C, et al. Adriamycin, 14-hydroxydaimomycin, a new antitumor antibiotic from S. Peucetius var. caesius. Biotechnology and Bioengineering. 1969;11(6):1101-10.

15. Cytotoksiske antibiotika Norsk Legemiddelhandbok: Foreningen for utgivelse av Norsk legemiddelhåndbok; 2015 [updated Dec 18. 2015; cited 2019 Dec 17.]. Available from: https://www.legemiddelhandboka.no/L2.1.4/Cytotoksiske_antibiotika.

16. Han Y, Zhang JP, Qian JQ, Hu CQ. Cardiotoxicity evaluation of anthracyclines in zebrafish (Danio rerio). J Appl Toxicol. 2015;35(3):241-52.

17. Doksorubicin Norsk Legemiddelhandbok: Foreningen for utgivelse av Norsk legemiddelhåndbok; 2016 [updated Apr 20. 2016; cited 2019 Dec 17.]. Available from: https://www.legemiddelhandboka.no/L2.1.4.1/Doksorubicin.

18. Weiss RB. The anthracyclines: will we ever find a better doxorubicin? Semin Oncol. 1992;19(6):670-86.

19. Brinch L. Behandling av akutt lymfatisk leukemi Oncolex - onkologisk oppslagsverk: Oncolex; 2010 [updated Jan 22. 2010; cited 2020 Jan 18.]. Available from: http://oncolex.no/Leukemi/Prosedyrekatalog/Behandling/Medikamentell-behandling/ALL?lg=procedure&chapter=2.

20. Kaklamani VG, Gradishar WJ. Epirubicin Versus Doxorubicin: Which Is the Anthracycline of Choice for the Treatment of Breast Cancer? Clinical Breast Cancer. 2003;4:S26-S33.

21. Yang F, Lei Q, Li L, He JC, Zeng J, Luo C, et al. Delivery of epirubicin via slow infusion as a strategy to mitigate chemotherapy-induced cardiotoxicity. PLoS One. 2017;12(11):e0188025-e.

22. Cerubidin «Sanofi-Aventis» Felleskatalogen: Legemiddelindustrien; 2019 [updated Nov 25. 2019; cited 2020 Apr 14.]. Available from: https://www.felleskatalogen.no/medisin/cerubidin-sanofi-aventis-547410.

23. Zavedos «Pfizer» Felleskatalogen: Legemiddelindustrien; [updated Oct 10. 2018; cited 2020 Apr 14.]. Available from: https://www.felleskatalogen.no/medisin/zavedos-pfizer-565616.

24. Lee JH, Kim H, Joo YD, Lee WS, Bae SH, Zang DY, et al. Prospective Randomized Comparison of Idarubicin and High-Dose Daunorubicin in Induction Chemotherapy for Newly Diagnosed Acute Myeloid Leukemia. J Clin Oncol. 2017;35(24):2754-63.

25. Owattanapanich W, Owattanapanich N, Kungwankiattichai S, Ungprasert P, Ruchutrakool T. Efficacy and Toxicity of Idarubicin Versus High-dose Daunorubicin for Induction Chemotherapy in Adult Acute Myeloid Leukemia: A Systematic Review and Meta-analysis. Clinical Lymphoma Myeloma and Leukemia. 2018;18(12):814-21.e3.

26. Chatterjee K, Zhang J, Honbo N, Karliner JS. Doxorubicin cardiomyopathy. Cardiology. 2010;115(2):155-62.
27. Lefrak EA, Piťha J, Rosenheim S, Gottlieb JA. A clinicopathologic analysis of adriamycin cardiotoxicity. Cancer. 1973;32(2):302-14.
28. Takemura G, Fujiwara H. Doxorubicin-induced cardiomyopathy from the cardiotoxic mechanisms to management. Philadelphia: Progress in Cardiovascular Diseases; 2007. p. 330-52.
29. Swain SM, Whaley FS, Ewer MS. Congestive heart failure in patients treated with doxorubicin: A retrospective analysis of three trials. Cancer. 2003;97(11):2869-79.
30. Jones RL, Swanton C, Ewer MS. Anthracycline cardiotoxicity. Expert Opinion on Drug Safety. 2006;5(6):791-809.
31. Henninger C, Fritz G. Statins in anthracycline-induced cardiotoxicity: Rac and Rho, and the heartbreakers. Cell Death Dis. 2018;8(1):e2564-e.
32. Henriksen PA. Anthracycline cardiotoxicity: an update on mechanisms, monitoring and prevention. Heart. 2018;104(12):971-7.
33. Wallace KB. Doxorubicin-Induced Cardiac Mitochondrionopathy. Pharmacology & Toxicology. 2003;93(3):105-15.
34. Mordente A, Meucci E, Silvestrini A, Martorana GE, Giardina B. Anthracyclines and Mitochondria. In: Scatena R, Bottoni P, Giardina B, editors. Advances in Mitochondrial Medicine. Dordrecht: Springer Netherlands; 2012. p. 385-419.
35. Hyperlipidemi Norsk Legemiddelhandbok: Foreningen for utgivelse av Norsk legemiddelhåndbok; 2016 [updated Sep 09. 2017; cited 2020 Feb 5.]. Available from: https://www.legemiddelhandboka.no/T8.13/Hyperlipidemi.
36. Reseptregisteret [Internet]. Folkehelseinstituttet. 2018. Available from: http://reseptregisteret.no/default.aspx.
37. Statiner Legemiddelhandboka: Foreningen for utgivelse av Norsk legemiddelhåndbok; 2017 [updated Jan 25. 2017; cited 2020 May 22.]. Available from: https://www.legemiddelhandboka.no/L8.15.1/Statiner.
38. Compound Summary - Simvastatin PubChem: U.S. National Library of Medicine; [updated Mar 21. 2020; cited 2020 Mar 27.]. Available from: https://pubchem.ncbi.nlm.nih.gov/compound/Simvastatin.

39. MSD. Zocor MSD - Summary of Product Characteristics (SPC) [updated Aug 26. 2019; cited 2020 Mar 27.]. Available from: https://www.legemiddelsok.no/_layouts/15/Preparatomtaler/Spc/0000-07907.pdf.
40. Rautio J, Kumpulainen H, Heimbach T, Oliyai R, Oh D, Järvinen T, et al. Prodrugs: design and clinical applications. Nature Reviews Drug Discovery. 2008;7(3):255-70.
41. Liao JK, Laufs U. Pleiotropic effects of statins. Annu Rev Pharmacol Toxicol. 2005;45:89-118.
42. Feleszko W, Młynarczuk I, Bałkowiec-Iskra EZ, Czajka A, Świtaj T, Stokłosa T, et al. Lovastatin Potentiates Antitumor Activity and Attenuates Cardiotoxicity of Doxorubicin in Three Tumor Models in Mice. Clinical Cancer Research. 2000;6(5):2044-52.
43. Allhoff F, Lin P, Moore D. What is nanotechnology and why does it matter : from science to ethics. Malden, MA: Wiley- Blackwell; 2010.
44. Definition of a Nanomaterial European Commision: European Commision of the European Union; 2019 [updated Aug 07. 2019; cited 2020 Mar 27.]. Available from: https://ec.europa.eu/environment/chemicals/nanotech/faq/definition_en.htm.
45. Yingchoncharoen P, Kalinowski DS, Richardson DR. Lipid-Based Drug Delivery Systems in Cancer Therapy: What Is Available and What Is Yet to Come. Pharmacol Rev. 2016;68(3):701-87.
46. Khan I, Saeed K, Khan I. Nanoparticles: Properties, applications and toxicities. Arabian Journal of Chemistry. 2019;12(7):908-31.
47. Cho K, Wang X, Nie S, Chen ZG, Shin DM. Therapeutic nanoparticles for drug delivery in cancer. Clinical cancer research : an official journal of the American Association for Cancer Research. 2008;14(5):1310.
48. Wang EC, Wang AZ. Nanoparticles and their applications in cell and molecular biology. Integr Biol (Camb). 2014;6(1):9-26.
49. Gelderblom H, Verweij J, Nooter K, Sparreboom A. Cremophor EL: the drawbacks and advantages of vehicle selection for drug formulation. Eur J Cancer. 2001;37(13):1590-8.
50. Cucinotto I, Fiorillo L, Gualtieri S, Arbitrio M, Ciliberto D, Staropoli N, et al. Nanoparticle albumin bound Paclitaxel in the treatment of human cancer: nanodelivery reaches prime-time? J Drug Deliv. 2013;2013:905091-.
51. Feng T, Wei Y, Lee RJ, Zhao L. Liposomal curcumin and its application in cancer. International journal of nanomedicine. 2017;12:6027-44.

52. Singh A, Myklebust NN, Furevik SMV, Haugse R, Herfindal L. Immunoliposomes in Acute Myeloid Leukaemia Therapy: An Overview of Possible Targets and Obstacles. Curr Med Chem. 2019;26(28):5278-92.
53. Sercombe L, Veerati T, Moheimani F, Wu S, Sood A, Hua S. Advances and Challenges of Liposome Assisted Drug Delivery. Front Pharmacol. 2015;6.
54. De Jong W, Borm P. Drug delivery and nanoparticles: Applications and hazards. International Journal of Nanomedicine. 2008;3(2):133-49.
55. Barenholz Y. Doxil® — The first FDA-approved nano-drug: Lessons learned. Journal of Controlled Release. 2012;160(2):117-34.
56. Iyer AK, Khaled G, Fang J, Maeda H. Exploiting the enhanced permeability and retention effect for tumor targeting. Drug Discovery Today. 2006;11(17):812-8.
57. Salimi A. Liposomes as a novel drug delivery system: fundamental and pharmaceutical application. Asian Journal of Pharmaceutics (AJP): Free full text articles from Asian J Pharm. 2018;12(01).
58. Bozzuto G, Molinari A. Liposomes as nanomedical devices. International Journal of Nanomedicine. 2015;10:975.
59. Aulton ME, Taylor K. Aulton's pharmaceutics : the design and manufacture of medicines. Fifth edition. ed. Amsterdam: Elsevier; 2018.
60. Mayer L, Bally M, Cullis P. Uptake of adriamycin into large unilamellar vesicles in response to a pH gradient. Biochimica Et Biophysica Acta (BBA)-Biomembranes. 1986;857(1):123-6.
61. Abraham SA, Waterhouse DN, Mayer LD, Cullis PR, Madden TD, Bally MB. The Liposomal Formulation of Doxorubicin: Elsevier Science & Technology; 2005. 71-97 p.
62. Letrado P, de Miguel I, Lamberto I, Diez-Martinez R, Oyarzabal J. Zebrafish: Speeding Up the Cancer Drug Discovery Process. Cancer Res. 2018;78(21):6048-58.
63. Bambino K, Chu J. Zebrafish in Toxicology and Environmental Health. Current topics in developmental biology. 2017;124:331-67.
64. Howe K, Clark MD, Torroja CF, Torrance J, Berthelot C, Muffato M, et al. The zebrafish reference genome sequence and its relationship to the human genome. Nature. 2013;496(7446):498-503.
65. Long HK, Sims D, Heger A, Blackledge NP, Kutter C, Wright ML, et al. Epigenetic conservation at gene regulatory elements revealed by non-methylated DNA profiling in seven vertebrates. eLife. 2013;2:e00348.

66. Kanungo J, Cuevas E, Ali SF, Paule MG. Zebrafish model in drug safety assessment. Curr Pharm Des. 2014;20(34):5416-29.
67. Willett CE, Cortes A, Zuasti A, Zapata AG. Early hematopoiesis and developing lymphoid organs in the zebrafish. Developmental Dynamics. 1999;214(4):323-36.
68. Asnani A, Peterson RT. The zebrafish as a tool to identify novel therapies for human cardiovascular disease. Disease Models & Mechanisms. 2014;7(7):763-7.
69. Santoriello C, Zon LI. Hooked! Modeling human disease in zebrafish. The Journal of Clinical Investigation. 2012;122(7):2337-43.
70. Langenau DM. Cancer and Zebrafish : Mechanisms, Techniques, and Models. Cham: Springer International Publishing : Imprint: Springer; 2016.
71. Westerfield M. The Zebrafish book. A guide for the laboratory use of zebrafish (Danio Rerio). Chapter 3 - Embryonic and Larval culture University of Oregon, Eugene: University of Oregon Press; 2000 [4th ed. :[Available from: https://zfin.org/zf_info/zfbook/zfbk.html.
72. Kimmel CB, Ballard WW, Kimmel SR, Ullmann B, Schilling TF. Stages of embryonic development of the zebrafish. Developmental dynamics : an official publication of the American Association of Anatomists. 1995;203(3):253.
73. Henn K, Braunbeck T. Dechorionation as a tool to improve the fish embryo toxicity test (FET) with the zebrafish (Danio rerio). Comparative Biochemistry and Physiology Part C: Toxicology & Pharmacology. 2011;153(1):91-8.
74. Avdesh A, Chen M, Martin-Iverson MT, Mondal A, Ong D, Rainey-Smith S, et al. Regular care and maintenance of a zebrafish (Danio rerio) laboratory: an introduction. J Vis Exp. 2012(69):e4196.
75. Directive 2010/63/EU of the European Parliament and of the Council of 22 september 2010 on the protection of animals used for scientific purposes, (2010).
76. Rafferty SA, Quinn TA. A beginner's guide to understanding and implementing the genetic modification of zebrafish. Progress in Biophysics and Molecular Biology. 2018;138:3-19.
77. Lawson ND, Weinstein BM. In Vivo Imaging of Embryonic Vascular Development Using Transgenic Zebrafish. 2002. p. 307-18.
78. Karlsson J, von Hofsten J, Olsson P-E. Generating Transparent Zebrafish: A Refined Method to Improve Detection of Gene Expression During Embryonic Development. Marine Biotechnology. 2001;3(6):522-7.

79. D'agati G, Beltre R, Sessa A, Burger A, Zhou Y, Mosimann C, et al. A defect in the mitochondrial protein Mpv17 underlies the transparent casper zebrafish. Developmental Biology. 2017;430(1):11-7.
80. MacRae CA, Peterson RT. Zebrafish as tools for drug discovery. Nature Reviews Drug Discovery. 2015;14(10):721-31.
81. Boston Children's Hospital. Drug developed based on zebrafish studies passes Phase I clinical trial ScienceDaily2013 [cited 2020 Feb 20.]. Available from: https://www.sciencedaily.com/releases/2013/10/131021131011.htm.
82. North TE, Goessling W, Walkley CR, Lengerke C, Kopani KR, Lord AM, et al. Prostaglandin E2 regulates vertebrate haematopoietic stem cell homeostasis. Nature. 2007;447(7147):1007-11.
83. Goldstone JV, McArthur AG, Kubota A, Zanette J, Parente T, Jönsson ME, et al. Identification and developmental expression of the full complement of Cytochrome P450 genes in Zebrafish. BMC Genomics. 2010;11(1):643.
84. Stanton MF. Diethylnitrosamine-Induced Hepatic Degeneration and Neoplasia in the Aquarium Fish, Brachydanio rerio. JNCI: Journal of the National Cancer Institute. 1965;34(1):117-30.
85. Wertman J, Veinotte CJ, Dellaire G, Berman JN. The Zebrafish Xenograft Platform: Evolution of a Novel Cancer Model and Preclinical Screening Tool. Advances in experimental medicine and biology. 2016;916:289.
86. Ceol CJ, Houvras Y. Uncharted Waters: Zebrafish Cancer Models Navigate a Course for Oncogene Discovery. Advances in experimental medicine and biology. 2016;916:3.
87. Mayrhofer M, Mione M. The Toolbox for Conditional Zebrafish Cancer Models. Advances in experimental medicine and biology. 2016;916:21.
88. Moore JC, Langenau DM. Allograft Cancer Cell Transplantation in Zebrafish. Advances in experimental medicine and biology. 2016;916:265.
89. Tulotta C, He S, van Der Ent W, Chen L, Groenewoud A, Spaink HP, et al. Imaging Cancer Angiogenesis and Metastasis in a Zebrafish Embryo Model. Advances in experimental medicine and biology. 2016;916:239.
90. Survival Rates for Breast Cancer American Cancer Society: American Cancer Society; [updated Jan 8., 2020; cited 2020 Jun 3.]. Available from: https://www.cancer.org/cancer/breast-cancer/understanding-a-breast-cancer-diagnosis/breast-cancer-survival-rates.html#references.

91. Hansen SH. HPLC/UHPLC. In: Müllertz A, Perrie Y, Rades T, editors. Analytical Techniques in the Pharmaceutical Sciences. New York, NY: Springer New York; 2016. p. 413-37.
92. Buxbaum E. Chromatography. Biophysical Chemistry of Proteins: An Introduction to Laboratory Methods. Boston, MA: Springer US; 2011. p. 147-62.
93. Østergaard J. UV/Vis Spectrophotometry and UV Imaging. In: Müllertz A, Perrie Y, Rades T, editors. Analytical Techniques in the Pharmaceutical Sciences. New York, NY: Springer New York; 2016. p. 3-27.
94. Reich G. Mid and Near Infrared Spectroscopy. In: Müllertz A, Perrie Y, Rades T, editors. Analytical Techniques in the Pharmaceutical Sciences. New York, NY: Springer New York; 2016. p. 61-138.
95. Simplified analysis of lipid or detergent content in biological samples using the IR-based Direct Detect® Spectrometer Merck Millipore: Merck Millipore; [cited 2020 Mar 20.]. Available from: https://www.merckmillipore.com/NO/en/life-science-research/protein-detection-quantification/direct-detect-spectrometer/applications/lipid-analysis/hGOb.qB.KHkAAAFB3eARRkxC,nav.
96. Ross Hallett F. Particle size analysis by dynamic light scattering. Food Research International. 1994;27(2):195-8.
97. Bigg C. Brownian Motion. In: Greenberger D, Hentschel K, Weinert F, editors. Compendium of Quantum Physics. Berlin, Heidelberg: Springer Berlin Heidelberg; 2009. p. 81-4.
98. Zetasizer Nano ZS Malvern Panalytical: Malvern Panalytical; [cited 2020 Mar 25.]. Available from: https://www.malvernpanalytical.com/en/products/product-range/zetasizer-range/zetasizer-nano-range/zetasizer-nano-zs#howitworks.
99. Kastner E, Perrie Y. Particle Size Analysis of Micro and Nanoparticles. In: Müllertz A, Perrie Y, Rades T, editors. Analytical Techniques in the Pharmaceutical Sciences. New York, NY: Springer New York; 2016. p. 677-99.
100. Shannon RR, Ford BJ. Microscope. Encyclopædia Britannica, inc Encyclopædia Britannica2019.
101. Confocal Microscopy Ibidi: Ibidi; [cited 2020 Apr 22.]. Available from: https://ibidi.com/content/216-confocal-microscopy.
102. Oreopoulos J, Berman R, Browne M. Chapter 9 - Spinning-disk confocal microscopy: present technology and future trends: Elsevier Science & Technology; 2014. 153-75 p.

103. Holtebekk T. Fluorescens Store Norske Leksikon2019 [updated Oct 28. 2019; cited 2020 Jan 8.]. Available from: https://snl.no/fluorescens.

104. Fluorescence Encyclopædia Britannica: Encyclopædia Britannica, inc.; 2017 [cited 2020 Jan 8.]. Available from: https://www.britannica.com/science/fluorescence.

105. Kaur G, Dufour JM. Cell lines: Valuable tools or useless artifacts. Spermatogenesis. 2012;2(1):1-5.

106. Introduction to Cell Culture ThermoFisher Scientific: ThermoFisher; [cited 2020 Apr 22.]. Available from: https://www.thermofisher.com/no/en/home/references/gibco-cell-culture-basics/introduction-to-cell-culture.html.

107. Soule HD, Vazquez J, Long A, Albert S, Brennan M. A Human Cell Line From a Pleural Effusion Derived From a Breast Carcinoma2. JNCI: Journal of the National Cancer Institute. 1973;51(5):1409-16.

108. Kimes BW, Brandt BL. Properties of a clonal muscle cell line from rat heart. Experimental Cell Research. 1976;98(2):367-81.

109. Protocol Guide: WST-1 Assay for Cell Proliferation and Viability Merck Life Science Merck; [cited 2020 Mar 18.]. Available from: https://www.sigmaaldrich.com/technical-documents/protocols/biology/roche/cell-proliferation-reagent-wst-1.html.

110. InvitrogenTM. Product Information Sheet: Lipophilic Tracers—DiI, DiO, DiD, DiA, and DiR ThermoFisher Scientific2008 [updated June 26. 2008; cited 2020 Mar 25.]. Available from: https://www.thermofisher.com/document-connect/document-connect.html?id=man0001776&version=1.0&pdfurl=https%3A%2F%2Fassets.thermofisher.com%2FTFS-Assets%2FLSG%2Fmanuals%2Fmp00282.pdf&title=TGlwb3BoaWxpYyBUcmFjZXJzICYjMTUxOyBEaUksIERpTywgRGlELCBEaUEgYW5kIERpUg==.

111. InvitrogenTM. Product Information Sheet: CellTrackerTM fluorescent probes [cited 2020 Feb 24.]. Available from: https://www.thermofisher.com/document-connect/document-connect.html?url=https%3A%2F%2Fassets.thermofisher.com%2FTFS-Assets%2FLSG%2Fmanuals%2FMAN0001826_CellTracker_Probes_PI.pdf&title=UHJvZHVjdCBTaGVldDogQ2VsbFRyYWNrZXIgRmx1b3Jlc2NlbnQgUHJvYmVz.

112. Förster F, Volz A, Fricker G. Compound profiling for ABCC2 (MRP2) using a fluorescent microplate assay system. European Journal of Pharmaceutics and Biopharmaceutics. 2008;69(1):396-403.

113. 2 Membrane-Permeant Reactive Tracers for Long-Term Cell Labeling Thiol-Reactive CellTracker Probes2002.
114. Knudsen KS, Universitetet i Bergen Kjemisk i. Development of nanocarriers for co-delivery of statins and anthracyclines. Bergen: Department of Chemistry, University of Bergen; 2017.
115. MCF7 Cell Line Human Merck: Merck; [cited 2020 Jun 10.]. Available from: https://www.sigmaaldrich.com/catalog/product/sigma/cb_86012803?lang=en&region=NO.
116. H9C2 (2-1) Cell Line from rat Merck: Merck; [cited 2020 Jun 10.]. Available from: https://www.sigmaaldrich.com/catalog/product/sigma/cb_88092904?lang=en&region=NO.
117. Gonzales JM, Jr. Preliminary evaluation on the effects of feeds on the growth and early reproductive performance of zebrafish (Danio rerio). J Am Assoc Lab Anim Sci. 2012;51(4):412-7.
118. Westerfield M. CHAPTER 1: GENERAL METHODS FOR ZEBRAFISH CARE The Zebrafish Information Network [cited 2019 oct. 23]. Available from: https://zfin.org/zf_info/zfbook/chapt1/1.3.html.
119. Westerfield M. The Zebrafish book. A guide for the laboratory use of zebrafish (Danio Rerio). CHAPTER 4 - MICROSCOPIC OBSERVATIONS. Removing embryos from their chorions. University of Oregon, Eugene: University of Oregon Press; 2000 [4th ed. :[Available from: https://zfin.org/zf_info/zfbook/zfbk.html.
120. Dunn N, Eagle A. TRICAINE [web page]. The zebrafish information network2018 [updated Jan 18, 2018; cited 2019 oct 21]. Available from: https://wiki.zfin.org/display/prot/TRICAINE.
121. Myhren L, Nilssen IM, Nicolas V, Døskeland SO, Barratt G, Herfindal L. Efficacy of multi-functional liposomes containing daunorubicin and emetine for treatment of acute myeloid leukaemia. European Journal of Pharmaceutics and Biopharmaceutics. 2014;88(1):186-93.
122. Selheim F, Herfindal L, Martins R, Vasconcelos V, Døskeland SO. Neuro-apoptogenic and blood platelet targeting toxins in benthic marine cyanobacteria from the Portuguese coast. Aquat Toxicol. 2005;74(4):294-306.
123. Benzodiazepines on Ascentis® Express Phenyl Hexyl HPLC Columns Merck: Merck Millipore; [cited 2020 Jun 10.]. Available from: https://www.sigmaaldrich.com/technical-documents/articles/analytical/brochures/phenyl-hexyl-hplc-columns.html.

124. Alyane M, Barratt G, Lahouel M. Remote loading of doxorubicin into liposomes by transmembrane pH gradient to reduce toxicity toward H9c2 cells. Saudi Pharm J. 2016;24(2):165-75.
125. Gundersen ET. The production and characterization of drug-loaded liposomal and PLGA nanocarriers for targeted treatment of acute myeloid leukemia. The University of Bergen; 2016.
126. Hovorka O, Šubr V, Větvička D, Kovář L, Strohalm J, Strohalm M, et al. Spectral analysis of doxorubicin accumulation and the indirect quantification of its DNA intercalation. European Journal of Pharmaceutics and Biopharmaceutics. 2010;76(3):514-24.
127. Calienni MN, Cagel M, Montanari J, Moretton MA, Prieto MJ, Chiappetta DA, et al. Zebrafish (Danio rerio) model as an early stage screening tool to study the biodistribution and toxicity profile of doxorubicin-loaded mixed micelles. Toxicology and Applied Pharmacology. 2018;357:106-14.
128. Campos LM, Rios EA, Guapyassu L, Midlej V, Atella GC, Herculano-Houzel S, et al. Alterations in zebrafish development induced by simvastatin: Comprehensive morphological and physiological study, focusing on muscle. Exp Biol Med (Maywood). 2016;241(17):1950-60.
129. Baardman ME, Kerstjens-Frederikse WS, Berger RMF, Bakker MK, Hofstra RMW, Plösch T. The Role of Maternal-Fetal Cholesterol Transport in Early Fetal Life: Current Insights1. Biology of Reproduction. 2013;88(1).
130. Maerz LD, Burkhalter MD, Schilpp C, Wittekindt OH, Frick M, Philipp M. Pharmacological cholesterol depletion disturbs ciliogenesis and ciliary function in developing zebrafish. Commun Biol. 2019;2:31-.
131. Evensen L, Johansen PL, Koster G, Zhu K, Herfindal L, Speth M, et al. Zebrafish as a model system for characterization of nanoparticles against cancer. Nanoscale. 2016;8(2):862-77.
132. Summary of Product Characteristics, Caelyx European Medicines Agency [cited 2019 nov 12.]. Available from: https://www.ema.europa.eu/en/documents/product-information/caelyx-epar-product-information_no.pdf.
133. Konantz M, Balci TB, Hartwig UF, Dellaire G, André MC, Berman JN, et al. Zebrafish xenografts as a tool for in vivo studies on human cancer. Annals of the New York Academy of Sciences. 2012;1266(1):124-37.

134. Berens EB, Sharif GM, Wellstein A, Glasgow E. Testing the Vascular Invasive Ability of Cancer Cells in Zebrafish (Danio Rerio). Journal of visualized experiments : JoVE. 2016(117):55007.

135. Eguiara A, Holgado O, Beloqui I, Abalde L, Sanchez Y, Callol C, et al. Xenografts in zebrafish embryos as a rapid functional assay for breast cancer stem-like cell identification. Cell cycle. 2011;10(21):3751-7.

136. Herbomel P, Thisse B, Thisse C. Ontogeny and behaviour of early macrophages in the zebrafish embryo. Development. 1999;126(17):3735-45.

137. Lee LMJ, Seftor EA, Bonde G, Cornell RA, Hendrix MJC. The fate of human malignant melanoma cells transplanted into zebrafish embryos: Assessment of migration and cell division in the absence of tumor formation. Developmental Dynamics. 2005;233(4):1560-70.

138. Strouse JJ, Ivnitski-Steele I, Waller A, Young SM, Perez D, Evangelisti AM, et al. Fluorescent substrates for flow cytometric evaluation of efflux inhibition in ABCB1, ABCC1, and ABCG2 transporters. Anal Biochem. 2013;437(1):77-87.

9 Appendix

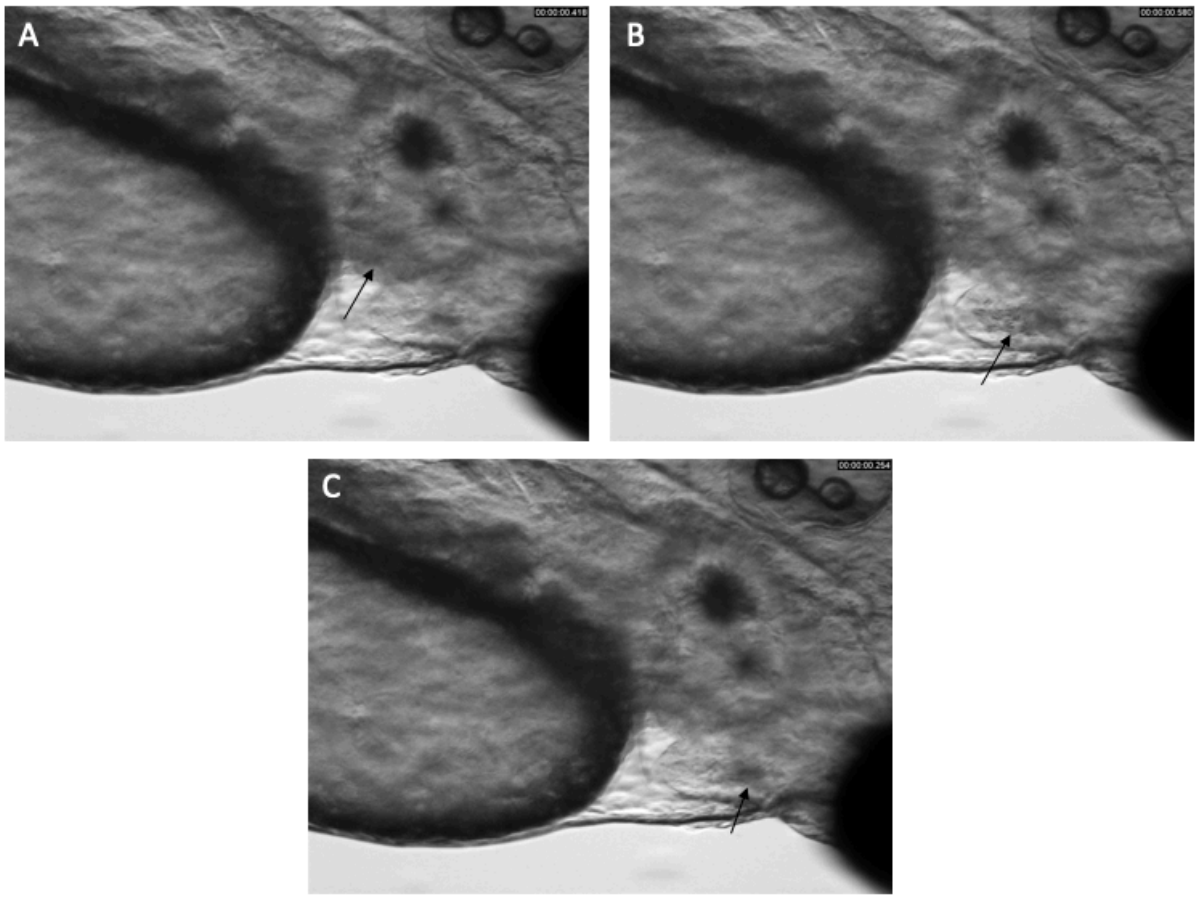

Supplementary Figure 1: Heart contraction of untreated zebrafish larvae. *The zebrafish larvae heart was for the heartrate toxicity assays filmed for ten seconds to calculate beats per minute. The zebrafish larvae were sedated in 0.2 mg/mL tricaine in embryo water and films obtained after placing the zebrafish larvae on an agarose gel. The images show the heartbeat of one zebrafish larva. A: A darker bolus of blood cells is observed in the zebrafish atrium. B: The blood has been pumped into the ventricle. C: The blood is pushed into circulation. Arrows point to the blood cell bolus. Still images captured from a film obtained using a Leica M205 stereo microscope. Scale not provided.*

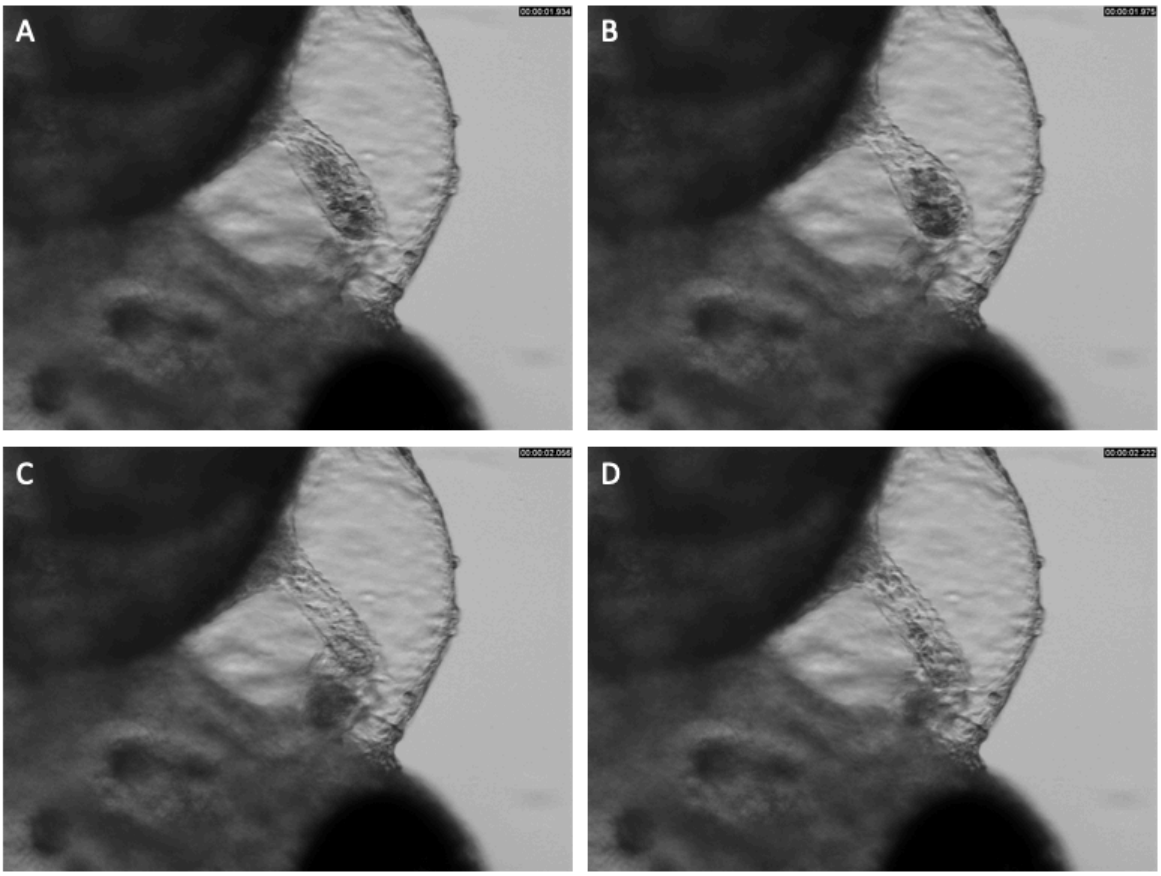

Supplementary Figure 2: Heart contraction of zebrafish larvae with pericardial effusion. *The zebrafish larvae heart was filmed for ten seconds to calculate beats per minute. The zebrafish larvae were sedated in 0.2 mg/mL tricaine in embryo water and films obtained after placing the zebrafish larvae on an agarose gel. The images show the heartbeat of a zebrafish larva pretreated with doxorubicin, and suffering from pericardial effusion as a result. A and B: The atrium is filled up with blood cells. C: The blood cells have entered the ventricle. D: The blood is leaving the ventricle and entering the circulatory system. Still images obtained from a film, using a Leica M205 stereo microscope. Scale not provided.*

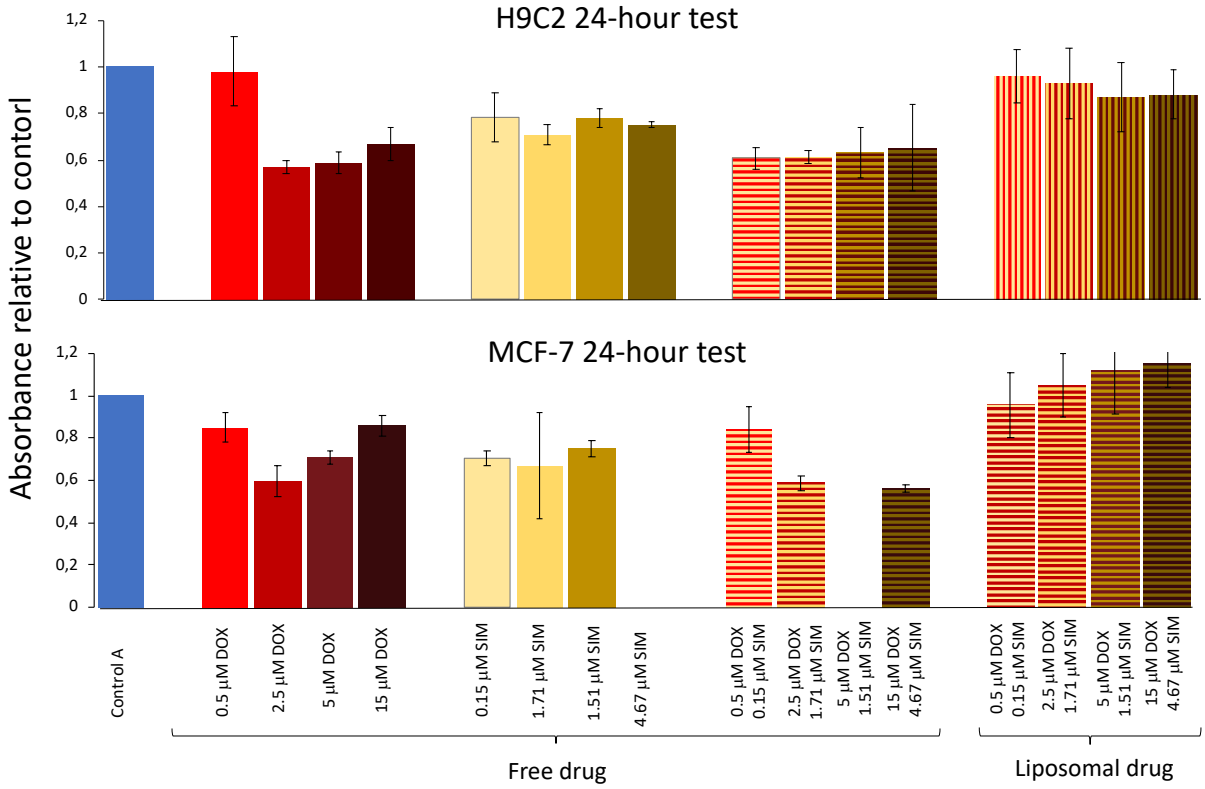

Supplementary Figure 3: WST-1 metabolic activity assay results from experiments with MCF-7 and H9C2 cells. *After 24 hours incubation with DOX, SIM or both, as liposomes or as free drugs, the cells were added ten µL WST-1 and incubated for two hours at 37 °C. The absorbance of MCF-7 and H9C2 was measured at 450 nm. The results are displayed as the relative absorbance at 450 nm in the treated wells compared to the absorbance of the control wells with cells only incubated with cell medium. Some of the wells in the MCF-7 test (4.67 µM SIM free and liposomal, 5 µM DOX free and 1.51 µM SIM free drug wells) were by a mistake not added WST-1 and are not displayed.*

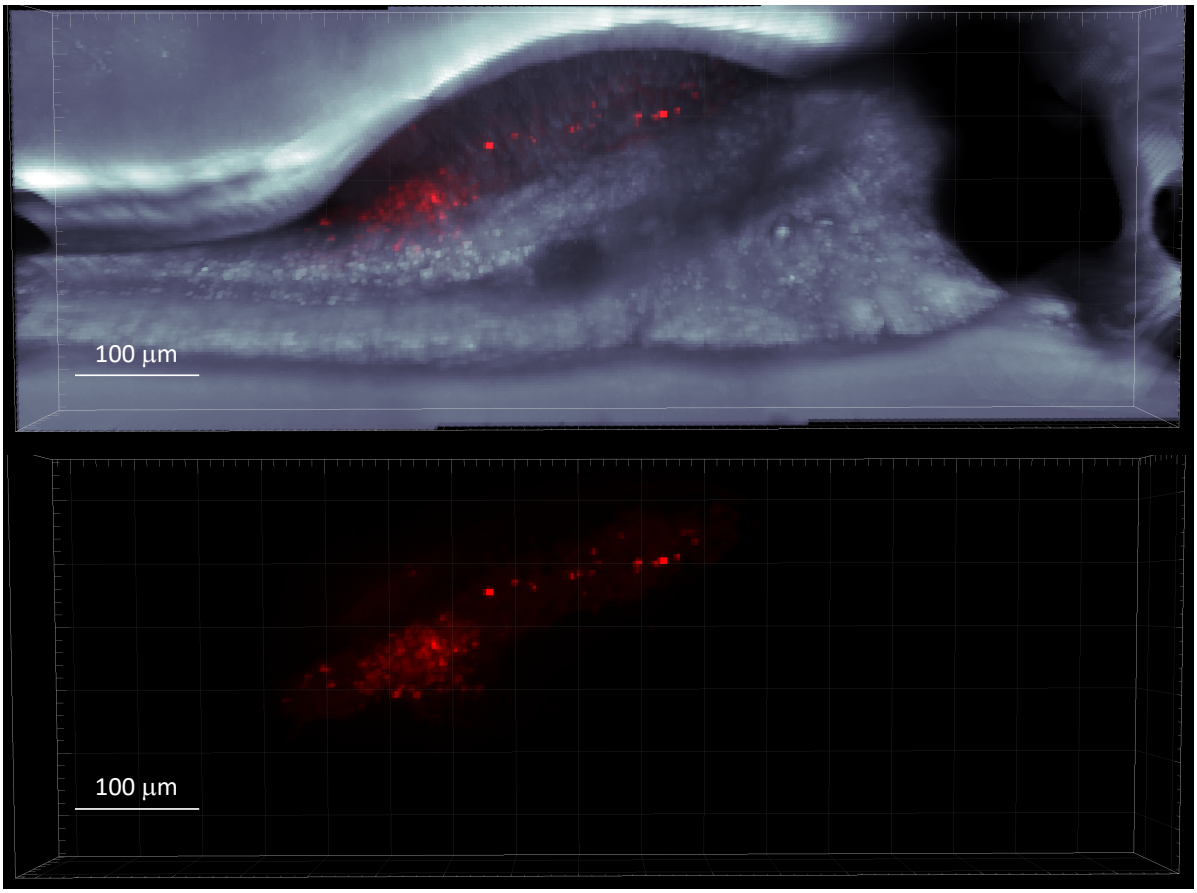

Supplementary Figure 4: DiI stained MOLM-13 injected in zebrafish larvae yolk sac. *DiI stained MOLM-13 acute myeloid leukemia cells were injected into the yolk sac of two days post fertilization zebrafish larvae and observed at one day post injection. The fluorescent signal was observed to be strong at one day post injection and was therefore also utilized to visualize MCF-7 cells. The images were obtained using Andor Dragonfly confocal microscope at 20x magnification. Scale bar: 100 µm*

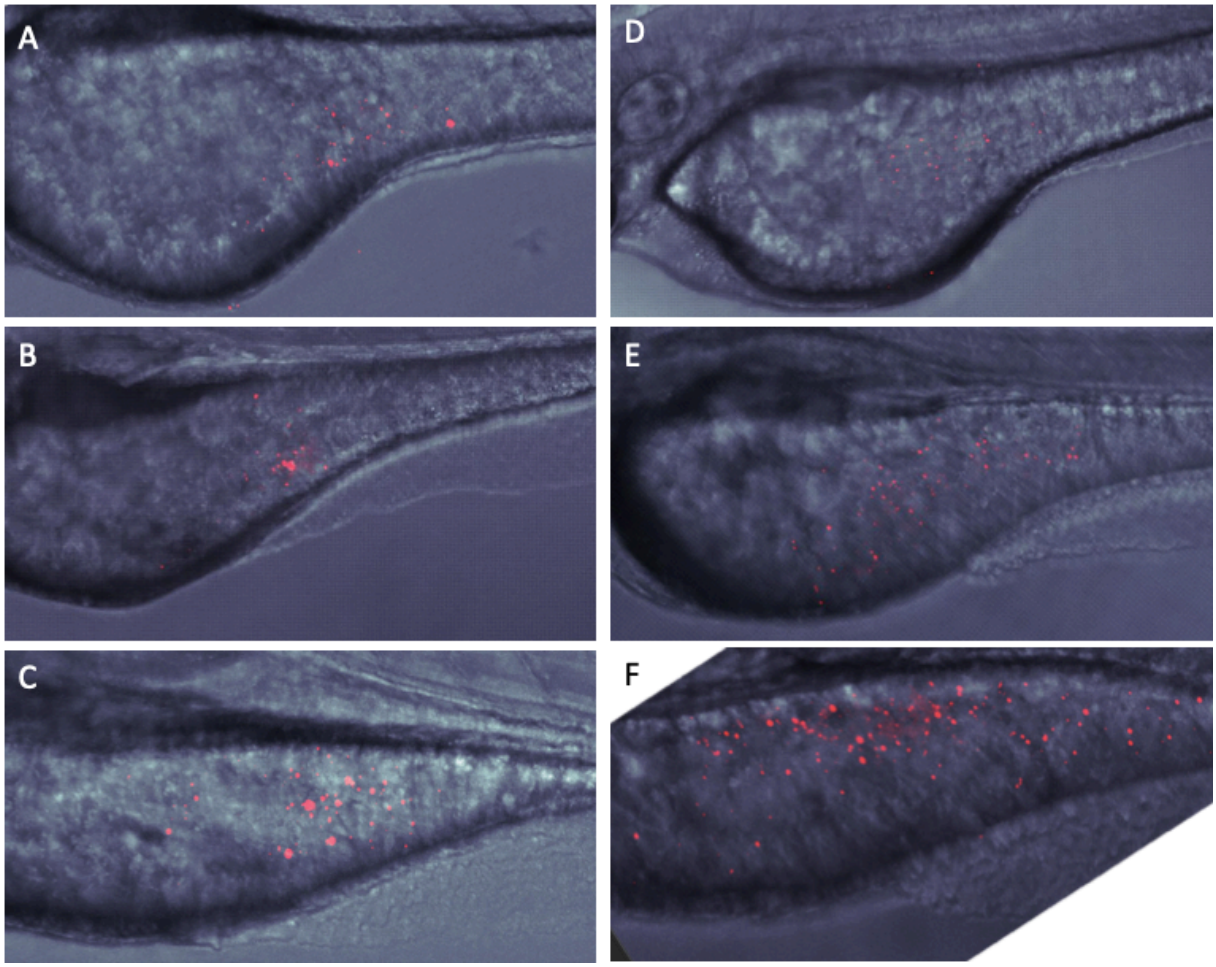

Supplementary Figure 5: DiI stained MCF-7 cells injected into the yolk sac of zebrafish larvae*. Two zebrafish larvae injected with DiI stained MCF-7 cells in the yolk sac at two days post fertilization. A and D: Yolk sac visualized two to four hours post injection. B and E: Yolk sac visualized one day post injection. C and F: Yolk sac visualized two days post injection. The images were obtained using Andor Dragonfly confocal microscope at 10x magnification. Scale not provided.*

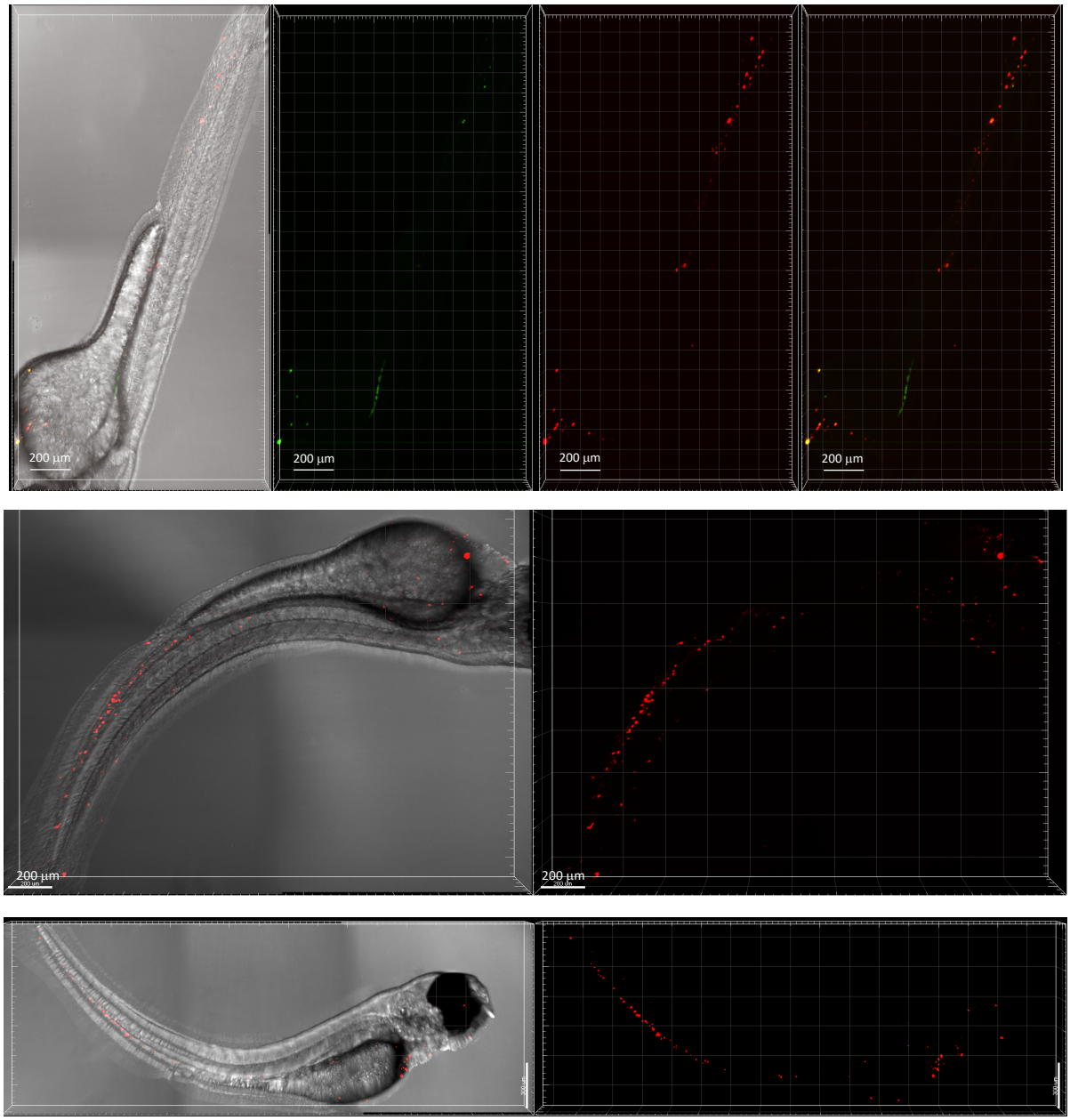

Supplementary Figure 6: CTG and DiI stained cell trackers injected into the posterior cardinal vein of zebrafish larve*. A zebrafish larva injected with MCF-7 cells at two days post fertilization, stained with both DiI and CellTracker green. A: CTG is visible in a few cells at the day of injection. B: CTG stain not visible at one dpi, and only DiI stain observed. C: CTG stain not visible at two dpi, and only DiI stained observed. The images were obtained using Andor Dragonfly confocal microscope at 10x magnification. Scale bar: 200 µm.*